DETECTION OF DECAY AND HOLLOWS IN LIVING TREES USING RESISTIVITY METHOD WITH MODIFIED SCHLUMBERGER ELECTRODE CONFIGURATION

Ayodele Olatunbosun SOGE

Matric No.: 79384

BSc (Hons) Physics (Ibadan); MPhil Electrical Engineering (Leicester)

A thesis in the Department of Physics submitted to the Faculty of Science in partial fulfilment of the requirements for the award of the degree of

DOCTOR OF PHILOSOPHY (PhD)

of the

UNIVERSITY OF IBADAN

MAY 2020

ABSTRACT

Decay and hollows in stems of Living Trees (LT) are responsible for some tree failures which may lead to loss of lives and damage to property, especially during stormy weather. This possible disaster and attendant economic loss could be prevented if such defects are detected early for timely intervention in cutting down the affected trees. Several attempts have been made to detect the Location, Extent of Decay and Hollows (LEDH) in LT using resistivity method with minimal success owing to the electrode configuration adopted. Therefore, this study was undertaken to detect LEDH in LT.

Eighty LT comprising forty candle trees (*Senna alata* L. Roxb.) and forty almond trees (*Terminalia catappa* L. Roxb.) were purposively selected within the University of Ibadan campus. The Resistivity Profiles (RP) were obtained from resistivity measurements for the selected LT, freshly-cut healthy, decayed and hollowed tree stems. The resistivity method implemented involved the use of an earth resistivity meter and a modified form of Schlumberger electrode configuration, which employed tiny electrodes with the spacing scaled down to centimetre range. A laboratory experiment was set up using three wood fabricated hollow cylinders filled with compacted sawdust to mimic stems of LT. The correlation between the RP of healthy LT and that of healthy tree replica was determined. The RP of healthy, decayed and hollowed trees were replicated in the Laboratory Prototypes (LP). Wood decay was modelled by inserting copper wire lumps into the LP at depths 5.00, 10.00, 15.00 and 20.00 cm from the centre of the modelled decay to the LP surface. Hollows were replicated in the LP using a plastic cylinder, at depths 4.00, 12.00 and 20.00 cm from the centres of the modelled hollows to the LP surface. The replicated RP were compared to those of selected LT to detect LEDH in LT. Data were analysed using descriptive statistics and ANOVA.

The Mean Resistivity Values (MRV) of decayed, healthy and hollowed trees were. 13.52±1.11, 62.59±8.61, 7388.17±1564.58 Ωm for candle trees; and 14.23±1.78, 171.24±33.43, 12430.70±1410.79 Ωm for almond trees. The sharp decrease in MRV of decayed trees may be due to mobile cations in the decayed region. The rapid increase in MRV of hollowed trees could be attributed to the non-conductivity of electric current by the hollows. The RP of healthy LT correlated strongly with that of healthy tree replica (r^2_{mean}=0.956 for candle trees and r^2_{mean}=0.998 for almond trees). Hence, the LP was a true replica of healthy LT. The resistivity values of the LP ranged between 45 and 80 Ωm. Wood decay replicated in the LP were detected as resistivity anomalies of 11–17 Ωm representing a decrease by a factor of four compared with

the healthy tree replica. The embedded hollows were detected as resistivity anomalies of 155–271 Ωm representing an increase by a factor of three compared with the healthy tree replica. The location and extent of the resistivity anomalies corresponded to LEDH in LT of similar dimensions.

The resistivity method with modified Schlumberger electrode configuration detected the location, extent of decay and hollows in living trees. The method would assist in non-invasive urban tree management.

Keywords. Wood decay, Tree hollows, Electrical resistivity method, Resistivity profiles, Schlumberger electrode configuration

Word count. 495

CERTIFICATION

This to certify that this research was carried out by **Ayodele Olatunbosun SOGE** in the Department of Physics, University of Ibadan, under the supervisions of:

O. I. Popoola
BSc (Hons), MSc, PhD (Ibadan), MNIP
Department of Physics
University of Ibadan

A. A. Adetoyinbo
BSc (Hons), MSc, PhD (Ibadan)
Department of Physics
University of Ibadan

ACKNOWLEDGEMENTS

My greatest gratitude goes to the Almighty God for divine protection, good health and wisdom to carry out this research successfully. All glory to His name!

I would like to express my profound gratitude to my supervisors, Dr O. I. Popoola and Dr A. A. Adetoyinbo, for their guidance, support, patience and immense contribution towards the success of this research.

My sincere appreciation also goes to all members of the Solid Earth Physics research group, University of Ibadan, such as Prof J. A. Adegoke, Dr E.O. Joshua, Dr Folashade L. Aderemi, Dr T. T. Ogunseye, and Dr I. A. Ojoawo for their advice, encouragement and moral support during the course of this work. I also acknowledge the assistance received from Mr F. O. Kayode and Mr O. G. Ajoje, staff members of the Wood Workshop in the Department of Physics, University of Ibadan, for the construction of wooden hollow cylinders used as laboratory prototypes for this research. I like to register my appreciation for the following: Prof O. E. Awe (Head of Department), Prof Janet A. Ademola, Prof F. O. Ogundare, Prof I. P. Farai, Dr Mojisola O. Adeniyi (Postgraduate Coordinator), Dr O. O. Faluyi, Dr Godwin Egbeyale, Dr A. K. Bello, Dr H. O. Efunwole and Mr Tunji Popoola.

I would like to thank Prof L. B. Kolawole, Redeemer's University, for his encouragement and fatherly advice. My gratitude also goes to my colleagues at Redeemer's University for their friendly advice and moral support – Dr Semiu Kareem, Dr Oluropo Dairo, Mr Muritala Osinowo, Engr. Olubunmi Onatoyinbo, Mr Gbenga Akinyemi, Dr A. A. Willoughby, Dr J. A. Falade and Prof U. E. Vincent.

I also express my deepest appreciation to my family for their prayers, encouragement and moral support throughout the course of this work. My special thanks and heartfelt gratitude to my loving wife, Rita Orevaoghene; and my beautiful children, Oluwafunmilayo Okeoghene, Oluwaferanmi Ovie, and Oluwafunke Efeoghene, for their sacrifice and understanding.

The relentless effort, constant encouragement and continuous support of my dearest parents – Late Elder F. A. Soge and Deaconess E. O. Soge – who sacrificed a lot for my education, are also greatly acknowledged and appreciated. Also, I wish to express my profound gratitude to my siblings and their spouses: Arc. Moses & Late Mrs Bose Dzungwe, Dr Bede & Mrs Busola Akpunne, Dr Olusegun & Mrs Valerie Soge and Mr Sunday & Mrs Lola Jegede.

DEDICATION

To the memory of my beloved father, **Elder Francis Abiodun Soge**

and my dearest sister, **Mrs Abosede Oluwatoyin Dzungwe**

TABLE OF CONTENTS

LIST OF TABLES

LIST OF FIGURES

LIST OF APPENDICES

CHAPTER ONE
INTRODUCTION

Trees are crucial for the conservation of our environment, which is presently experiencing the negative impacts of global warming and climate change. The critical roles played by trees in our environment include temperature regulation, absorption of greenhouse gases such as carbon dioxide, production of oxygen via photosynthesis, prevention of erosion, and the supply of fruits for consumption (Campbell and Reece, 2005). However, trees, if not monitored and managed correctly, can wreak havoc on human lives and property in our communities (Appendices 1 and 2). Lack of adequate and prompt action in felling decayed and hollowed trees before crumpling by strong wind is a primary cause of disaster by fallen trees (Johnstone *et al*., 2010; Goh *et al*., 2018). Timely intervention is only possible if monitoring systems capable of detecting defects in living trees are available. On the contrary, such monitoring systems are not readily available in Nigeria. Besides, researchers in Nigeria have not thoroughly considered the risks to lives and property posed by collapsed trees with a concerted effort in proffering scientific solutions to the menace.

Wood decay is the process by which wood is decomposed by micro-organisms to provide nutrients for their survival (Harris *et al*., 2004). A prolonged bacterial attack on wood usually results in physical degradation such as mass loss, decrease in mechanical properties, and biological decay by white-rot, brown-rot, or soft-rot fungi (Smith and Shortle, 1988). Hollows in tree trunks may develop due to either an abnormality in the tree growth or dried decayed wood falling off at the advanced stage of the decay process. Wood decay and hollows within a tree trunk have been identified to be responsible for some tree failures which often lead to human tragedy and property destruction (Lonsdale, 1999; Schwarze *et al*., 2000; Mortimer and Kane, 2004; Johnstone *et al*., 2010; Goh *et al*., 2018). Moreover, the ecological purpose of a standing tree in preserving the environment from climate change is severely hampered by wood decay. Also, the replacement of urban trees with high monetary values could be time-consuming and expensive (Heikura *et al*., 2008). In terms of economic worth, a decayed wood would not attract equal market value as a healthy wood since decay causes a

decrease in wood density or mass (Beall and Wilcox, 1987; Johnstone *et al*., 2010; Goncz *et al*., 2017; Gao *et al*., 2019). Therefore, an accurate method of detecting decay and hollows in trees is germane for the maintenance and routine monitoring of both urban and forest trees.

1.1 Tree Anatomy

The anatomy of a tree is described in Fig. 1.1 while the sectional view of a wood structure is presented in Fig. 1.2 and consists of the following layers:

I. The **outer bark (or periderm)** is the tree's protection from the outside word and injuries. Continually renewed from within, it helps keep out moisture in the rain, and prevents the tree from losing moisture when the air is dry (Arteca, 1996). It insulates against cold and heat and wards off insect enemies (Arteca, 1996).

II. The **inner bark (or phloem)** is involved in the transport of the sap containing the sugars made by photosynthesis to other parts of the tree (Lalonde *et al*., 2004; Campbell and Reece, 2005). It is a soft spongy layer of living cells, some of which are arranged end to end to form tubes (Raven, 1992). It lives for only a short time, then dies and turns to cork to become part of the protective outer bark (Mauseth, 1991). These are supported by parenchyma cells which provide padding and include fibres for strengthening the tissue (Lalonde *et al*., 2004).

III. **Vascular cambium** is a layer of undifferentiated cells that are continually dividing and creating phloem cells on the outside and wood cells known as xylem on the inside (Bannan, 1962).

IV. **Cambium cell** is the growing part of the trunk, situated between phloem and xylem. It annually produces new bark and new wood in response to hormones that pass down through the phloem with food from the leaves (Larson, 1994). These hormones, called "auxins", stimulate growth in cells and are produced by leaf buds at the ends of branches (Davies, 1995; Taiz and Zeiger, 2010).

V. **Sapwood** acts as the tree's pipeline transporting sap from the roots to leaves (Fig.1.1). It is the new wood formed by cambium. As newer rings of sapwood are formed, inner cells lose their vitality and become heartwood (Larson, 1994).

VI. **Heartwood** is usually darker in colour than the sapwood. It is the dense central core of the trunk giving it rigidity. Although dead, it would not decay or lose

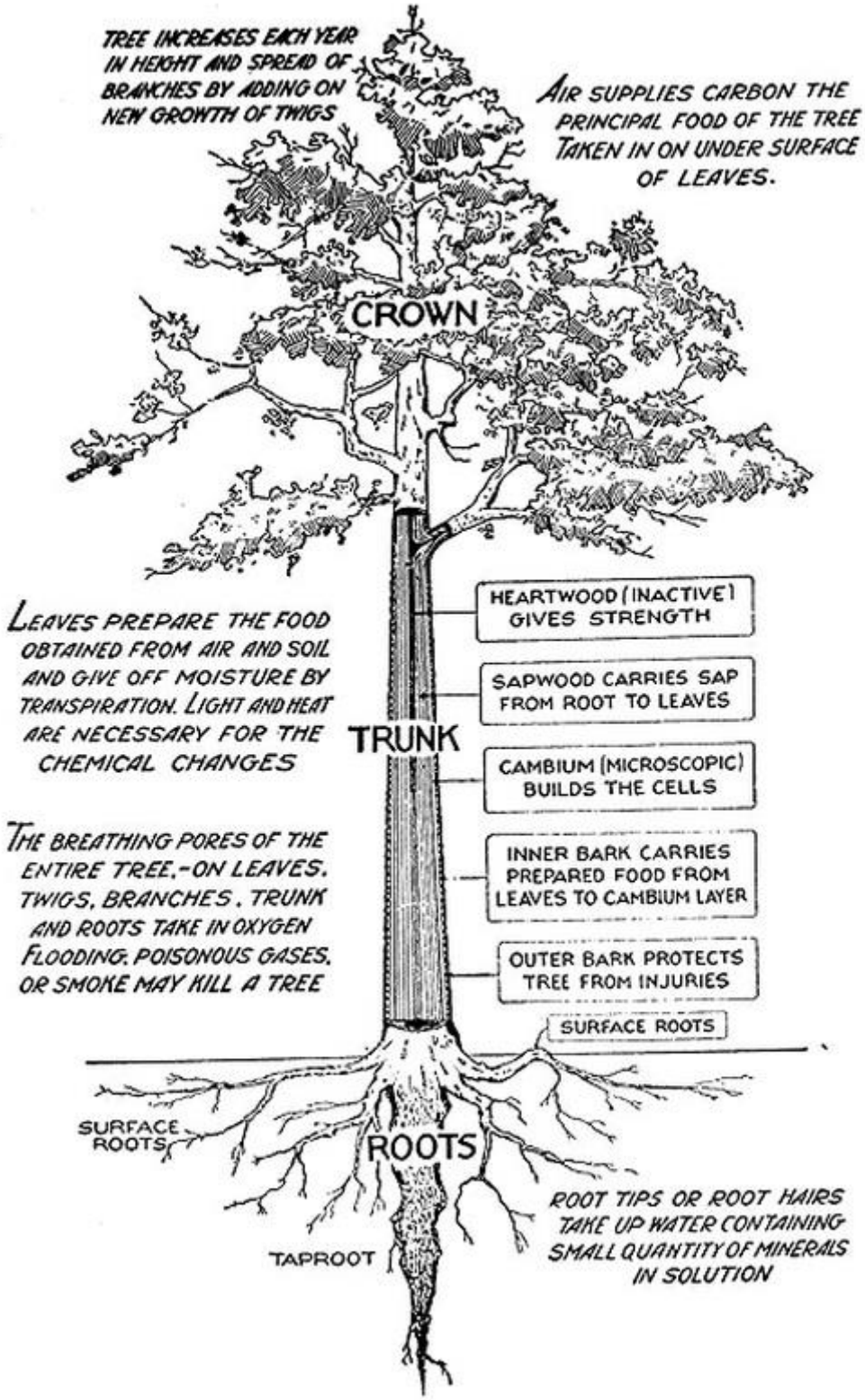

Fig. 1.1. The anatomy of a tree showing the three major parts – the crown, trunk and roots

Source: Anatomy Note, www.anatomynote.com, retrieved on 20 February 2020

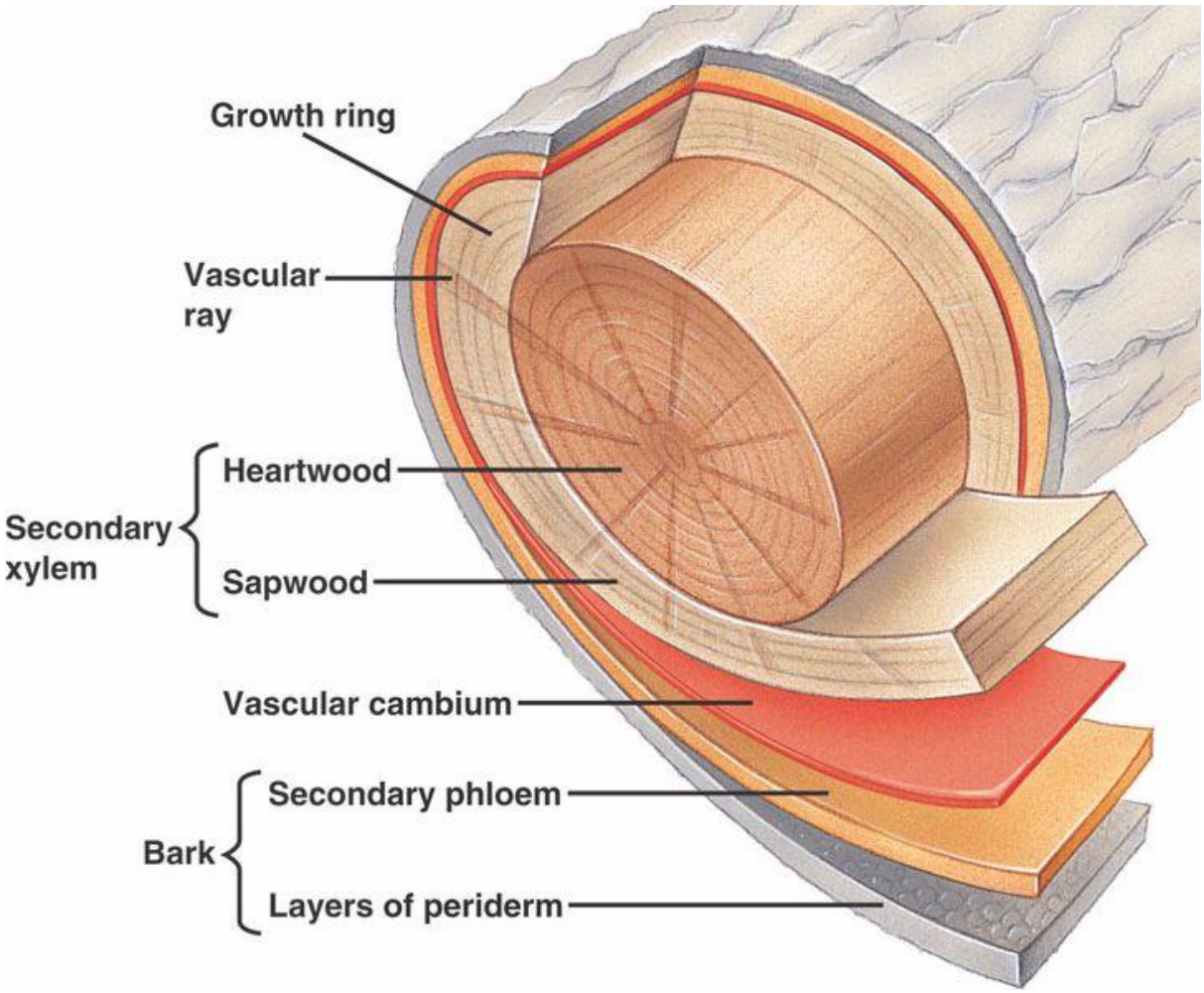

Fig. 1.2. Wood sectional view showing the different layers

Source: Anatomy Note, www.anatomynote.com, retrieved on 20 February 2020

strength while the outer layers are intact except it is attacked by decay fungi (Lalonde *et al*., 2004). It is a composite of hollow, needle-like cellulose fibers bound together by a chemical glue called **lignin** – a class of complex organic polymers that form key structural materials in the support tissues of vascular plants and some algae (Martone *et al*., 2009). Lignins are particularly important in the formation of cell walls, especially in wood and bark, because they lend rigidity and do not rot easily (Martone, 2009).

VII. **Xylem** are thick walled consisting of the sapwood and heartwood and sited nearest the centre of stem (Larson, 1994). It consists of the sapwood and heartwood layers. Xylem, together with phloem and cambium, forms the vascular bundle – a strand of conducting vessels in the stem (Campbell and Reece, 2005).

1.1.1 Growth Layers

Cambial activity in temperate areas is usually periodic and yields a growth layer (Larson, 1994). In the transverse section of stem and roots, these layers appear as definite rings or concentric circles known as **growth rings** (Fritts, 2001). In plant with definite seasonal growth or when growth takes place during a season, growth layer is called annual layer and growth ring may be termed as annual ring, respectively (Fritts, 2001). There may also be rays running at right angles to growth rings. These are vascular rays which are thin sheets of living tissue permeating the wood (Bannan, 1962; Fritts, 2001). Approximate age of trees can be estimated by counting the number of growth rings (Mauseth, 1991). For instance, the age of yew (*Taxus baccata*) in Fig. 1.3 with 27 annual rings is approximately 27 years.

Wood is produced in an inconstant environment and is subjected to developmental control, xylem cells are formed that are of different shape, size, cell wall structure, composition and texture (Fahn and Werker, 1972). In plants that have experienced bad environmental condition like stress, disease etc. and growth is interrupted but resumed later, an additional or second growth layer may be observed in wood (Mauseth 1991; Fritts, 2001). Such layer is called false annual ring and the two or more rings formed are termed as multiple annual ring (Mauseth 1991; Fritts, 2001).

Fig. 1.3. A section of yew (*Taxus baccata*) showing 27 annual rings, pale sapwood and dark heartwood

Source: Wikipedia, www.wikipedia.org, retrieved on 25 February 2020.

1.1.2 Chemical Components of Wood

Wood is a carbohydrate composed principally of carbon, hydrogen, and oxygen (Kollmann and Cote, 1968). Table 1.1 details the typical chemical composition of wood and shows carbon to be the dominant element on a basis (Kollmann and Cote, 1968). Additionally, wood contains inorganic compounds that remain after high-temperature combustion in the presence of abundant oxygen. Such residues are known as ash. The elemental constituents of wood are combined into three organic compounds: cellulose, hemicellulose and lignin (Kollmann and Cote, 1968). Table 1.2 shows the approximate percentage of dry weight of each in hardwood and softwood. Cellulose, perhaps the most important component of wood, constitutes slightly less than one half the weight of both hardwoods and softwoods (Kollmann and Cote, 1968). The proportion of lignin and hemicellulose varies widely among species and between the hardwood and softwood groups (Kollmann and Cote, 1968).

1.2 Wood Decay Fungi

Fungi are overwhelmingly the most important causative agent of wood decay as first reported by Herman Schacht in 1863 (Blanchette, 1991). Wood decay fungi are unique owing to their capacity to decompose lignified cell wall through their enzymatic activities [Blanchette, 1991). Decay fungi need oxygen, water and a food source to exist (Seweta, 2013). Wood as a food source is limited to those fungi which can utilise the components and, in the process, break down the wood (Seweta, 2013). Wood decay fungi may form fruiting structures called conks on affected branches and trunks as displayed in Fig. 1.4 but not always (Lyon, 2005). Moreover, wood decay fungi can degrade wood strength leading to stem or branch failure (Lyon, 2005). Decay fungi require free water so the moisture content of wood must be above 28% to decay (Seweta, 2013). Fungi have an external method for breaking down their food by secreting digestive enzymes and other chemicals into the substrate where they are growing (Eriksson *et al*., 1990). This enables the fungi to then absorb pre-digested food products. This external digestion process requires liquid water for the secretion of enzymes and then the useable food products can diffuse back into the fungus (Eriksson *et al*., 1990). Without this moisture, the fungus cannot be active or grow. Hence, it may either become dormant or die in the absence of water (Eriksson *et al*., 1990).

Table 1.1. Elemental composition of wood

Elements	Percentage of dry weight (%)
Carbon	49
Hydrogen	6
Nitrogen	Slight amount
Ash	0.1

Source: Kollmann and Cote, 1968.

Table 1.2. Organic constituents of wood

Type	Percentage of dry weight (%)		
	Cellulose	**Hemicellulose**	**Lignin**
Hardwood	40 – 44	15 – 35	18 – 25
Softwood	40 – 44	20 – 32	25 – 35

Note: Pectins and starch commonly compose approximately 6% of the dry weight

Source: Kollmann and Cote, 1968.

Fig. 1.4. Fruity bodies by Poroid wood decay fungi *Ganoderma* spp. P. Karst.

Source: George Hudler, Cornell University, www.bugwood.org, retrieved on 20 February 2020.

Decay fungi colonise wood via the anatomical paths of least resistance, and quickly move into areas containing easily assimilated nutrients (Blanchette, 1991).

Wood decay is generally classified into two main groups, **white rots** and **brown rots**, based on the wood residue left behind following fungal digestion (Seweta, 2013). The fungi responsible for white rots and brown rots are Basidiomycota (Blanchettes, 1991). Two other types include "dry rot", which is a form of brown rot caused by water conducting decay fungi, and "soft rot", referring to decay caused by certain Ascomycetes and asexual fungi (Seweta, 2013). Table 1.3 summarises different types of wood decay.

1.2.1 White Rots

White-rot fungi are more numerous than brown-rot fungi. They include both Ascomycota, such as *Xylaria* spp. (Fig. 1.5), and Basidiomycota (e.g. *Armillariella mellea*) (Seweta, 2013). All white-rot fungi can cause lignin degradation, but some can selectively remove lignin leaving large concentrations of cellulose (Blanchette, 1991). These areas of cellulose appear as bright, white zones in the heartwood of living trees or in sapwood and heartwood of downed timber (Blanchette, 1991). This process is called **selective delignification**.

There is a tremendous amount of interest in using these fungi in industry, because many uses of wood involve removing lignin e.g., biopulping (Blanchette, 1991). White rot fungi are typically associated with hardwood decay and their wood decay patterns can take on different forms (Blanchette, 1991; Seweta, 2013).

An oak tree with white rot is shown in Fig. 1.6. The fungus has decayed the sapwood and dark heartwood turning it white (Fig. 1.6a). This white rot fungus attacked all cell wall components. Figure 1.6b is the scanning electron micrograph (SEM) showing the hypha (basic structural unit) of a white rot fungus in the cell lumen of a wood cell. The SEM revealed that extracellular enzymes are degrading all the cell wall components simultaneously causing erosion troughs to form in the cell wall (Seweta, 2013). The selective delignification of the cell wall components by white rot fungus is depicted in Fig. 1.6c. The most remarkable feature of white-rot fungi is their ability to completely degrade lignin – they are the only organisms known to do this.

Table 1.3. Types of Wood Decay

Type	Agent	Colour	Colour Texture	Chemistry
White Rot	Basidiomycota	Bleached	Fibrous	Decays mostly lignin and secondarily cellulose. All components removed.
Brown Rot	Basidiomycota	Brown	Fibrous texture lost easily, cross-checking	Primarily carbohydrates lost, lignin mostly remains. Great strength loss occurs in initial stage of decay.
Soft Rot	Asco- and Deuteromycota	Bleached or brown	Usually on surface, some fibrous texture lost, cross-checking in some cases	Carbohydrates preferred, but some lignin lost too

Source: Seweta, 2013

Fig. 1.5. **Upper row:** Two common Ascomycota that cause white rots. **Left:** *Xylaria hypoxylo*, the "candle snuff" fungus often seen on rotting stumps. The upper parts of the fork-shaped structures are covered with white, powdery conidia. **Right:** *Xylaria polymorpha*, the "dead man's fingers" which often grows from the bases of rotting wood stumps. **Bottom:** A section cut through one of the "dead man's fingers" showing numerous perithecia just below the surface of the fruitbody.
Source: Seweta, 2013

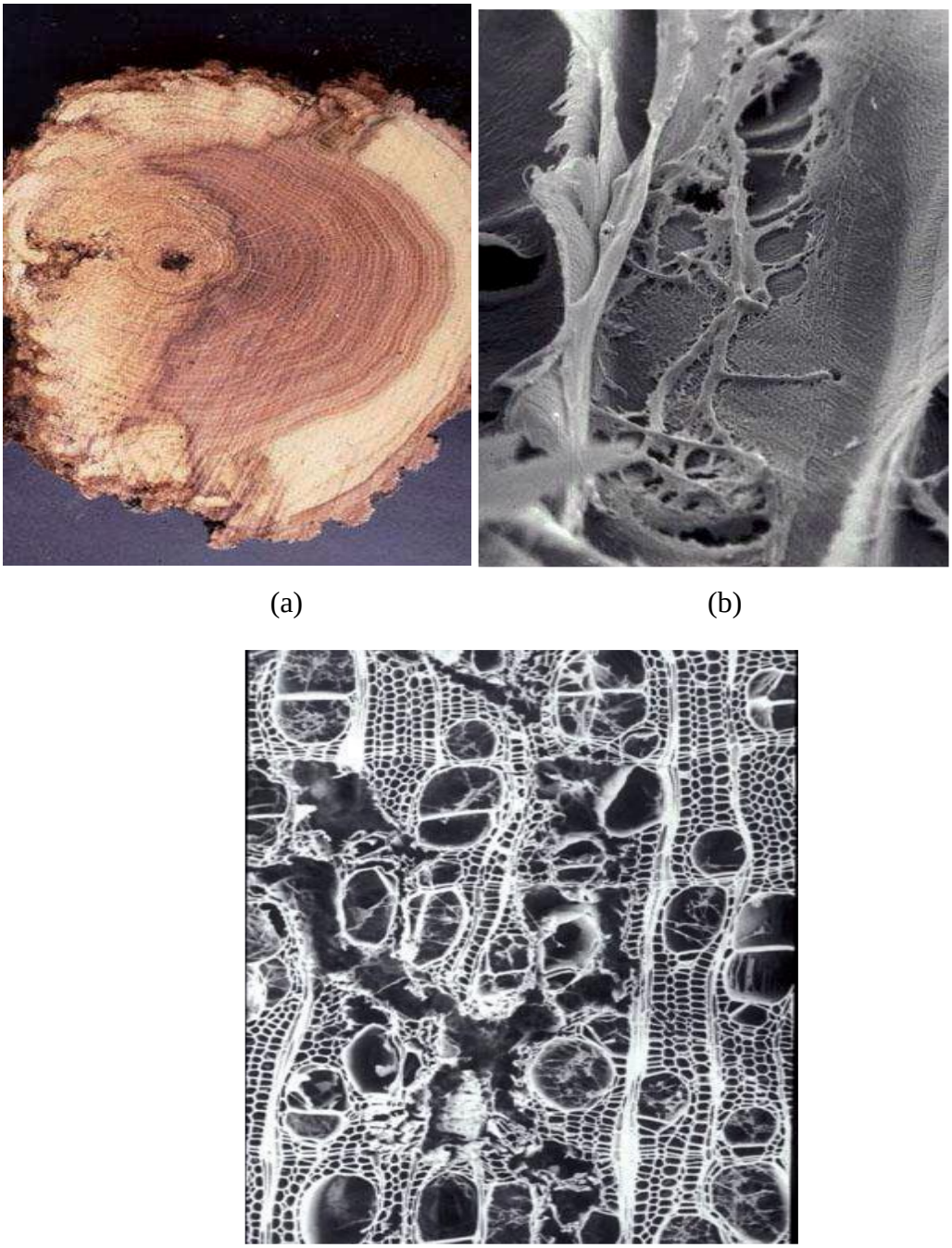

(a) (b)

(c)

Fig. 1.6. A decayed oak tree showing two different forms of white rot – selective delignification and simultaneous decay of all cell components. (a) Cross section of an oak tree with white rot. (b) Scanning electron micrograph showing the hypha of a white rot fungus in the cell lumen of a wood cell. (c) A cross section of wood with white rot showing the fungus has degraded some cells completely but not others.

Source: Seweta, 2013

A split section of a pine tree with white-pocket rot caused by *Phellinus pini* is displayed in Fig. 1.7a. The white areas are delignified zones where the fungus has removed lignin but not the cellulose. White-pocket rot fungi cause a selective attack on lignin and hemicellulose in wood. A mottled white rot in wood decayed by *Ganoderma applanatum* is illustrated in Fig. 1.7b. This fungus causes a combination of delignification and a simultaneous white rot attack in the wood (Seweta, 2013). White areas with black spots containing manganese (deposited by the fungus) are delignified while the tan areas have a simultaneous white rot. In the tan areas, large degraded zones form and these holes fill with white mycelium of the fungus (Seweta, 2013). Figure 1.7c depicts a cross section of wood from a white-pocket area of decayed wood showing delignified wood cells. These cells have no middle lamella (this is the area between cells that has high lignin concentration). Only the cellulose-rich secondary walls remain after advanced decay.

1.2.2 Brown Rots

Brown-rot fungi are predominantly members of the Basidiomycota, including common species such as *Schizophyllum commune*, *Fomes fomentarius* (the "hoof fungus" of Scottish birch woods) and the dry-rot fungus, *Serpula lacrymans* (Eriksson *et al*., 1990; Seweta, 2013). Many of the brown-rot fungi produce bracket-shaped fruitbodies on the trunks of dead trees (Fig. 1.8) but the characteristic feature of these fungi is that the decaying wood is brown and shows brick-like cracking – a result of the uneven pattern of decay, causing the wood to split along lines of weakness as shown in Fig.1.9 (Blanchette, 1991; Seweta, 2013).

The wood decayed by brown rot fungi is typically brown and crumbly and it is degraded via both non-enzymatic and enzymatic systems (Seweta, 2013). A series of cellulolytic enzymes are employed in the degradation process by brown rot fungi, but no lignin degrading enzymes are typically involved (Seweta, 2013). Hence, brown rotted wood is characterised by selective removal of cellulose and hemicellulose, leaving a brown amorphous residue that usually cracks into cubical blocks and consists largely of slightly modified lignin (Blanchette, 1991; Seweta, 2013). Brown rot fungi can hollow out branches and tree trunks and the tree will show no symptoms; these trees are prone to sudden breakage in storms (Blanchette, 1991). An urban tree with brown rot is displayed in Fig. 1.10a. The large branch failed and broke off due to the presence of decay.

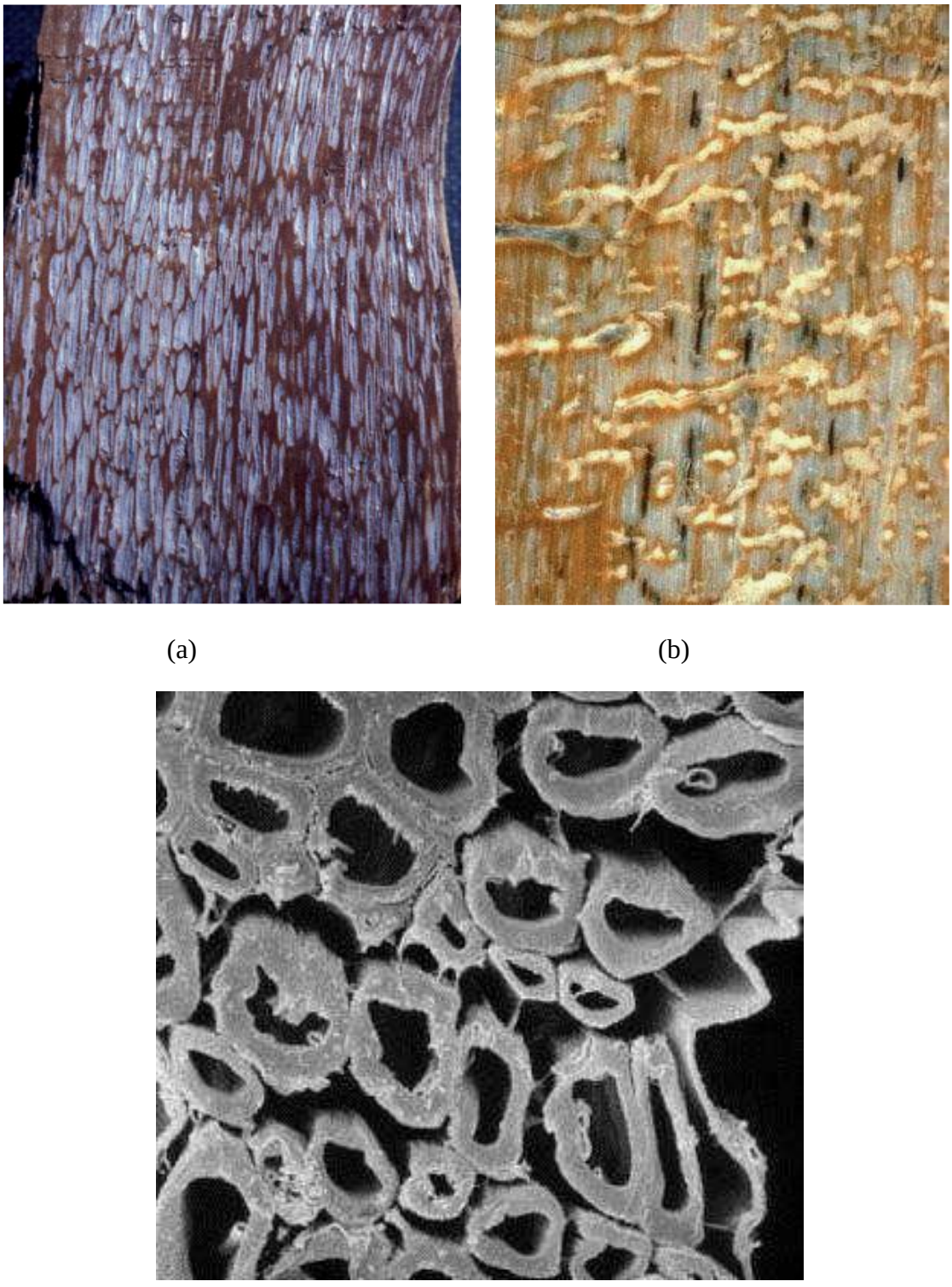

(a) (b)

(c)

Fig. 1.7. Different forms of white rots (a) A split section of a pine tree with white-pocket rot caused by *Phellinus pini*. (b) A mottled white rot in wood decayed by *Ganoderma applanatum*. (c) A cross section of wood from a white-pocket area of decayed wood showing delignified wood cells. Source: Seweta, 2013

Fig. 1.8. Small, leathery, bracket-shaped fruitbodies of a white-rot fungus

Source: US Pest Protection, www.uspest.com, retrieved on 20 February 2020

Fig. 1.9. Cross-section of a tree with brown rot

Source: Utah Pests, Utah State University, www.utahpests.usu.edu, retrieved on 20 February 2020

(a) (b)

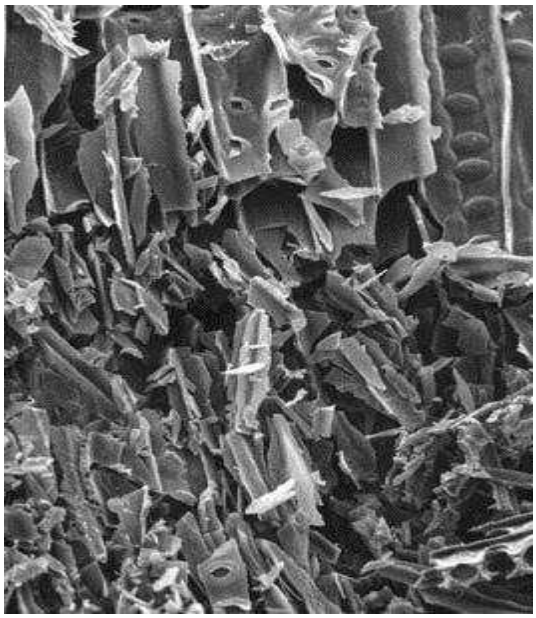

(c)

Fig. 1.10. (a) An urban tree with brown rot. (b) A closer view of brown-rotted Wood. (c) Scanning electron micrograph of brown-rotted wood.

Source: Seweta, 2013

Brown rot has little structural integrity and large losses of wood strength occur early in the decay process, often before decay characteristics are visually evident (Seweta, 2013). A closer view of the brown-rotted wood is shown in Fig. 1.10b. In advanced stages of decay, the wood cracks and checks into cubicle pieces. Little to no integrity remains in this decayed wood. Figure 1.10c is the scanning electron micrograph of a brown-rotted wood. Only slight pressure causes the wood cell walls to crumble into minute fragments.

1.2.3 Soft Rots

Fungi that cause soft-rot are taxonomically classified in the subdivisions, Ascomycota and Deuteromycota (Lyon, 2005; Seweta, 2013). Soft rot was first characterized as a soft, decayed surface of wood in contact with excessive moisture. However, soft rots can occur in dry environments and may be macroscopically similar to brown rot (Lyon, 2005; Seweta, 2013). Two distinct types of soft rot are currently recognised. Type 1 is characterised by longitudinal cavities formed within the secondary wall of wood cells and Type 2 used to describe an erosion of the entire secondary wall (Lyon, 2005; Seweta, 2013). The middle lamella is not degraded (in contrast to cell wall erosion by white-rot fungi) but may be modified in advanced stages of decay (Lyon, 2005; Seweta, 2013). Large strength losses in wood can be associated with soft rot attack. Cavities formed in the wood as well as extensive cellulose degradation can result in extremely poor strength characteristics when soft-rot wood is visually evident (Lyon, 2005; Seweta, 2013). As decay progresses, extensive carbohydrate loss occurs, and lignin concentrations increase in the residual wood (Lyon, 2005; Seweta, 2013). Soft rot is different from other types of wood decay. Chains of cavities are produced inside the cell wall as illustrated in Fig. 1.11.

1.3 Statement of Problems

It has been observed that several trees could have decay or hollows without showing any external sign. One major cause of disaster by tree is lack of timely intervention in cutting down decayed and hollowed trees before collapsing by wind pressure. Timely intervention is only possible if there is monitoring system in place for early detection of decay and hollows in living trees. Early detection of wood decay and hollows has not been seriously addressed by researchers in Nigeria.

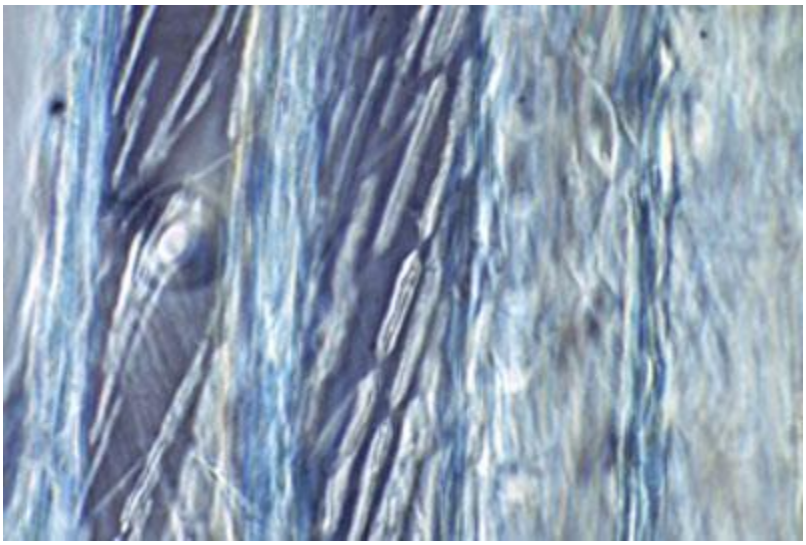

Fig. 1.11. Micrograph of a section from soft-rotted wood showing cavities within the cell walls when viewed with a light microscope (Seweta, 2013)

1.4 Justification for the Research

Early detection of wood decay and tree hollows would prevent loss of human lives and property by fallen decayed trees. Also, an accurate method of detecting decay and hollows in trees would reduce economic loss by the buyers when forest trees are evaluated for sale. Additionally, the possibility of assessing incipient wood decay could afford the forest managers ample time to take corrective measures on the trees if necessary. The conventional resistivity method for detecting decay and hollows in trees involves the use of specially designed resistivity meter with computer interface which is expensive. Hence, the improvisation of earth resistivity meter for detecting decay and hollows in trees would be cost effective.

1.5 Aim and Objectives of the Research

The aim of this research was to detect the location and extent of wood decay and hollows in living trees using resistivity method for the purpose of non-invasive forest and urban tree management.

The objectives of this work are to:

I. adapt earth resistivity meter to detect decay and hollows in living trees;
II. determine the resistivity patterns of healthy trees, decayed trees and hollowed trees;
III. develop resistivity profile models for healthy, decayed and hollowed trees, and;
IV. apply the resistivity profile models to detect the location and extent of wood decay and hollows in living trees.

1.6 Thesis Outline

The implementation of the electrical resistivity method for the detection of wood decay and hollows in living trees was discussed extensively in this thesis. Chapter Two is the literature review on the various techniques for detecting decay and hollows in living trees as reported by researchers in several publications. The methodology adopted for this research was reported in detail in Chapter Three. Field and laboratory results were presented and discussed in Chapter Four. The conclusions, field applications of the resistivity method, contribution to knowledge and further work were presented in Chapter Five.

CHAPTER TWO
LITERATURE REVIEW

2.1 Techniques for Detecting Decay and Hollows in Living Trees

There are several methods for detecting decay and hollows in living trees, as reported by various authors and researchers. These techniques can be classified into two broad categories: **Invasive methods** and **Non-invasive methods** (Lawday and Hodges, 2000). The invasive methods involve exposing the wood either by removing the bark discs or in extreme cases by drilling holes into the wood to probe for evidence of decay and cavity or hollow (Lawday and Hodges, 2000). However, the non-invasive methods allow the probing of the internal structure of the tree through the aid of sensors and other probing devices, without exposing the wood or drilling holes into the tree (Lawday and Hodges, 2000). One crucial drawback of invasive methods is that the holes drilled into the wood tissue expose the tree to fungi invasion and encourage the spread of any compartmentalised infection to healthy wood – a possible phenomenon when increment borers and drills with the capability of creating deep holes are used (Toole and Grammage, 1959; Lawday and Hodges, 2000).

The primary examples of invasive methods for identifying decay and hollows in standing trees include: electrical resistivity techniques, acoustic techniques (those using ultrasonic and stress-wave devices), traditional techniques (involving the use of tools such as a decay detecting drill, increment borer and boroscope), X-Ray or Gamma Ray radiographic technique, acoustic tomography and impedance tomography (Weihs *et al*., 1999). Some examples of non-invasive methods reported by researchers are microwave scanning (Martin *et al*., 1987), magnetic resonance imaging (Müller *et al*., 2001), X-ray tomography (Habermehl, 1982a, 1982b), and traditional techniques involving the use of mallets (Dolwin *et al*., 1998).

2.1.1 Traditional Methods

The traditional technique is a visual inspection of trees for external signs of decay usually undertaken by experienced arboriculturist to ascertain whether further inspection is necessary (Kennard *et al*., 1996). The external signs of decay in trees include dead

cambium, deadwood in the crown, exposed wood with decay, swollen trunks, cracks and sunken areas (Dolwin *et al*., 1998). The traditional technique also involves the use of some specialised tools such as mallets, decay detecting drill, increment borers, and borescopes.

The resulting sound from a mallet striking a suspect surface can be interpreted with experience to acquire some information on the presence and extent of wood decay. This is a non-invasive method undertaken with an inexpensive tool (Dolwin *et al*., 1998). Decay detecting drill (also known as the resistograph method) penetrate the sound tree with a constant drilling pressure, speed and rotation (Johnstone *et al*., 2007; Nowak *et al*., 2016; Goh *et al*., 2018). The turning moment (or torque), which is equal to drilling resistance, is recorded graphically and relatively to the drilling depth (Goh *et al*., 2018). An abrupt change in spacing between the lines on the resistograph indicates the presence of wood decay (Goh *et al*., 2018). Figure 2.1a illustrates the use of a resistance drill in a standing tree to obtain the relative resistance profile. Figure 2.1b shows an example of a drilling profile obtained from Norway spruce (*Picea abies*) revealing density variations inside tree rings caused by earlywood and latewood zones.

The increment borer is a standard forestry tool which consists of a hollow tube with a screw thread at one end. It is usually used to extract a core of wood from a tree trunk (Fig. 2.2) which can then be investigated for the evidence of discolouration or decay along the wood cross-section (Mattheck *et al*., 1995; Goh *et al*., 2018). The increment borer is highly invasive because its head is typically 9 – 10 mm in diameter and thus, exposes the tree to fungi invasion (Dolwin *et al*., 1998).

Borescope provides a remote visual inspection of the interior of a tree for the presence of wood decay. Like increment borer, it involves the drilling of numerous holes into the xylem (or sapwood) (Goh *et al*., 2018). Its accessories include a small video camera and zoom lenses for the purpose of visual documentation (Goh *et al*., 2018).

2.1.2 Radiographic Technique

The radiographic technique is an invasive method for sensing decay and cavities in trees using an X-ray or gamma radiation. The wood samples can be obtained destructively (harvesting the trees and cutting wood cross-sections) or non-destructively (extraction with increment borer) under laboratory experiments (Tomazello *et al*., 2008). The radiographic technique involves measuring the attenuation of X-rays or gamma rays at their transmission through the wood samples under examination (Ouis, 2003).

(a)

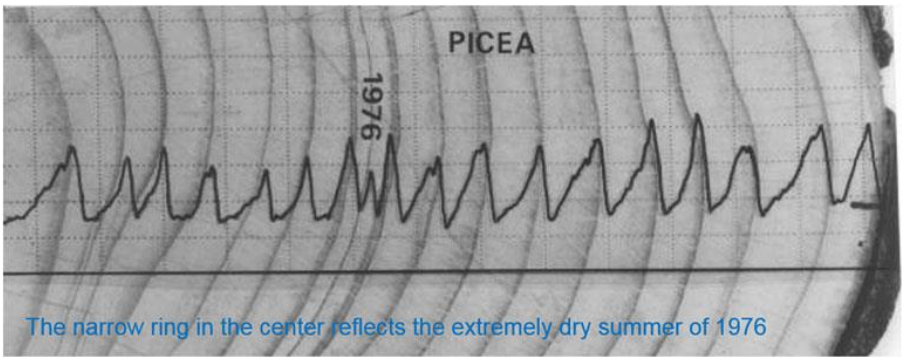

(b)

Fig. 2.1. (a) Electronically regulated resistance drilling in a standing tree using a resistograph tool, and (b) Resistance drilling profile obtained from a Norway spruce (*Picea abies*) revealing density variations inside tree rings. The narrow ring in the centre reflects the extremely dry summer of 1976 (Gao *et al*., 2017).

Fig. 2.2. Increment borer being used to extract a core sample from a tree (Gao *et al*., 2017)

Wood decay is detected by a decreasing wood density resulted from the biodegradation of the wood cell wall (Osborne *et al*., 2016).

2.1.3 Acoustic Techniques

Acoustic techniques for decay detection in trees involve the use of sonic devices which measure the transit time of a pulse of ultrasound or a stress wave across a tree stem. Any deviation from the expected transit time suggests a peculiarity or degradation of a wave path. Ultrasonic waves typically take a longer time to travel through a decayed tree than a healthy tree due to signal attenuation by the decayed wood (Waid and Woodman, 1957; Wilcox, 1988; Bethge *et al*., 1996; Axmon, 2000). Ultrasonic tree testing tools exploit this phenomenon by measuring the increased transit time when ultrasonic waves evade decay within a tree trunk. However, the interpretation of the data acquired from these techniques was unable to offer accurate information on the location and extent of decay in a tree trunk (Lawday and Hodges, 2000). The velocity of sound in wood is dependent on specific properties which are altered by wood decay such as modulus of elasticity, moisture content and density (Dolwin *et al*., 1998). The presence of high moisture content in the tree stem increases the attenuation of ultrasonic waves (Sakai *et al*., 1990).

The main difference between ultrasonic and stress waves is that ultrasonic wave is generated with sound pulses of known frequency while stress wave is a sound wave produced manually with a complex combination of frequencies (Wade, 1975; Bulleit and Falk, 1985; Mattheck and Bethge, 1993). Ultrasonic pulses are generated by a transmitting transducer, as shown in Fig. 2.3a. The wave is more than 20 kHz and above the range of human hearing (Goh *et al*., 2018). In the early 1990s, ultrasound decay detectors (UDD) have been commercially available. One of the UDD implementations is Arborsonic Decay Detector – a portable device that delivers an ultrasound pulse of 77 kHz which can transverse a tree of any species at a relatively constant speed of approximately 2000 m/s. The maximum tree diameter was 1.4 m (Wade, 1975). The UDD operates using a transducer (which sends the signal) and a receiver (that receives the signal) on opposite sides of the tree. The time required for the wave to travel between them is measured, and if the tree is not intact or decayed, it takes longer time to travel through than the nearest path of sound wood (Xu *et al*., 2000; Kazemi-Najafi *et al*., 2009; Goh *et al*., 2018).

(a)

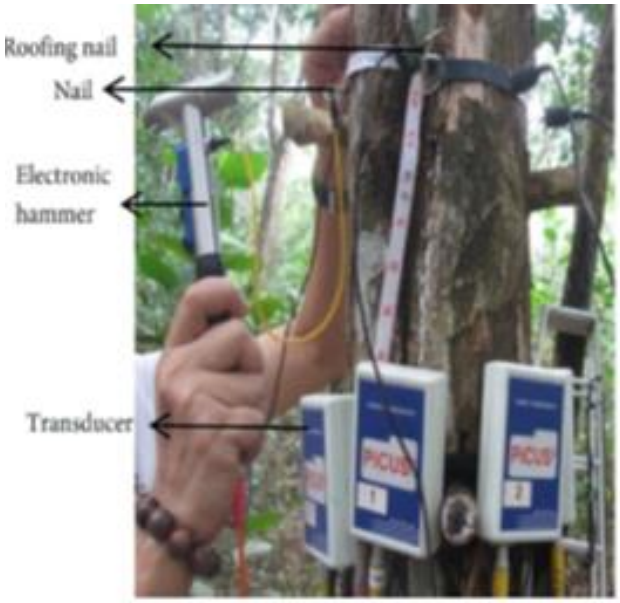

(b)

Fig. 2.3. The set-up of Acoustic Techniques: (a) Ultrasonic wave (b) Stress wave (Karlinasari *et al*., 2015)

In the stress wave approach, the sound wave is generated by tapping a hammer on pins inserted a few millimetres into the xylem (hard interior layer of a tree) as demonstrated in Fig. 2.3b (Gilbert and Smiley, 2004; Karlinasari *et al*., 2015). Like ultrasonic wave approach, detection of wood decay using stress wave technique is based on the claim that stress waves travel relatively slower in decayed wood compared to sound wood (Goh *et al*., 2018). The transit time of stress wave in the decayed regions is markedly increased (Rabe *et al*., 2004; Wang and Allison, 2008; Schwarze, 2008), and internal defects can be detected by the difference between the measured and the reference transit time (Pellerin and Ross, 2002). Stress wave method is not as accurate as the ultrasonic technique because of the large number of frequencies involved (Goh *et al*., 2018). The foremost disadvantage of the stress wave method over the ultrasonic wave is that the stress wave method does not deliver a sound pulse of known frequency, which can lead to inaccuracies in recording the speed and propagation time of the stress wave (Nicolotti *et al*., 2003). Besides, inconsistencies in readings can occur because the hammer is not always struck with the same force and in some cases, inaccurate measurements due to excessive wind speed may arise (Mattheck and Bethge, 1993; Yamaguchi *et al*., 2001).

Acoustic techniques involving the use of ultrasonic and stress-wave devices are classified as invasive methods since the ultrasonic device is generally used on wood exposed by the removal of bark discs, whereas the stress wave operates via screws inserted a short distance from the wood (Dolwin *et al*., 1998). Although acoustic techniques can offer comprehensive information on the wood quality, they may be unable to distinguish between decay and cavities in a tree. Besides, single pulse ultrasound and stress wave equipment is expensive (Johnstone *et al*., 2010). The focus of ultrasonic wood characterisation has been on wave velocity (v), which decreases in the case of a decayed tree (Ouis *et al*., 2003). Wave velocity can be expressed as

$$v = \sqrt{\frac{E}{\rho}} \quad \text{(m/s)} \qquad (2.1)$$

where E is the modulus of elasticity, MOE (N/m) which is a measure of the strength of the wood and ρ is the wood density (kg/m^3). The MOE of a decayed wood is relatively lower than that of sound wood resulting in the reduction of the wave velocity. It has been verified that velocity is dependent on factors such as tree species, moisture content, temperature, and sound wave direction (Mishiro, 1996). However, it is difficult to

translate the velocity of sound to physical properties, because wood is an anisotropic material (Socco *et al*., 2004; Bucur, 2006a; Maurer *et al*., 2006; Schubert *et al*., 2009).

2.1.4 Tomographic Methods

Tomographic methods are the least invasive methods for assessing internal decay in trees (Bucur, 2005). However, X-ray tomography and radar tomography are classified as non-invasive methods by Larsson *et al*. (2004) and Johnstone (2010). Sonic tomography (SoT), an example of acoustic tomography, is a technique for generating an image of the internal structure of a solid object by recording differences in the speed of sound wave transmission. SoT measures the velocity of sound waves through the wood, which depends on the modulus of elasticity and the wood density. Brazee *et al*. (2010) reported that decay causes a decrease in the modulus of elasticity and wood density.

Acoustic tomography can detect internal decay, locate the defects, and estimate their size, shape and characteristics (Bucur, 2005; Wang *et al*., 2007, 2009; Deflorio *et al*., 2008; Lin *et al*., 2008, 2013; Wang and Allison, 2008). In addition, sonic tomography determines the relative strength loss (Rinn, 2011; Lin and Yang, 2015). A decreasing velocity of the ultrasonic propagation could be indicative of fungal invasion of the wood cell wall since ultrasonic velocity is related to the density and dynamic elasticity modulus (Bucur, 1995). Besides, sonic tomography has proven to be very suitable for the early detection of wood decay (Wilcox, 1988; Bauer *et al*. 1991).

Electrical impedance tomography (EIT) can detect wood decay at the early stage, which may not be detected by SoT (Brazee *et al*., 2010; Weihs *et al*., 1999). EIT provides the resistivity image of the wood under investigation by determining its electrical conductivity (Brazee *et al*., 2010). The electrical impedance decreases due to an increased conductivity as moisture accumulates in the decayed wood from fungal colonisation (Brazee *et al*., 2010). However, EIT is unsuitable for routine monitoring for wood decay because of the numerous sensors required and long duration for taking measurements (Brazee *et al*., 2010).

Computerised tomography can employ acoustic rays, electrical resistance, and thermal or radar techniques (Johnstone *et al*., 2010). For electrical resistance and acoustic measurements, sensors are usually placed around a tree (from 8–16 but occasionally more), and multiple measurements are gained by sending a signal from one sensor to the others (Gilbert and Smiley, 2004; Bucur, 2006b). In radar or thermal imaging techniques, the signal is delivered and allowed to bounce off internal, and in

the case of thermal imaging, external structures (Bucur, 2003; Nicolotti *et al*., 2003; Catena and Catena, 2008). These instruments produce cross-sectional "pictures" of the stem, via a computer programmed with complex conversion algorithms.

Thermal imaging with an infrared camera scans for wood defects but cannot accurately quantify the amount of wood decay (Catena and Catena, 2008). Images are species specific. This method is based on the phenomenon that the existence of decayed wood tissue or hollows is related to the surface temperature of the tree (Ouis, 2003). Thermography cannot assess residual wall thicknesses (Catena, 2003). Thermal imaging has the advantage of being non-invasive. It can detect wood decay in large tree roots or the root collar (Catena, 2003; Catena and Catena, 2008).

2.1.5 Nuclear Magnetic Resonance (NMR)

Nuclear Magnetic Resonance (NMR), also known as Magnetic Induction Technique, is a non-invasive method for identifying decay and cavities in trees. Generally, this technique involves the use of inductive coils and eddy current to map the passive electromagnetic properties (PEP's) of a material such as conductivity, permeability and permittivity (Goh *et al*., 2018). The NMR system consists of excitation coils that generate the electromagnetic primary field, which then induces an eddy current in the material under investigation to have magnetic field perturbations, also known as the secondary magnetic field. The eddy current is induced in the material due to the PEP's of the material itself. The secondary magnetic field is acquired by the receiver of the NMR system to assess the PEP's distribution of the tested material (Zakaria *et al*., 2013). Measurements of NMR are based on the resonance frequency, the magnitude of the signal proportional to the density of the nuclei, the spin-lattice and the spin-spin relaxation durations, the diffusion coefficient, the flow velocity, and the spin-spin coupling time (Araujo *et al*., 1992). These parameters, in turn, depend on tree species, moisture content, physiological parameters of the wood, and measurement factors including the Larmor precession frequency, temperature, etc. (Bucur, 2003).

The chief advantage of the NMR technique, besides non-invasive, is that the method is contact-less (Zakaria *et al*., 2013). Hence, the galvanic coupling between the tree and the NMR device is not required. However, the NMR technique being a new technology has not been thoroughly investigated in wood science and technology (Goh *et al*., 2018). In addition, the utilisation of the NMR technique may possibly be limited by the high cost of the equipment (Bucur, 2003; Goh *et al*., 2018).

Magnetic Resonance Imaging (MRI) can be applied to determine the fresh water within a wooden specimen (Araujo *et al*., 1992; Muller, 2001), and provides excellent and spatial high-resolution information about the morphology and pathology of fresh wood samples in a non-invasive manner (Kucera, 1986; Hall *et al*., 1986a). MRI has also been successfully implemented for imaging wood samples (Hall *et al*., 1986b; Wang and Chang, 1986; Chang *et al*., 1989; Flibotte *et al*., 1990; Olson *et al*., 1990).

Muller *et al*. (2001) reported that MRI could accurately and reliably detect fungal decay at an early stage. This was demonstrated using a beech wood sample (*Fagus sylvatica* L.) infected with the brown rot fungus *Coniophora puteana* (Schum.) Karst. cultured on an agar medium in a sterile glass-bottle, as described in Fig. 2.4. The wood sample was examined 12 and 26 days after incubation using MRI, which was able to detect areas containing fresh water attributed to fungal activity 12 days after incubation. Thus, MRI was useful in identifying the early stages of fungal decay in wood prior to any visual evidence. Brown rot fungi decompose cell wall carbohydrate into carbon-dioxide and water, resulting in the increased moisture content of the infected wood sample (Muller *et al*., 2001). With moisture variation inherent in wood, the MRI technique is particularly suited for detecting internal features of wood (Chang *et al*., 1989).

2.1.6 Microwave Scanning

Microwave scanning or imaging is a non-invasive technique for studying physical properties of wood, and for diagnosing wood decay, hollows or cavities and other defects in trees. Microwaves are electromagnetic waves with speed and attenuation dependent on the propagating medium, especially its electric permittivity or dielectric constant which in turn depends on the moisture content and density (Martin *et al*.,1987). The microwave signal transmission through trees is usually attenuated due to absorption and scattering by the wood tissue (Ulaby and Jedlicka, 1984; Choffel, 1999; Goh *et al*., 2018). It has been reported that microwave scanning can be applied to determine the physical characteristics of wood (e.g. density, moisture content and slope of grain) and the detection of defects (knots, metallic objects, sapwood) from the estimation of attenuation, dephasing, and degree of polarisation of microwaves (Martin *et al*., 1987).

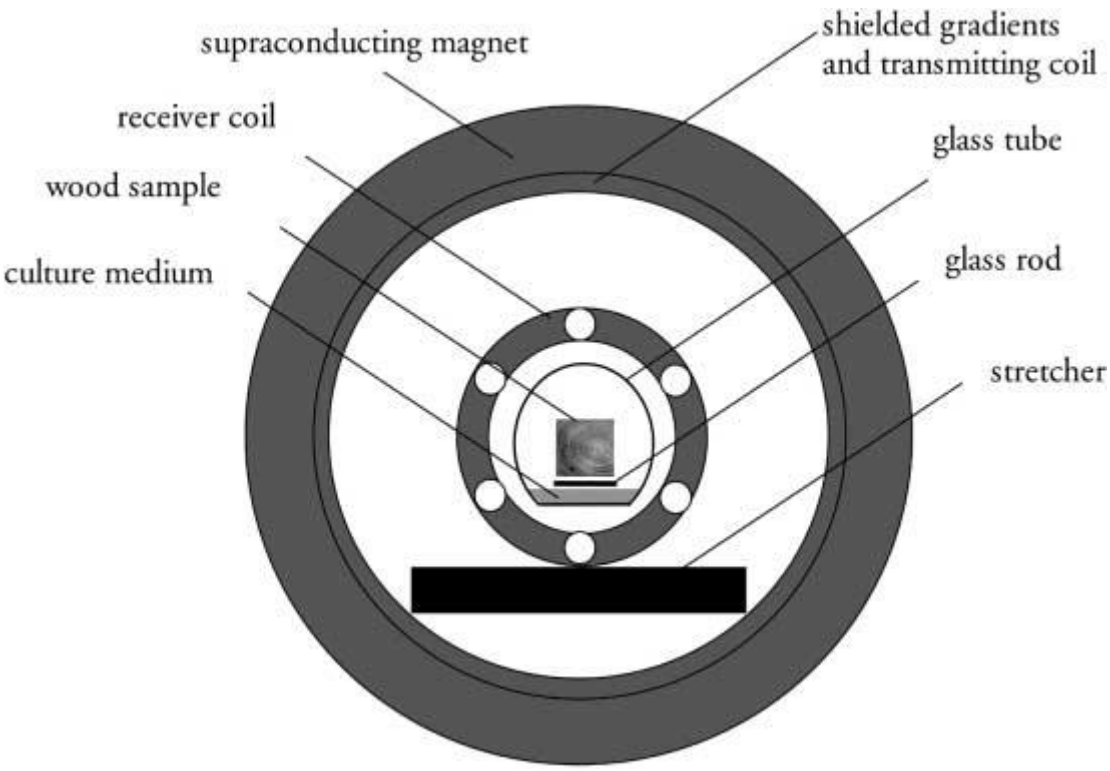

Fig. 2.4. Cross section of the wood sample within the supra-conducting magnet (Muller *et al*., 2001)

The two principal measurement configurations in microwave technique are free space transmission in a focused beam (FB) and near field probing using a modulated scattering technique (MST), as illustrated in Fig. 2.5. Kaestner and Baath (2005) developed a microwave system based on FB concept for locating knots in the tree trunks. In this system, the polarisation measurements were made using a vector network analyser connected to a wide-band horn antenna. It was reported that the system could diagnose fungal attacks and cavities in trees.

The non-invasive nature of the microwave technique and the use of relatively small antenna are the principal advantages of the method (Bucur, 2003; Goh *et al*., 2018). However, the difficulties of applying microwave imaging to wood material arise from inherent material properties, such as the anisotropy, heterogeneity and the presence of natural defects in wood (Larsson *et al*., 2004; Goh *et al*., 2018).

2.1.7 Ground Penetrating Radar Methods

Ground penetrating radar (GPR) is potentially an accurate method for detecting decay in hardwoods (Butnor *et al*., 2009). GPR uses an antenna to propagate short bursts of electromagnetic energy in solid materials and measure the two-way travel time and amplitude of reflected signals. GPR detects wood decay by measuring the degree of reflectivity of a short radar signal at the boundary between the sound and decayed parts which have different electrical and magnetic properties (Ouis *et al*., 2003). Georadar or radar tomography is constituted by the images generated from the reflection of electromagnetic waves at the sound-decayed wood interface (Nicolotti *et al*. 2003).

The GPR methodology is a non-invasive technique that exploits the variable electromagnetic properties (i.e. dielectric permittivity) of the wood in living trees (Butnor *et al*., 2009). A decayed wood has a characteristic dielectric permittivity which differs from that of sound wood owing to the difference in their moisture content and density (Nicolotti *et al*., 2003). Miller and Doolittle (1990) reported that GPR accurately located knots and incipient brown rot in four different angiosperm tree species. A good correlation was observed between high dielectric values and the decayed inner core of two *Platanus hybrida* Brot (Nicolotti *et al*., 2003).

Butnor *et al*. (2009) claimed that the GPR method was effective in estimating the volume of hollows in three conifer species. It was also discovered that exterior wood decay, hollows and dry trunks had exceptional electromagnetic properties different from other defects.

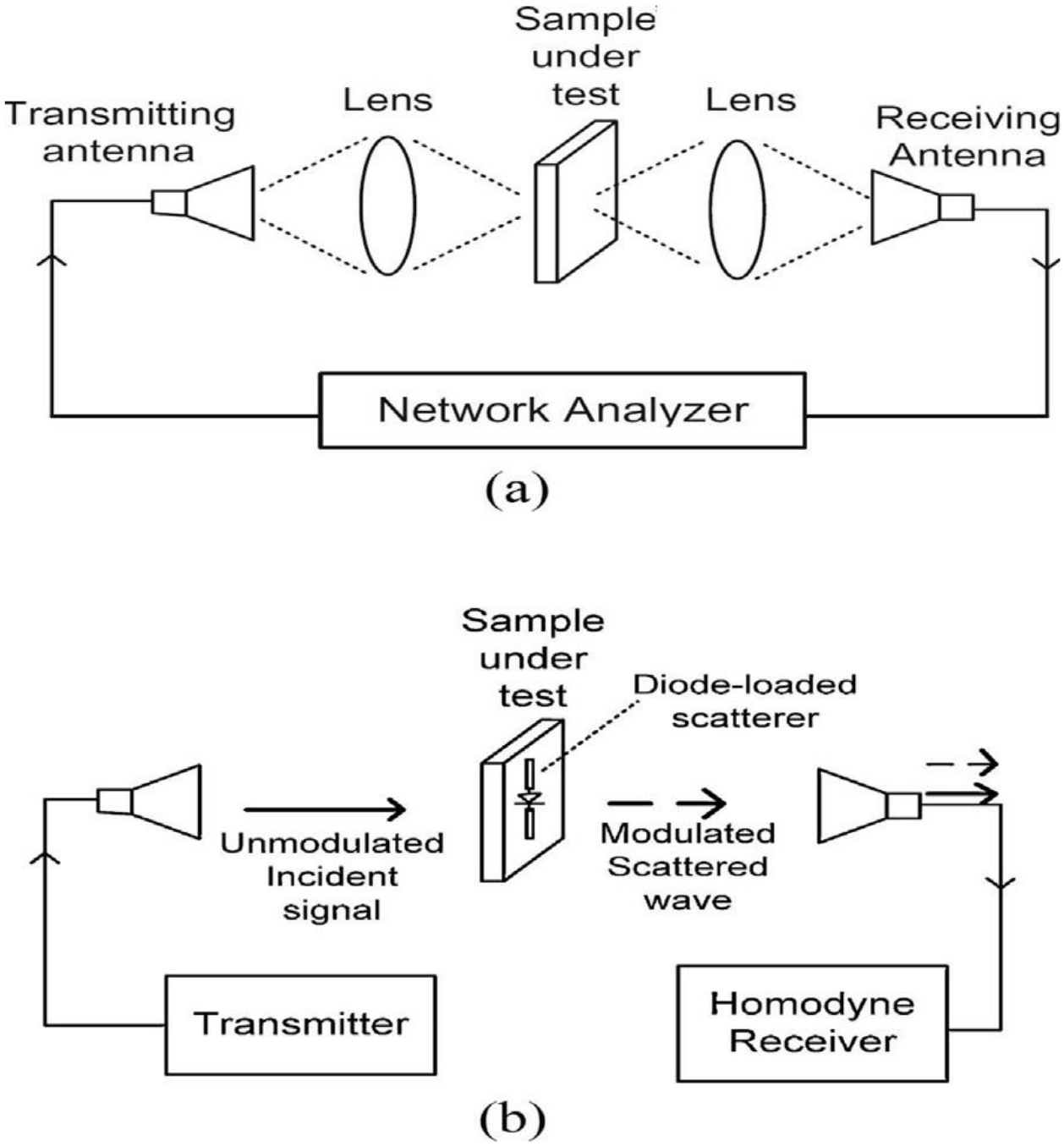

Fig. 2.5. Two measurement configurations in microwave technique (a) Focussed beam, and (b) Modulated scattering technique (Kaestner and Baath, 2005)

2.1.8 Electrical Resistivity Methods

Electrical resistivity methods were initially designed and are commonly used for the ground survey (Reynolds, 2011; Herman, 2001). However, their viability in detecting wood decay in standing trees has been reported by many researchers (Tattar and Shigo, 1972; Shortle and Smith, 1987; Smith and Shortle, 1988; Ostrofsky and Shortle, 1989; Shortle, 1990; Manyazawale and Ostrofsky, 1992; Butin, 1995; Larsson *et al*., 2004; Martin, 2009). The critical factor determining the electrical resistance of a tree is the concentration of mobile cations, which is usually very different between sound and degraded wood (Johnstone *et al*., 2010). It has been observed that in the region adjacent to wood decay, the concentration of cations in the wood would increase and therefore, electrical resistance would decrease (Shigo, 1991). A noticeable number of ions was produced by decay fungi during the wood degradation process of two plane trees *(Platanus hybrida* Brot.*)* investigated by Nicolotti *et al*. (2003). Hydrogen (H) and Potassium (K) ions are produced by brown rot and white rot, respectively, and which ultimately decrease the electrical resistivity of a decaying tree (Tattar and Shigo,1972; Tattar and Saufley, 1973; Shortle and Smith, 1987). A decrease in electrical resistance for bacterial wet wood was also reported by Nicolotti and Miglietta (1998). Moreover, Martin and Gunther (2013) attributed the low resistivity of the fungi-infected wood to the high moisture content and the varying ion concentration caused by the fungi invasion. It has also been reported that fungi play an important role in the translocation of ions from the soil to wood (Kirker *et al*., 2017; Gao *et al*., 2019). Fungi contributed to the active transport of some ions such as iron (Fe), manganese (Mn), and calcium (Ca) from the soil in an inoculated flask into wood, and an increased concentration of metals is often associated with an increased decay-related mass loss (Kirker *et al*., 2017; Gao *et al*., 2019). Additionally, the wood resistivity depends on the wood porosity and texture, which are susceptible to change by the fungi decaying activities (Skaar, 1988).

Gao *et al*. (2019) investigated the relationship between wood decay and electrical resistance by systematically examining the changes in the electrical resistance, wood mass loss, moisture content, and ion concentrations in larch and poplar wood progressively decayed by brown-rot fungi. The results showed that the decreasing electrical resistance of decaying wood is related to both the mass loss and the changes in the cation concentrations – Fe, Mn, K, Ca, and Mg (magnesium). Additionally, the degradation of wood was more severe as the exposure time to fungi attack increased,

and there was an equivalent increase in the mass loss. It was also reported that the electrical resistance of decaying wood significantly decreased as the exposure time increased. The decrease in the electrical resistance during the decay of wood was accompanied by a rapid increase in the cation concentrations. Also, the moisture content of fungus-treated wood significantly increased to various degrees for decayed wood. However, the effect of the change in the moisture content on the electrical resistance was insignificant compared with that of the cation concentrations.

The electrical resistivity of tree trunks can be determined using a shigometer which is a device that applies a pulsed electric current to the wood tissue and measures the electrical resistance of the wood tissue (Larsson *et al*., 2004; Tattar and Shigo, 1972). The shigometer electrodes are usually inserted into a narrow hole drilled toward the stem centre to measure the resistivity variation along the length of the hole. This technique can detect internal decay of living trees using the resistivity measurements, and it is nearly non-destructive, that means, the end-use capabilities of the trees under investigation are not altered (Pellerin and Ross, 2002). Compared to other methods, this technique offers a better quantitative measure of wood tissue decay status and capable of detecting decay at the early stages (Shortle, 1990). The extent of injury to the trunk is relatively reduced with the use of a narrow hole (Larsson *et al*., 2004).

The Relative Impedance in Situ Examination (RISE) method for detecting decay in living trees was reported by Bengtsson (1997). RISE is a four-point electrical resistivity method which exploits the effective resistivity and voltage difference between two points along a trunk to locate defects in living trees. The effective resistivity of a single tree was compared to that of other trees measured under similar conditions (temperature, humidity, site conditions and time of year) to detect wood decay.

Larsson *et al*. (2004) also implemented the four-point resistivity (RISE) method to detect the presence of wood decay in living trees. A low-frequency alternating current was passed to the tree stem with a pair of electrodes while measuring the voltage difference with another pair of electrodes to obtain four-point measurements, as illustrated in Fig. 2.6. A lower voltage difference was recorded for a decaying tree than a healthy tree because decay reduces tissue resistivity.

The electrical resistance of the wood tissue is normalised for stem cross-sectional area to obtain an absolute value of resistivity that corresponds to the amount of decay.

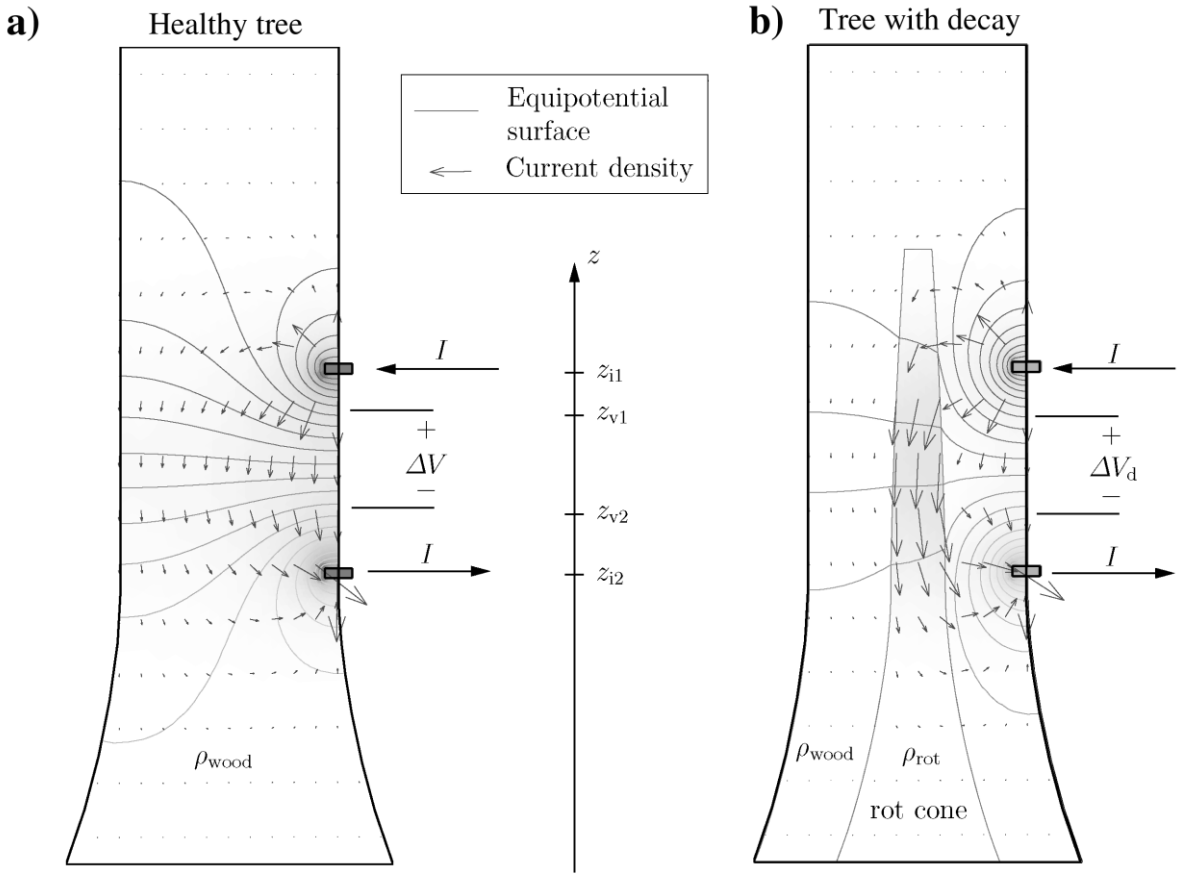

Fig. 2.6. Four-point resistivity method. (a) Healthy tree showing that the current is distributed over the whole stem cross-section. (b) Tree with decay showing that resistivity is relatively low in the cone-shaped decayed region and that the current is concentrated in the region of decay (Larsson *et al*., 2004)

Effective resistivity ρ (also known as *true resistivity*) is defined as the resistance of a stem section when a constant current is passed vertically through the stem, and the voltage is measured at two points on the stem surface:

$$\rho = \frac{\Delta V A}{I l} \tag{2.2}$$

where ΔV is voltage difference, I is current, l is the distance between the measuring points, and A is the stem cross-sectional area.

The resistivity of an individual tree could not be used to detect decay because the effective resistivity (or true resistivity) of wood depends on water content and temperature (Larsson *et al*., 2004). Therefore, the resistivity of an individual tree was compared with that of other trees measured under similar conditions, i.e., temperature, humidity, site conditions and time of year.

Relative resistivity (ρ_r) is defined as:

$$\rho_r = \frac{\rho}{\rho_h} \tag{2.3}$$

where ρ_h is the mean resistivity of healthy trees. Thus, relative resistivity normalised to approximately one for healthy trees.

Larsson *et al*. (2004) reported that the resistivities of Norway spruce trees with decay decreased by a factor of two compared to healthy trees. Also, the use of relative resistivities reduced the effect of temperature and seasonal changes on the tree resistivity. However, the RISE method does not provide information on the exact location and extent of stem decay. This shortcoming will be examined in this research to improve the method.

Goncz *et al*. (2017) demonstrated that electrical resistance method using four electrodes was highly reliable in detecting red heart in beech trees (*Fagus sylvatica*) of diameter 40 – 60 cm. Red heart – a visual defect in beech wood – was detected with a measured voltage drop of 1/3 to 1/5 of that measured on unaffected wood. However, the method was unable to determine the extent of red heart in beech trees reliably.

Martin (2009) successfully implemented Complex Resistivity (CR) technique to examine the location and extent of defects in wood and standing trees. CR, a conventional geophysical method, uses alternating current to measure the difference in

the voltage within a broad frequency range (1 mHz to 1000 Hz). The frequency spectra produced by the CR measurements can be interpreted using various models. Complementary information about the wood decay and the extent of decay or damage can be obtained from the amplitude and the phase of the complex resistivity (Martin, 2009). The complex resistivity tomogram of a fungi-infected oak tree is displayed in Fig. 2.7. A region of very high resistivity values and extremely low phases due to a hole in the centre of the oak tree (Fig. 2.7a) is displayed in Figs. 2.7b and 2.7c. The healthy sections exhibit moderate resistivities and high phases. However, the fungi-infected regions are characterised by both relatively lower resistivity values and phases compared to the healthy sections.

2.2 True Resistivity (or Effective Resistivity)

Electrical resistivity is a fundamental and diagnostic physical property that can be determined by a wide variety of techniques, including electromagnetic induction (Reynolds, 2011). The electrical resistivity of a material is defined as a measure of the ability of the material to oppose the flow of electric current. Consider an electrically uniform cube of side L through which a current I is flowing through, as illustrated in Fig. 2.8 (Reynolds, 2011). The material within the cube opposes the electric current, creating a potential difference V between opposite sides. The resistance R is proportional to the length L of the resistive material and inversely proportional to the cross-sectional area A as expressed in Eq. (1.1):

$$R \propto \frac{L}{A} \tag{2.4}$$

Thus,

$$R = \frac{\rho L}{A} \tag{2.5}$$

where the constant of proportionality ρ is the **true resistivity** and can be written as:

$$\rho = \frac{RA}{L} \tag{2.6}$$

Resistivity is measured in ohm-metre (Ωm). Rewriting Eq. (2.6) using the Ohm's law, i.e. $R = V/I$, we have:

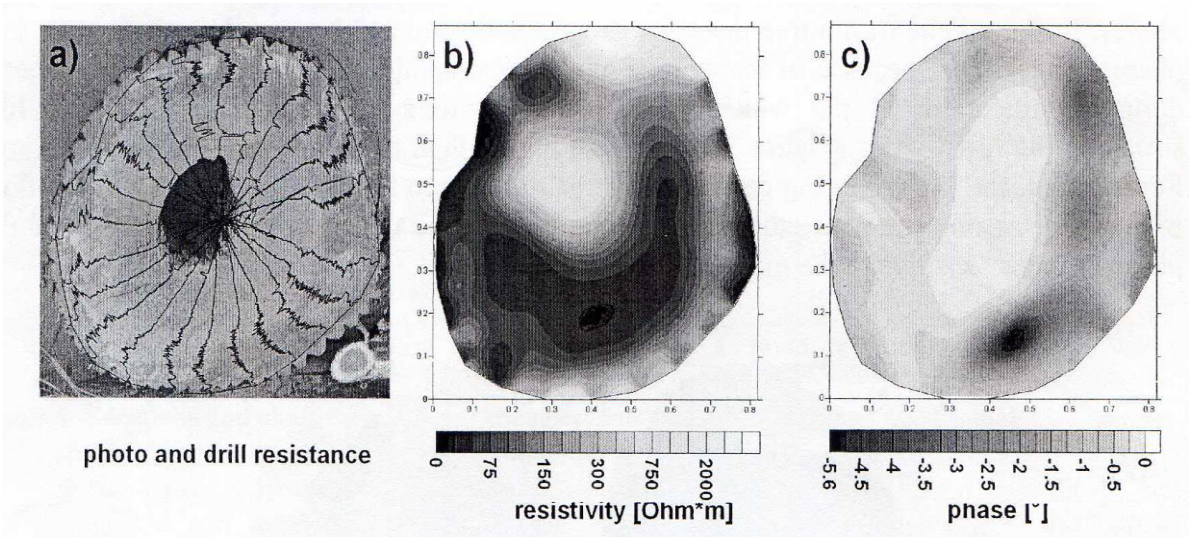

Fig. 2.7. (a) Photo with the drill resistance results, (b) tomograms of resistivity, and (c) phase, of a fungi-infected tree (Martin, 2009)

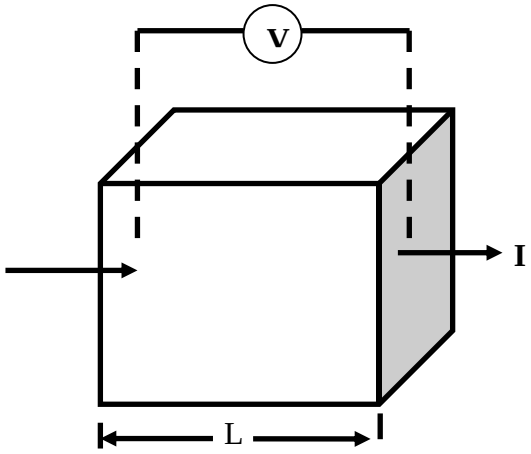

(a)

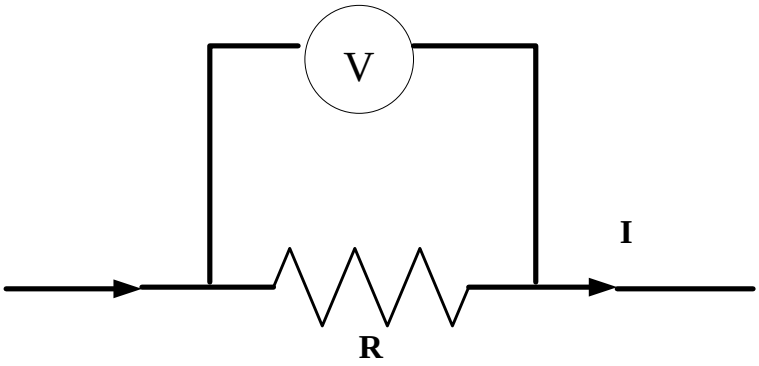

(b)

Fig. 2.8. (a) Electrical uniform cube (b) Electrical circuit equivalent (Reynolds, 2011)

$$\rho = \frac{VA}{IL} \tag{2.7}$$

Alternatively, the electrical resistivity can be expressed in terms of the electric field strength E (volts/m) and current density J (amps/m^2) as:

$$\rho = \frac{E}{J} \qquad (\Omega\text{m}) \tag{2.8}$$

The inverse of electrical resistivity is called the electrical conductivity σ which is measured in siemens/metre (S/m), an equivalent of $(\Omega\text{m})^{-1}$.

$$\sigma = \frac{1}{\rho} \tag{2.9}$$

2.3 Apparent Resistivity

The apparent resistivity ρ_a is the product of a measured resistance R_a and a geometric factor K for a given electrode array. The geometric factor accounts for the geometric spread of the electrodes and has the unit of length (metre). Hence, apparent resistivity is measured in ohm-metre (Ωm). The apparent resistivity of a homogeneous block of side length L with an applied current I and potential difference V between opposite faces of the block (Fig. 2.8) can be written as:

$$\rho_a = \left(\frac{V}{I}\right)\left(\frac{A}{L}\right) = R_a K \tag{2.10}$$

where $R_a = \frac{V}{I}$ is the apparent resistance, and $K = \frac{A}{L}$ is the geometric factor which provides information about the geometry of the block.

2.4 Electrode Configurations

The generalised form of electrode configuration in resistivity surveys comprises a current source, an ammeter for measuring the total current I flowing via the electrodes at points A and B into the material as described in Fig. 2.9. A voltmeter connected to the two electrodes at points M and N measures the potential difference V between the two points. The apparent resistance of the material, given by the ratio V/I, in conjunction with the geometric factor K of the electrode array, constructs the apparent resistivity ρ according to Eq. (2.10). Thus, the apparent resistivity depends on the geometry of the electrode array as expressed by the geometric factor K (Herman, 2001; Reynolds, 2011). The four main types of electrode configurations are Wenner, Schlumberger, dipole-dipole and square arrays, as shown in Fig. 2.10.

2.5 Vertical Electrical Sounding (VES)

The Vertical Electrical Sounding (VES) or depth sounding is the vertical variation of resistivity with depth (Reynolds, 2011). It is conducted by increasing the current electrode separation in order to increase the depth of current penetration. The midpoint of the electrode array is taken as the reference point for measurements. For a VES, the resistance ($\delta V/I$) measurements are taken at the shortest electrode separation and then at progressively larger spacings. For each electrode spacing, the apparent resistivity value ρ_a is estimated using the measured resistance and the appropriate geometric factor for the electrode configuration adopted (Reynolds, 2011). In the case of Wenner array, all four electrodes must be relocated to new positions as the inter-electrode spacings are increased (Fig. 2.11a). This constitutes a significant disadvantage for the deployment of Wenner array (Herman, 2001; Reynolds, 2011).

For the Schlumberger array, the potential electrodes (P_1, P_2) are placed at a fixed spacing (b) as illustrated in Fig. 2.11b. The current electrodes are placed at increasingly greater distances (a_1, a_2, a_3, a_4, a_5, a_6 …). The potential electrodes are spaced more widely apart (spacing b_2) when the voltage between P_1 and P_2 drops to very low values, due to the decreasing potential gradient caused by increasing current electrode spacings (Reynolds, 2011). The advantage of using the Schlumberger array for VES is that it requires both less space and physical movement of electrodes than the Wenner array (Reynolds, 2011).

The dipole-dipole array is seldom used for VES as large and powerful electrical generators are usually required to combat the problem of relatively low vertical resolution from its signal. Another major drawback of the dipole-dipole array is the lack of theoretical support for the analysis of the signal obtained with this array, especially when the four electrodes are not collinear (Reynolds, 2011; Telford, 1990). Nevertheless, vertical sounding can be carried out with this electrode arrangement by first choosing the dipole length, which is the distance between the two current electrodes, and between the potential electrodes. Then the distance between the two dipoles (C_1C_2 and P_1P_2) is increased progressively to produce the depth sounding, as depicted in Fig. 2.11c. Likewise, the square array is rarely used for large-scale soundings as its deployment is very cumbersome compared to other configurations (Fig. 2.11d). The essential advantage of the electrode configuration is the simplicity of the method when setting out small grids (Reynolds, 2011).

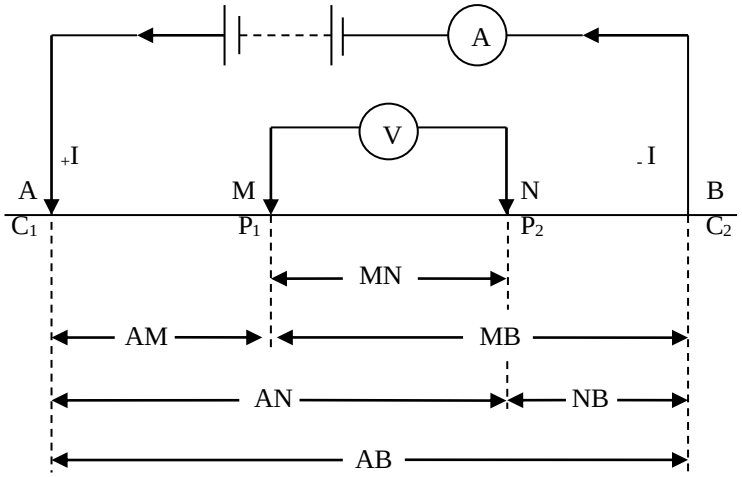

Fig. 2.9. Generalised form of electrode configuration in resistivity surveys. C_1 and C_2 are the current electrodes, while P_1 and P_2 are the potential electrodes. (Reynolds, 2011)

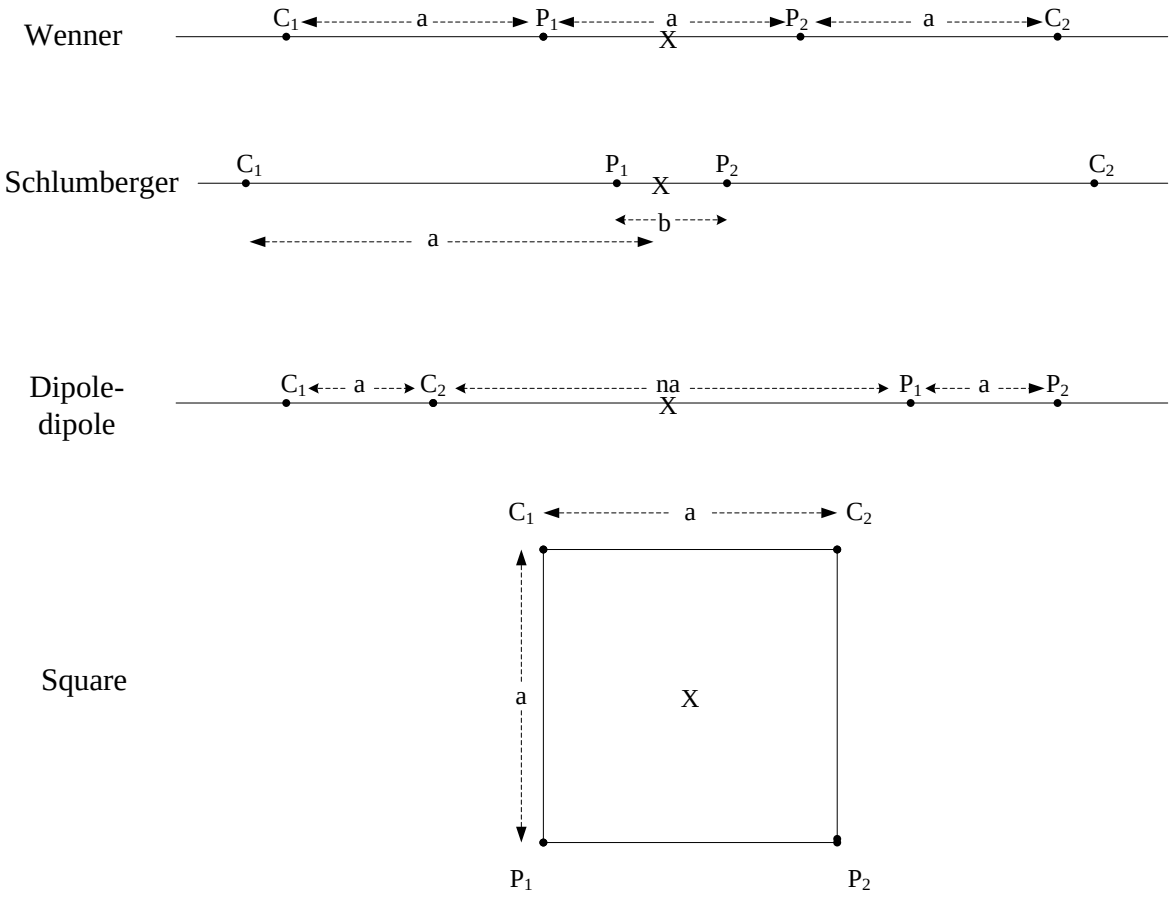

Fig. 2.10. The main types of electrode configurations (Reynolds, 2011)

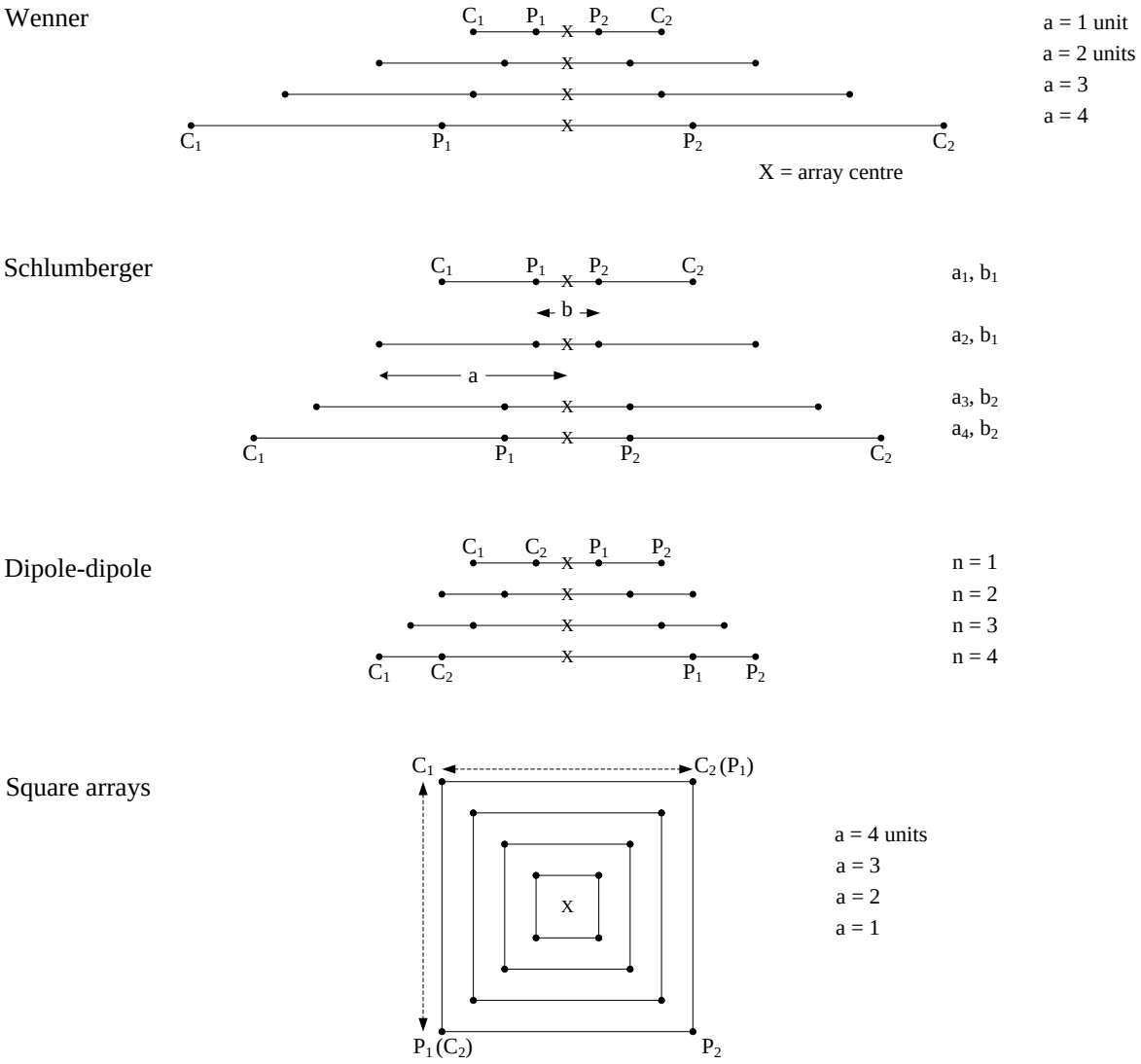

Fig. 2.11. Electrode configurations for vertical electrical sounding (Reynolds, 2011)

2.6 Mathematical Formulation of the Resistivity Theory

The Ohm's law in vector form can be written as:

$$J = \sigma E = -\frac{1}{\rho}E = -\frac{1}{\rho}\nabla V \tag{2.11}$$

Where,

J = current density vector (A/m^2),

E = electric field vector (V/m),

V = electric potential (Volt),

σ = conductivity (Ωm)$^{-1}$,

ρ = resistivity measured (Ωm),

Consider a subsurface of uniform composition of infinite extent with one source and one sink electrode for the current as described in Fig. 2.12. The total current I flows away from or toward each electrode across the surface of a half sphere (or hemisphere) with area $\frac{1}{2}(4\pi r^2)$. Ohm's law for one electrode can be expressed as:

$$J = \frac{I}{\frac{1}{2}(4\pi r^2)} = -\frac{1}{\rho}\frac{dV}{dr} \tag{2.12}$$

This is a first-order differential equation and its solution gives the potential $V(r)$ at a distance r from the electrode:

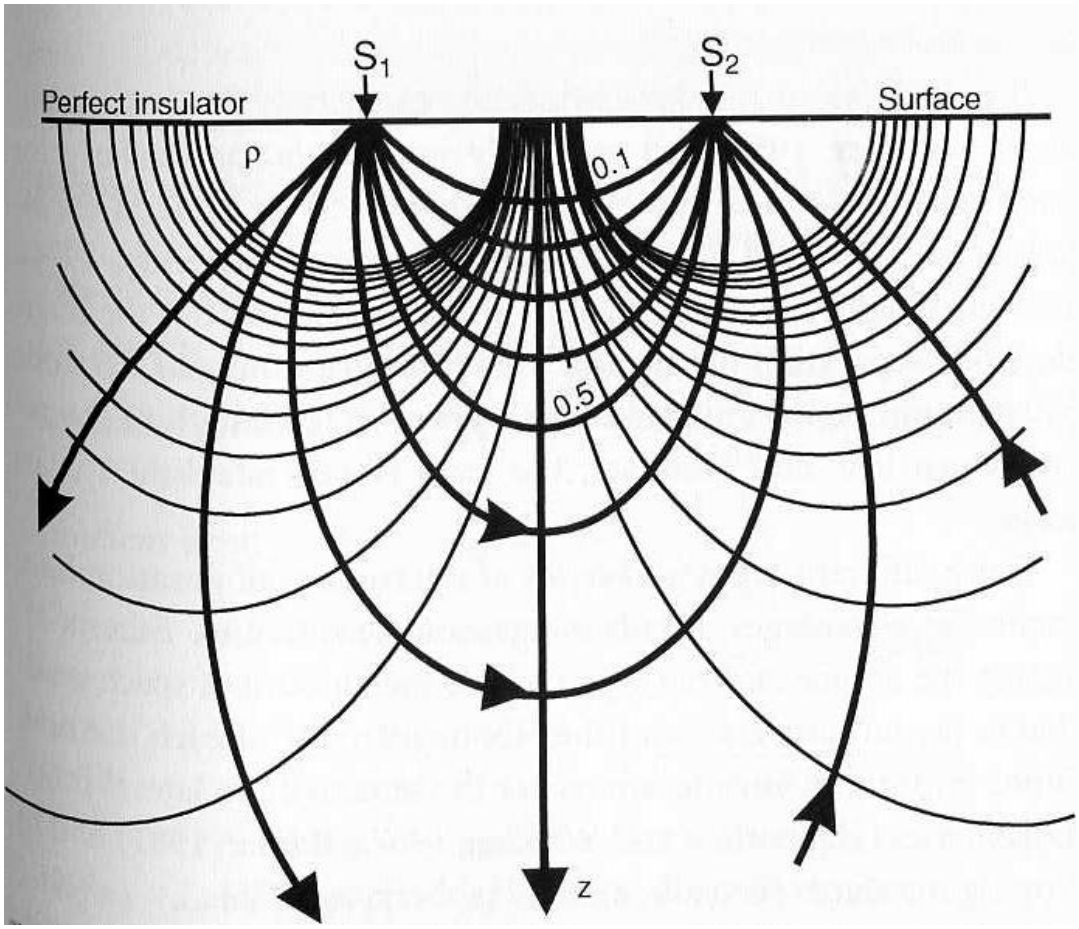

Fig. 2.12. Current and equipotential lines produced by a current source S_1 and sink S_2 (Reynolds, 2011)

$$\frac{dV}{dr} = -\rho \frac{I}{2\pi r^2} \quad , \tag{2.13}$$

$$V(r) = -\int \rho \frac{I}{2\pi r^2} dr = \frac{\rho I}{2\pi r} \quad . \tag{2.14}$$

The electric potentials measured at *M* and *N* in the general linear array of Fig. 2.9 are superpositions of the potential of Eq. (2.14) due to each of the two source electrodes located at *A* and *B*. With the separations of the electrodes given by *AM*, *MB*, *AN*, and *NB*, the potentials at *M* and *N* are given by:

$$V_M = \frac{\rho I}{2\pi}\left(\frac{1}{AM} - \frac{1}{MB}\right) \quad , \tag{2.15}$$

and

$$V_N = \frac{\rho I}{2\pi}\left(\frac{1}{AN} - \frac{1}{NB}\right) \quad . \tag{2.16}$$

The total potential difference between the electrodes M and N is thus:

$$V_{MN} = V_M - V_N = \frac{\rho I}{2\pi}\left[\left(\frac{1}{AM} - \frac{1}{MB}\right) - \left(\frac{1}{AN} - \frac{1}{NB}\right)\right]^{-1} \tag{2.17}$$

This may be rearranged to yield:

$$\rho = \frac{V_{MN}}{I} K \quad , \tag{2.18}$$

where,

$$K = 2\pi\left[\left(\frac{1}{AM} - \frac{1}{MB}\right) - \left(\frac{1}{AN} - \frac{1}{NB}\right)\right]^{-1} \tag{2.19}$$

is the **geometric factor** which has a particular value for a given electrode spacing.

The sub-surface ground is not homogeneous and hence, the resistivity obtained in Eq. (2.18) is the apparent resistivity as measured by the surface electrodes. The apparent resistivity value depends on the apparent resistance $\left(\frac{V_{MN}}{I}\right)$ and the geometric factor *K* that accounts for the electrode spacing (Reynolds, 2011; Herman, 2001).

CHAPTER THREE
METHODOLOGY

3.1 Resistivity Method with Modified Schlumberger Electrode Configuration

Resistivity method, initially designed for ground measurement, was adapted to detect the location and extent of tree decay and hollows. This is an improvement over the four-point resistivity (RISE) method by Larsson *et al*. (2004) which was unable to detect the location of tree decay. Soil resistivity meter Miller 400D (Appendix 3) designed for a shallow ground survey, was used to measure the electrical resistance of the tree stem. Tiny electrodes of thickness 0.382 cm (Appendix 4) were improvised for the trees because the conventional electrodes of thickness 1.40 cm may cause short-circuit due to the small electrode spacings used. The Schlumberger electrode configuration was used on the trees after scaling to centimetres (Appendices 5 and 6).

3.2 Field Measurements

Electrical resistivities of living trees were estimated using the four-point electrical resistivity method. Eighty living trees comprising forty candle trees (*Senna alata* L. Roxb.) and forty almond trees (*Terminalia catappa* L. Roxb.) of diameter between 40 and 120 cm respectively, were purposively selected from different locations within University of Ibadan campus. The selection of the almond and candle trees took place from 1 June to 30 September 2013 and 1 May to 31 July 2014, respectively. Vertical variation of resistivity with depth, otherwise known as Vertical Electrical Sounding (VES), was conducted on the living trees using the Schlumberger electrode configuration with a reduced scale in centimetres (Appendices 5 and 6). The Schlumberger array was chosen because it requires less space and movement of electrodes than the Wenner array (Reynolds, 2011).

Potential electrode spacings of 4 and 6 cm respectively were used while changing the current electrode positions by 2 cm to increase the current penetration depth. Generally, the current electrode separation AB is proportional to the current penetration depth (Herman, 2001). The electrode spacings (Appendices 5 and 6) used in this research require tiny electrodes to avoid short circuit that could occur if conventional electrodes

of typical thickness 1.40 cm designed for soil resistivity measurement were used. Therefore, locally fabricated tiny electrodes of thickness 0.382 cm (Appendix 4) suitable for the small electrode spacings were deployed for this research. Resistance measurements were taken at different points on the trees using Miller 400D digital resistance meter (Appendix 3) between 1 m and 2 m respectively above ground. For each resistance measurement, an estimation was made for the geometric factor K of the electrode configuration using Eq. (2.19). The apparent resistivity ρ_a was also calculated as

$$\rho_a = R_a K \tag{3.1}$$

where R_a is the measured electrical resistance of the living tree.

Freshly-cut almond and candle trees with decay and hollows were also obtained from different locations on the University of Ibadan campus between 1 June – 30 September 2013 and 1 May – 31 July 2014, respectively as shown in Fig. 3.1. These trees were cut down after showing visual evidence of internal decay such as (i) exposed wood showing decay due to mechanical damage or broken bark, (ii) indications of excessive mechanical stress, e.g. trunk swellings, cracks, sunken areas etc., (iii) presence of deadwood or dieback in crown, and (iv) presence of dead cambium under the bark. They are also of different stem diameters ranging from 20.5 to 58.5 cm, respectively. Several logs of wood of different lengths were obtained from the trees for resistivity measurement.

Some of the logs of wood comprised two sections – hollowed and decayed segments, while others comprised only healthy segments or hollowed segments. The electrical resistivity of the logs of wood was measured immediately the trees were cut down using the same approach for living trees.

3.3 Laboratory Measurements

A laboratory experiment was conducted to replicate the resistivity profiles of healthy trees, and the resistivity anomalies due to wood decay and hollow in living trees. Three wooden hollow cylinders of height 60 cm and diameters 20, 35 and 50 cm were fabricated and filled with compacted sawdust to mimic stems of living trees (Fig. 3.2a). The soft, outer layers of the tree (cambium) were modelled using compacted wet sawdust while the hard, interior layers of the tree (xylem) were reproduced using compacted dry sawdust. VES was conducted on the laboratory prototype using a similar approach adopted for the trees (Fig. 3.2b), and as described in **Section 3.2**.

Fig. 3.1. Freshly-cut decayed trees and trees with hollows

(a)

(b)

Fig. 3.2. (a) Laboratory prototype filled with sawdust, and (b) laboratory experimental set-up.

The resistivity plot of the laboratory prototype was compared to that of the healthy trees for similarity in profile by determining the correlation between the two resistivity plots. Once a similarity in the profile is established, the resistivity profile of the laboratory prototype serves as a replica for the healthy tree. Besides, one-way analysis of variance (ANOVA) was carried out using IBM SPSS Statistics 23 to investigate if there are statistical differences between the mean resistivities of the healthy trees and the laboratory prototype.

Moreover, the extent of wood decay or hollow was modelled in the laboratory prototype that serves as a replica for the healthy tree. This was done using good electrical conductors, e.g. copper wire lumps (Fig. 3.3a), since wood decay process is characterised by an increase in electrical conductivity owing to the accumulation of mobile cations in the decayed region (Shigo and Shortle, 1986; Shortle and Smith, 1987; Nicolotti *et al*., 2003). A copper wire lump of 5-cm thickness and 20-cm length was inserted into the laboratory prototype at depths of 5, 10, 15 and 20 cm from the centre of the wire lump to the laboratory prototype surface.

Similarly, electrical insulators, e.g. plastic cylinders, replicated hollows in the laboratory prototypes (Fig. 3.3b), since hollows or cavities are non-conductor of electric current (Larsson *et al*., 2004); thus, the hollowed region in a tree would have a relatively high resistivity (Shigo and Shortle, 1986; Shortle and Smith, 1987). The hollows in the laboratory prototype are of diameter 14 cm and length 20 cm and were sited at depths 4, 12 and 20 cm from the centres of the modelled hollows to the laboratory prototype surface.

VES was conducted (as described in **Section 3.2)** to identify the presence and location of the resistivity anomalies created by the decay and hollows modelled into the laboratory prototypes. The impact of the anomalies on the resistivity profiles of the laboratory prototype was determined by comparing the resistivity plots before and after introducing the anomalies. The resistivity profiles of the laboratory prototype with anomalies serve as the replica for decayed and hollowed living trees. Consequently, the electrical resistivity profiles of the laboratory prototype were deployed for the detection of wood decay and hollows in living trees by matching resistivity curves.

(a)

(b)

Fig. 3.3. A laboratory prototype with (a) a copper wire lump inserted to replicate wood decay (b) a hollow modelled by a plastic cylinder

A laboratory experiment was also conducted to determine the effects of tree decay and hollow size on the resistivity profile. Tree decay of various sizes were modelled into the laboratory prototype replicating a healthy almond tree, using copper wire lumps of different thicknesses 5, 8 and 12 cm inserted at depths of 5, 6.5 and 8.5 cm from the centre of the wire lumps to the laboratory prototype surface, respectively. Hollows of different diameters 8, 10 and 14 cm were also modelled into the laboratory prototype at 4 cm, 5 cm and 7 cm depths from the centre of the hollows to the laboratory surface, respectively. VES was carried out (as described in **Section 3.2**) to identify the presence and location of the resistivity anomalies due to the wood decay and hollows replicated in the laboratory prototypes.

3.4 2-D Images of Tree Cross-Sections

2-D images representing the cross-sections of decayed and hollowed trees were developed using the resistivity plots derived from the laboratory measurements. The cross-section of a healthy tree was modelled with two concentric circles representing the cambium and xylem of the tree. The diameters of the concentric circles correspond to the diameters of the tree or cambium and xylem. In the case of a decayed tree or a tree with hollow, minimum of three concentric circles were used for modelling the tree. The third circle, representing decay or hollow, has a diameter equivalent to the diameter of the decay or hollow. Circles of different diameters were used to capture multiple decay or hollows in a tree trunk.

The resistivity plots from the laboratory experiments provide the following information for modelling the 2-D images of tree cross-sections:

I. The location of the anomaly (evidence of decay or hollow) in terms of the current electrode separation (i.e. AB/2).
II. The extent of the decay or hollow in terms of the range of AB/2 values corresponding to the region covered by the anomaly in the resistivity plot.
III. The diameter of the xylem is determined by considering the portion of the resistivity plot with a series of high resistivity values.

3.4.1 The Equation of a Circle

The equation of a circle was used to model the cross-section of the tree, which is assumed to be circular. Mathematically, a circle of radius *r* with its centre at coordinate (*a*, *b*) can be expressed as:

$$(x-a)^2 + (y-b)^2 = r^2 \tag{3.2}$$

If the centre of the circle is at the origin, i.e. $a = b = 0$, Eq. (3.2) reduces to

$$x^2 - y^2 = r^2 \tag{3.3}$$

The radius *r* of the circle corresponds to the radius of the tree. Similarly, for a circle representing a wood decay or hollow, the radius *r* of the circle corresponds to the radius of the decay or hollow.

In the modelling of the 2-D images, the cross-section of a tree can be generated by choosing the values of *x* such that, $-r \leq x \leq r$, where *r* is the radius of the tree. Also, the values of *y* for the 2-D images as derived from Eq. (3.2) is given by

$$y = b \pm \sqrt{r^2 - (x-a)^2} \tag{3.4}$$

Similarly, for a circle with its centre at the origin, we have

$$y = \pm\sqrt{r^2 - x^2} \tag{3.5}$$

since $a = b = 0$

The *y* values were computed based on Eq. (3.5) using Microsoft Excel 2007. Different concentric circles (representing the cross-sections of healthy trees, decayed trees and trees with hollow) were modelled in MATLAB R2016a by plotting the *y* values obtained from Eq. (3.5) against *x* values with the range, $-r \leq x \leq r$, where *r* is the radius of the tree. The concentric circles, as illustrated in Figs. 4.42 – 4.58, constitute the modelled 2-D images of the cross-sections of living trees.

CHAPTER FOUR
RESULTS AND DISCUSSION

4.1 Field Results: Candle Trees

4.1.1 Resistivities of Healthy Candle Trees

The results of the electrical resistivity measurements of four healthy candle trees (*Senna alata* L.) of similar diameter situated at the same location are presented in Table 4.1. The resistivity values of the laboratory prototype are included for comparison. Figures 4.1 and 4.2 compare the resistivity profiles of the candle trees to that of the laboratory prototype of diameter 50 cm. A significant trend was observed in the resistivities of the healthy candle trees presented in Table 4.1 – a series of low resistivities followed by a series of high resistivities. The low resistivities represent the cambium (soft, external layer) of the tree while the high resistivities correspond to the xylem (hard, inner layer) of the tree. Candle trees 1 and 2 were 54.5 cm in diameter while candle trees 3 and 4 were of diameter 50.4 cm. Figures 4.1 and 4.2 show that the resistivity profiles of the candle trees match that of the laboratory prototype. There was a high correlation between the resistivities of the laboratory prototype and those of the candle trees ($r^2 = 0.983,\ 0.941,\ 0.902$ and 0.996 for candle trees 1, 2, 3 and 4, respectively) as illustrated in Figs. 4.3 – 4.6. The mean value of the four correlation coefficients $r^2{}_{mean}$ is 0.956. Similarly, a high correlation was recorded between the mean values of candle tree resistivity and laboratory prototype resistivity ($r^2 = 0.983$), as displayed in Fig. 4.7. Therefore, the laboratory prototype truly replicated healthy candle trees of similar diameter.

4.1.2 Statistical Analysis Results: Analysis of variance in the resistivities of the healthy candle trees and their replica

The results of the one-way analysis of variance (ANOVA) conducted using IBM SPSS Statistics 23 to test if there are statistical differences among the mean resistivities of the healthy candle trees and the laboratory prototype confirmed that the laboratory prototype is a replica of the healthy candle trees of similar diameter. The significant value obtained, p = 0.634 is not statistically significant since it is higher than 0.05, (the

cut-off for statistical significance) meaning that there are no statistical differences between the mean resistivities of the healthy candle trees and the laboratory prototype.

4.1.3 Resistivities of a Decayed Candle Tree with Hollow

The results of the resistivity measurement of a freshly-cut decayed candle tree with hollow and of stem diameter 40.5 cm are presented in Tables 4.2 and 4.3. The log of wood comprises two sections – hollowed and decayed segments, as shown in Fig. 4.8. Additionally, the resistivity measurement of the two segments of the tree was carried out separately. Table 4.2 shows the resistivity values of the decayed cambium in comparison to that of the healthy cambium of the same stem diameter, while Table 4.3 presents the resistivity values of the hollowed xylem as compared to that of the healthy xylem. From the results in Table 4.2, the resistivity values of the decayed section of the tree varied between 12 and 15 Ωm. Thus, the resistivity values of the decayed tree were relatively lower than those of the healthy tree which ranged between 51 and 77 Ωm. Also, the resistivity values of the hollowed segment were comparatively higher than those of the healthy tree and varied between 5,622 and 10,573 Ωm, as displayed in Table 4.3.

4.1.4 Resistivities of a Candle Tree with Hollow

Moreover, the results of the resistivity measurement of a freshly cut hollowed candle tree of stem diameter 41.5 cm are presented in Table 4.4. The hollow laterally filled the whole length of the wood, as shown in Fig. 4.9. Table 4.4 shows that the resistivities of the candle tree with hollow were markedly higher than those of the healthy tree of stem diameter 40.5 cm. This trend was also observed in the resistivity plots presented in Figs. 4.10 and 4.11 – showing the resistivity plot of the candle tree with hollow noticeably above that of the healthy tree. The resistivities of the candle tree with hollow as presented in Table 4.4 serve as a benchmark for a candle tree with hollow of similar dimension – hollow diameter 17 cm, hollow length 65 cm, and stem diameter 41.5 cm.

4.1.5 Resistivities of Selected Candle Trees

The resistivity values of all the 40 purposively selected candle trees are presented in Tables 4.5 – 10. Thirty-two out of the 40 trees were healthy (i.e. without wood decay and hollow) as at the time of measurement, three had wood decay, three were with hollows or cavities, and two had both wood decay and hollow. The health status of the selected trees was determined by comparing or matching their resistivity profiles with

those of healthy, decayed and hollowed trees of similar diameters. The results are summarised below:

I. Table 4.5 shows that one candle tree (Tree 5) out of the eight candle trees sampled from the Department of Archaeology and Anthropology, University of Ibadan, had wood decay in the xylem. The remaining seven candle trees (Trees 1 – 4, 6 – 8) were healthy trees.

II. According to Table 4.6, four candle trees (Trees 11 – 14) out of the six candle trees sampled from the Department of Physics were healthy trees. The other two candle trees consist of a decayed tree (Tree 10) and a hollowed tree (Tree 9). The wood decay in Tree 10 was sited in the xylem while the hollow in Tree 9 was located in the cambium, possibly due to deformation in the tree growth.

III. Table 4.7 shows that one of the four candle trees (Tree 18) sampled from the Department of Chemistry had both wood decay and hollow in the xylem and cambium, respectively. The remaining three candle trees (Trees 15 – 17) were healthy trees.

IV. Four candle trees (Trees 19, 20, 23, 24) out of the six candle trees sampled from the Department of Microbiology were healthy trees, as presented in Table 4.8. The other two candle trees comprised a decayed tree (Tree 22) and a hollowed tree (Tree 21). The wood decay in Tree 22 was sited in the xylem while the hollow in Tree 21 was located in the cambium possibly due to deformation in the tree growth.

V. Table 4.9 shows that one of the eight candle trees (Tree 28) sampled from the Faculty of Social Sciences had a cavity or hollow. The cavity, which extended from the xylem to the cambium, was possibly formed at the advanced stage of the decay process by the drying and crumpling of the decayed wood. The remaining seven candle trees (Trees 25 – 27, 29 – 32) were healthy trees.

VI. According to Table 4.10, one of the eight candle trees (Tree 33) sampled from the Department of Botany had wood decay and hollow in the xylem and cambium, respectively. The other seven candle trees (Trees 34 – 40) were healthy trees.

4.2 Field Results: Almond Trees

4.2.1 Resistivities of Healthy Almond Trees

The results of the resistivity measurements of four healthy almond trees (*Terminalia catappa* L. Roxb.) of similar diameter situated at the two different locations are shown in Table 4.11. The resistivities of the laboratory prototype are also included for comparison. Figures 4.12 and 4.13 compares the resistivity profiles of the almond trees to that of the laboratory prototype of diameter 50 cm. The resistivities of the healthy almond trees presented in Table 4 have a similar trend compared with those of healthy candle trees – a sharp rise in resistivity at the boundary between the cambium and xylem. The diameter of trees 1 and 2 is 52.50 cm while that of trees 3 and 4 is 50.89 cm. Figures 4.12 and 4.13 show that the resistivity profiles of the almond trees and that of the laboratory prototype are the same. There was a high correlation between the resistivities of the laboratory prototype and those of the almond trees ($r^2 = 0.9979, 0.9948, 0.9996$ and 0.9999 for almond trees 1, 2, 3 and 4 respectively) as displayed in Figs. 4.14 – 4.17. The mean value of the four correlation coefficients $r^2{}_{mean}$ is 0.998. Similarly, a high correlation was recorded between the mean values of almond tree resistivity and laboratory prototype resistivity ($r^2 = 0.9998$), as illustrated in Fig. 4.18. Hence, the laboratory prototype truly modelled healthy almond trees of similar diameter.

4.2.2 Statistical Analysis Results: Analysis of variance in the resistivity values of the healthy almond trees and their replica

The results of the one-way analysis of variance (ANOVA) conducted using IBM SPSS Statistics 23 to test if there are statistical differences between the mean resistivities of the healthy almond trees and the laboratory prototype established that the laboratory prototype is a replica of the healthy almond trees of similar diameter. The significant value obtained, p = 0.999 is not statistically significant since it is larger than 0.05, (the cut-off for statistical significance) meaning that there are no statistical differences among the mean resistivities of the healthy almond trees and the laboratory prototype.

4.2.3 Resistivities of a Decayed Almond Tree with Hollow

The results of the resistivity measurement of a freshly-cut decayed almond tree with hollow and of stem diameter 45 cm are presented in Tables 4.12. The log of wood comprises two sections – hollowed and decayed segments, as shown in Fig. 4.19. The

resistivity values of a healthy tree of the same stem diameter are included for comparison. Table 4.12 shows that the almond tree had wood decay in its cambium indicated by the relatively lower resistivities than the healthy almond tree. The resistivity values of the decayed cambium ranged from 12 to 17 Ωm, and those of the healthy cambium varied between 134 and 232 Ωm. Table 4.12 also indicates that there was a hollow in the xylem represented by the relatively higher resistivities than the healthy almond trees. The resistivities of the hollowed xylem ranged from 10,243 to 14,538 Ωm, and those of the healthy xylem varied between 3,621 and 4,071 Ωm.

4.2.4 Resistivities of Selected Almond Trees

The resistivity values of all the 40 purposively selected almond trees are presented in Tables 4.13 – 4.18. Thirty-three out of the 40 trees were healthy (i.e. without wood decay and hollow) as at the time of measurement, three had wood decay, three were with hollows or cavities, and one had both wood decay and hollow. The health status of the selected trees was determined by comparing or matching their resistivity profiles with those of healthy, decayed and hollowed trees of similar diameters. The results are summarised below:

I. Table 4.13 shows that one almond tree (Tree 6) out of the eight almond trees sampled from the Department of Microbiology, University of Ibadan, had decayed in the xylem. The remaining seven almond trees (Trees 1 – 5, 7 and 8) were healthy tees.

II. According to Table 4.14, all the eight almond trees (Trees 9 – 16) sampled from the Department of Mathematics were healthy trees.

III. Table 4.15 shows that the eight almond trees sampled from the Department of Zoology comprised one decayed tree (Tree 23), two hollowed trees (Trees 18 and 19), and five healthy trees (Trees 17, 20 – 22, 24).

IV. One of the six almond trees (Tree 25) sampled from the Faculty of Social Sciences had wood decay sited in the xylem while the remaining five trees (Trees 26 – 30) were healthy trees as depicted in Table 4.16.

V. Tables 4.17 and 4.18 show that the ten almond trees sampled from the Department of Botany comprised a hollowed tree (Tree 34), a decayed tree with hollow or cavity (Tree 40), and eight healthy trees (Trees 31 – 33, 35 – 39).

4.3 Laboratory Results

4.3.1 Resistivities of the Laboratory Prototype with Modelled Tree Decay

The resistivities of the laboratory prototype with copper wire lumps inserted at various depths to model tree decay, and thereby creating an anomaly in the resistivity profile of the prototype, are presented in Tables 4.19 – 4.22. For comparison, the resistivities of the laboratory prototype modelling a healthy tree (i.e. without anomaly) are included. The diameter of the laboratory prototype is 50 cm. The depths of placement of the copper wire lumps in the laboratory prototype were 5, 10, 15 and 20 cm, with the centre of the wire lump as the reference point. A copper wire lump of thickness 5 cm and length 20 cm was used. Resistivity plots of the laboratory prototype with anomaly (i.e. modelled tree decay) and without anomaly are shown in Figs. 4.20 – 4.27.

The copper wire lump implanted in the laboratory prototype to model tree decay was detected by a rapid decrease in the resistivities, as illustrated in Figs. 4.20 – 4.27. Also, the corresponding current electrode half separations, AB/2, constitute detection points of the anomaly (or modelled tree decay). Hence, depths of placement of the modelled tree decay can be matched with the detection points AB/2. This would be useful in determining the location of tree decay with similar resistivity anomalies given the detection points of the anomalies.

4.3.2 Resistivities of the Laboratory Prototype with Modelled Hollows

The resistivities of the laboratory prototype with hollows or cavities modelled into the prototype using electrical insulators are presented in Tables 4.23 – 4.25. For comparison, the resistivities of the laboratory prototype representing a healthy tree (i.e. without anomaly) are also included. The diameter of the laboratory prototype is 50 cm. The hollows in the laboratory prototype are of diameter 14 cm and length 20 cm and were sited at depths 4, 12 and 20 cm, with the centres of the hollows as the reference points. Resistivity plots of the laboratory prototype with anomaly (i.e. modelled hollow) and without anomaly are displayed in Figs. 4.28 – 4.33.

The hollow replicated in the laboratory prototype at different depths caused the relatively high resistivities observed at the detection points of the anomaly as contained in Tables 4.23 – 4.25 and graphically in Figs. 4.28 – 4.33. Similarly, matching can be carried out between the depths of placement of the hollows and the detection points AB/2. This would be useful in determining the location of hollows in trees with similar resistivity anomalies given the detection points of the anomalies.

4.3.3 Multiple Anomalies

The resistivities of a laboratory prototype with a copper wire lump implanted to replicate tree decay and a hollow modelled into the prototype using a plastic cylinder are shown in Tables 4.26 and 4.27. The resistivities of the laboratory prototype, which represents a healthy tree, are also included for comparison. Figs. 4.34 – 4.37 show resistivity plots of the laboratory prototype with multiple anomalies (modelled tree decay and hollows) and without anomaly.

Moreover, the outcome of the experiments on the detection of multiple resistivity anomalies further confirmed that relatively low resistivities indicate the presence of a conducting medium in the laboratory prototype while relatively high resistivities signify the presence of hollow as shown in Tables 4.26 and 4.27 and Figs. 4.34 – 4.37. This result also implies that tree decay and hollows can be detected simultaneously, with characteristic low resistivities for the tree decay and typical high resistivities for the hollows.

4.3.4 Resistivity Anomalies: Effects of Decay and Hollow Size on the Resistivity Profiles

The results of the experiments conducted on the effects of the size of decay and hollow on the resistivity profiles are presented in Tables 4.28 and 4.29 and Figs. 4.38 – 4.41. The results showed that the extent of decrease or increase in resistivities depends on the thickness of the copper wire lump or the diameter of the hollow, respectively. The most substantial decrease in resistivity values of an average factor 6.4 was observed for 12-cm thick copper wire lump placed at 8.5-cm depth, with the centre of the wire as the reference point; followed by 8-cm thick copper wire lump, placed at 6.5-cm depth, with an average factor of 5.1; and the lowest decrease was observed for 5-cm thick copper wire lump, placed at 5-cm depth, with an average factor of 3.8. Likewise for the hollow, the largest increase in resistivity values of an average factor 5.6 was observed for 14-cm hollow diameter placed at 7-cm depth, with the centre of the hollow as the reference point; followed by 10-cm hollow diameter with an average factor of 4.0, placed at 5-cm depth; and the lowest increase was observed for 8-cm hollow diameter with an average factor of 3.1, placed at 4-cm depth. The experimental results also showed that as the conducting medium and hollow increase in size, the detection points of the anomalies also widen.

4.4 Two-Dimensional Images of Tree Cross-sections

The 2-D images of tree cross-sections developed using the resistivity plots obtained from the laboratory experiments are presented in Figs. 4.42 – 4.58. The 2-D images display different cross-sections of living trees under five broad cases:

Case 1: Healthy Tree

This is a living tree without wood decay or hollow. The xylem and cambium of the tree are represented with two concentric circles of different colours – blue for the cambium and green for the xylem, as illustrated in Fig. 4.42. The radius of the tree or cambium is 25 cm, while the xylem is of radius 17 cm. This 2-D image was developed from the resistivity plot of the laboratory prototype, which replicated a healthy candle tree in Figs. 4.1 and 4.2.

Case 2: Decayed Trees

The cross-sections of five decayed trees are presented in Figs. 4.43 – 4.47 with wood decay of diameter 5 cm sited at different depths across the cambium and xylem. The wood decay was located at depths 5 cm, 10 cm, 15 cm, 20 cm and 25 cm, from the centre of the decay to the stem surface. The 2-D images show the progression of the decay from the cambium to the xylem as the depth increases. Besides, the images under this case are pictorial representations of the resistivity plots of the laboratory prototype with modelled decay presented in Figs. 4.20 – 4.27. The 2-D images illustrate the cross-sections of the decayed trees with three concentric circles of different colours – red, blue and green denoting wood decay, cambium and xylem respectively.

Case 3: Hollowed Tress

The cross-sections of three living trees with hollows of equal diameter 8 cm situated at different depths across the cambium and xylem are displayed in Figs. 4.48 – 4.50. The hollows were sited at depths 4, 12 and 20 cm from the centre of the hollow to the stem surface. The 2-D images clearly show the hollow progression with depth from the cambium to the xylem. The cross-sections of the hollowed trees are represented with three concentric circles of different colours – black, blue and green indicating hollow, cambium and xylem respectively. Also, the 2-D image evolved from the resistivity plots of the laboratory prototype with hollows, as illustrated in Figs. 4.28 – 4.33.

Case 4: Trees with both wood decay and hollows

The 2-D images showing the cross-sections of two living trees with both wood decay and hollows are presented in Figs. 4.51 and 4.52. One of the trees has wood decay of diameter 5 cm located in the cambium at 5-cm depth from the centre of the decay to the stem surface, and a hollow of diameter 14 cm located in the xylem at 14.5-cm depth from the centre of the hollow to the stem surface (Fig. 4.51). The second tree has a hollow of diameter 14 cm, located in both cambium and xylem at 8-cm depth from the centre of the hollow to the stem surface; and a decay of diameter 5 cm located in the xylem only at 22.5-cm depth from the centre of the decay to the stem surface (Fig. 4.52). In this case, the 2-D images were developed based on the resistivity plots of the laboratory prototype with multiple anomalies presented in Figs. 4.34 – 4.37.

Case 5: Trees with diverse decay and hollow sizes

The 2-D images displaying the cross-sections of three decayed trees are presented in Figs. 4.53 – 4.55 with wood decay of different diameters 5, 8 and 12 cm, sited at depths 5, 6.5 and 8.5 cm respectively, from the centre of the decay to the stem surface. Additionally, the 2-D images describing three standing trees with hollows of various diameters and situated at different depths are displayed in Figs. 4.56 – 4.58. The hollows are of diameters 8, 10 and 14 cm, and are situated at depths 4, 5 and 7 cm respectively, from the centre of the hollow to the stem surface. The 2-D images presented under this case evolved from the resistivity plots of the laboratory prototype with diverse modelled decay and hollow sizes as shown in Figs. 4.38 – 4.41.

Table 4.1. Resistivity values of four healthy candle trees with similar diameter located at Archaeology and Anthropology Department, University of Ibadan

AB/2[a] (cm)	MN[b] (cm)	Resistivity (Ωm)					
		Tree 1	Tree 2	Tree 3	Tree 4	Mean Value	Laboratory Prototype
4	4	46	61	51	61	55	45
6	4	40	70	62	77	62	62
8	4	46	71	57	74	62	63
10	4	45	68	52	71	59	80
12	4	1847	2705	1880	2760	2298	1141
14	4	1855	2775	1915	2790	2334	1508
16	6	2989	4077	3266	3444	3444	2101
18	6	3116	4046	3116	4448	3682	3040
20	6	3266	4168	3029	4665	3782	3296
22	6	3502	4109	3114	4788	3878	3474
24	6	3684	4191	3154	4987	4004	3890
26	6	3874	4338	3278	5257	4187	4061

[a]Current electrode half separation
[b]Potential electrode separation

Diameter of trees 1 and 2: 54.5 cm
Diameter of trees 3 and 4: 50.4 cm

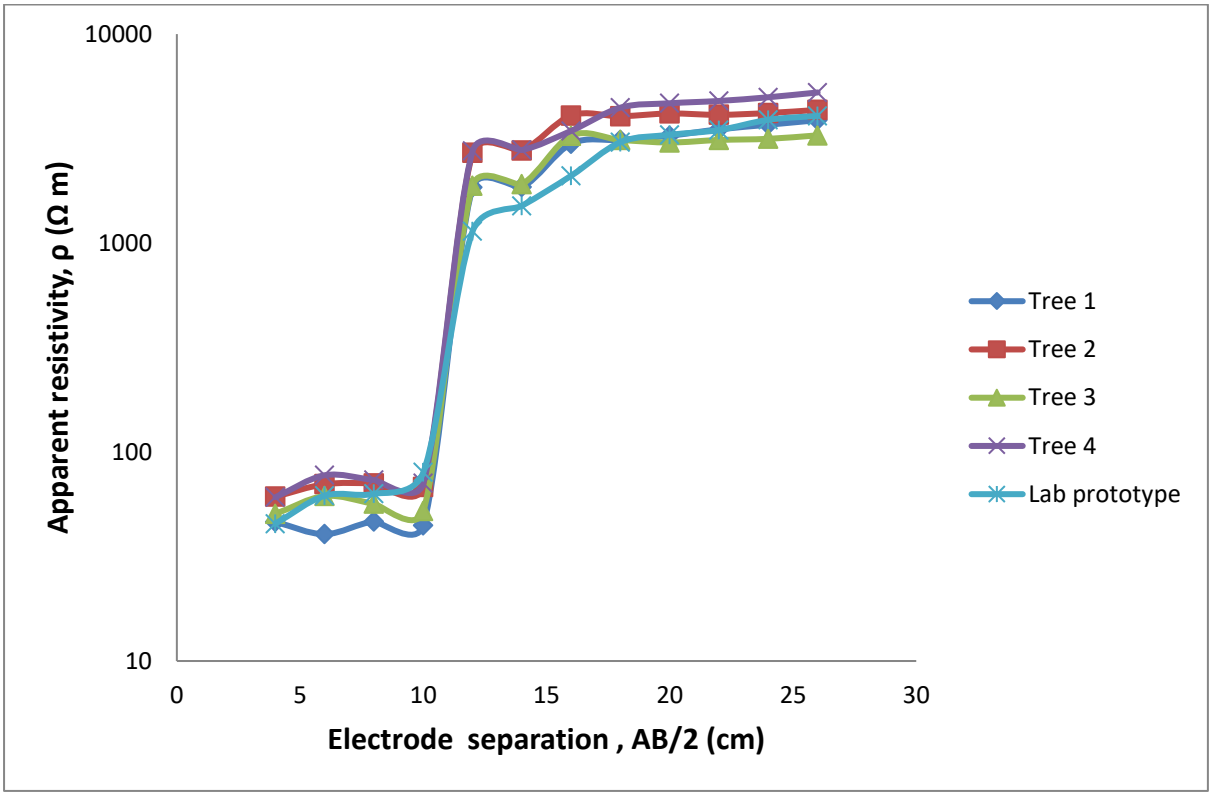

Fig. 4.1. Resistivity plots of candle trees of similar diameter and their replica

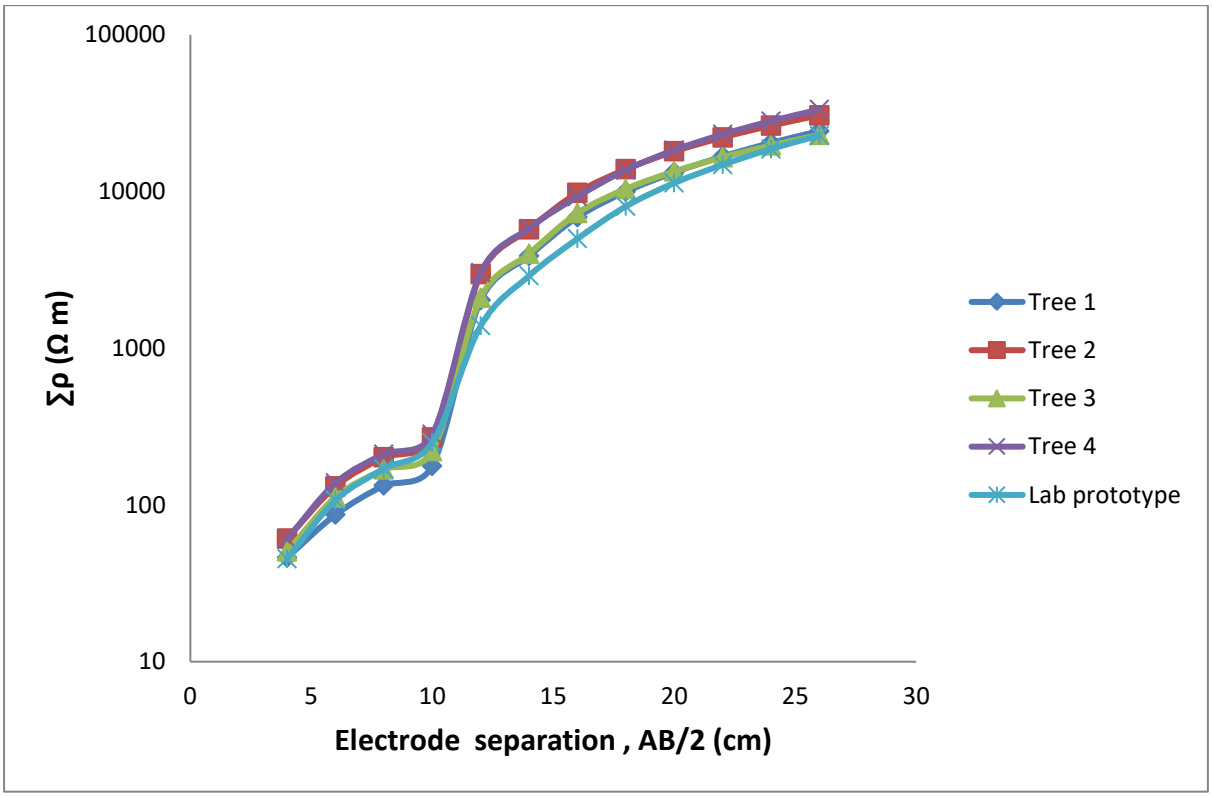

Fig. 4.2. Cumulative resistivity plots of candle trees of similar diameter and their replica

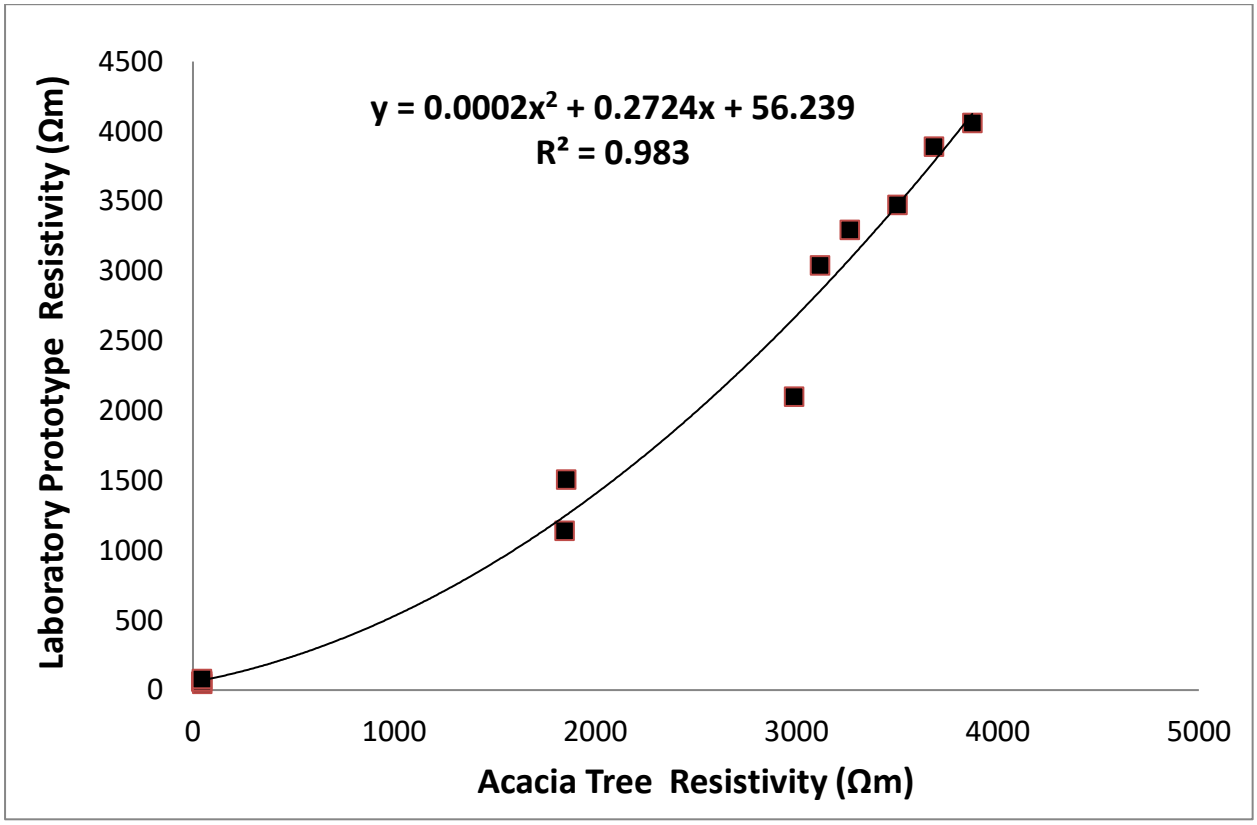

Fig. 4.3. Resistivity of laboratory prototype versus resistivity of candle tree 1

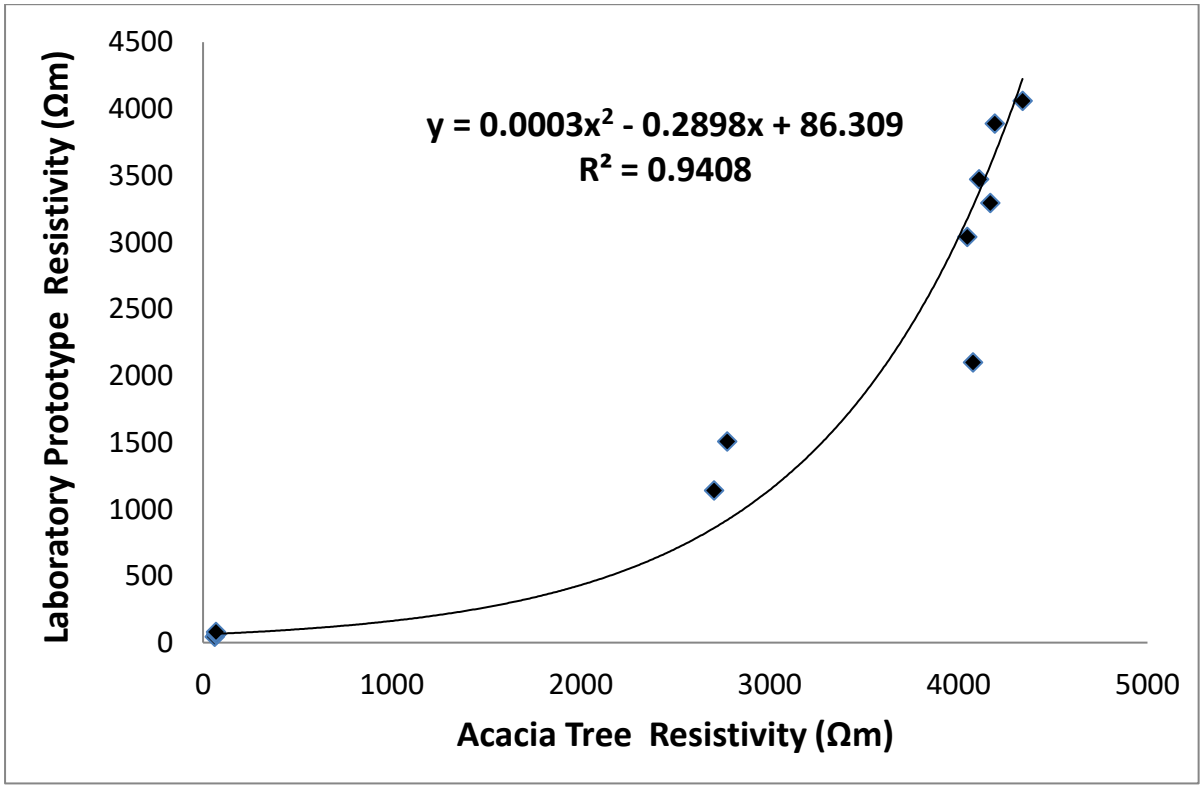

Fig. 4.4. Resistivity of laboratory prototype versus resistivity of candle tree 2

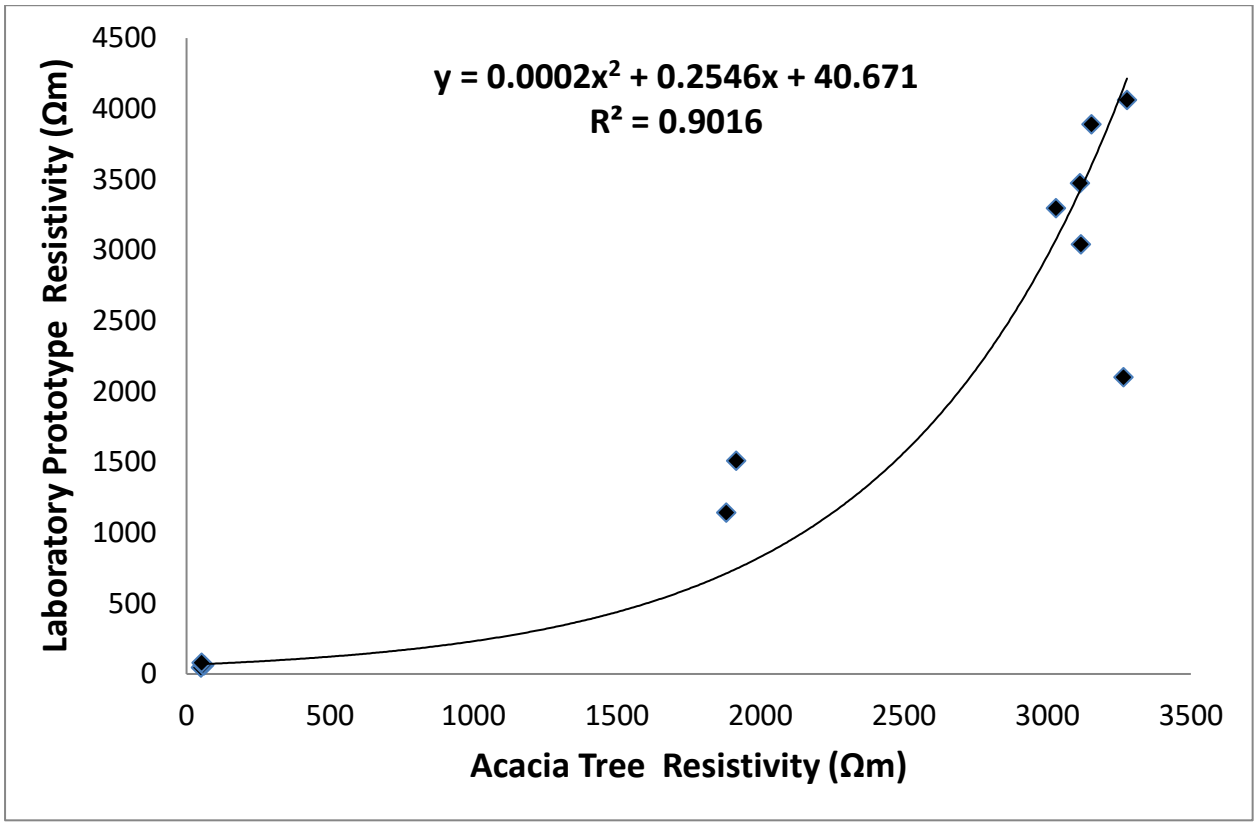

Fig. 4.5. Resistivity of laboratory prototype versus resistivity of candle tree 3

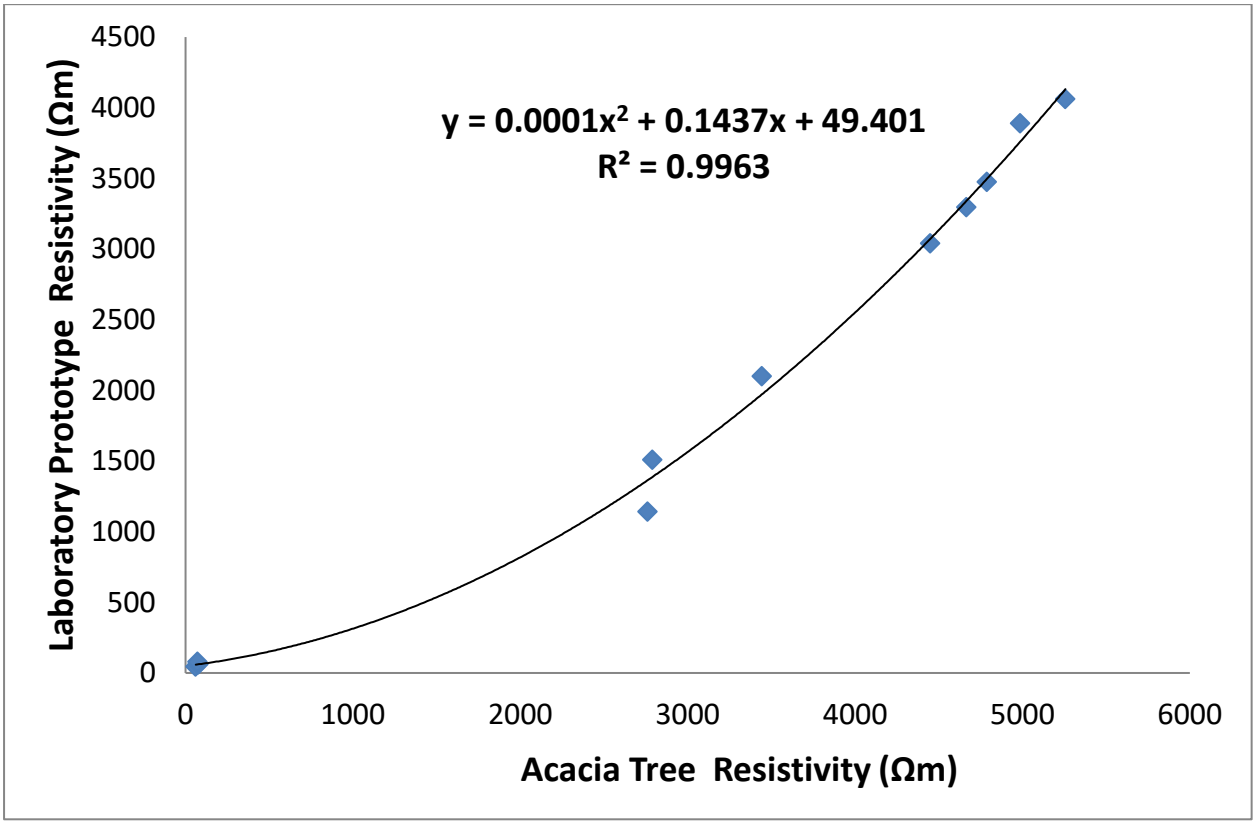

Fig. 4.6. Resistivity of laboratory prototype versus resistivity of candle tree 4

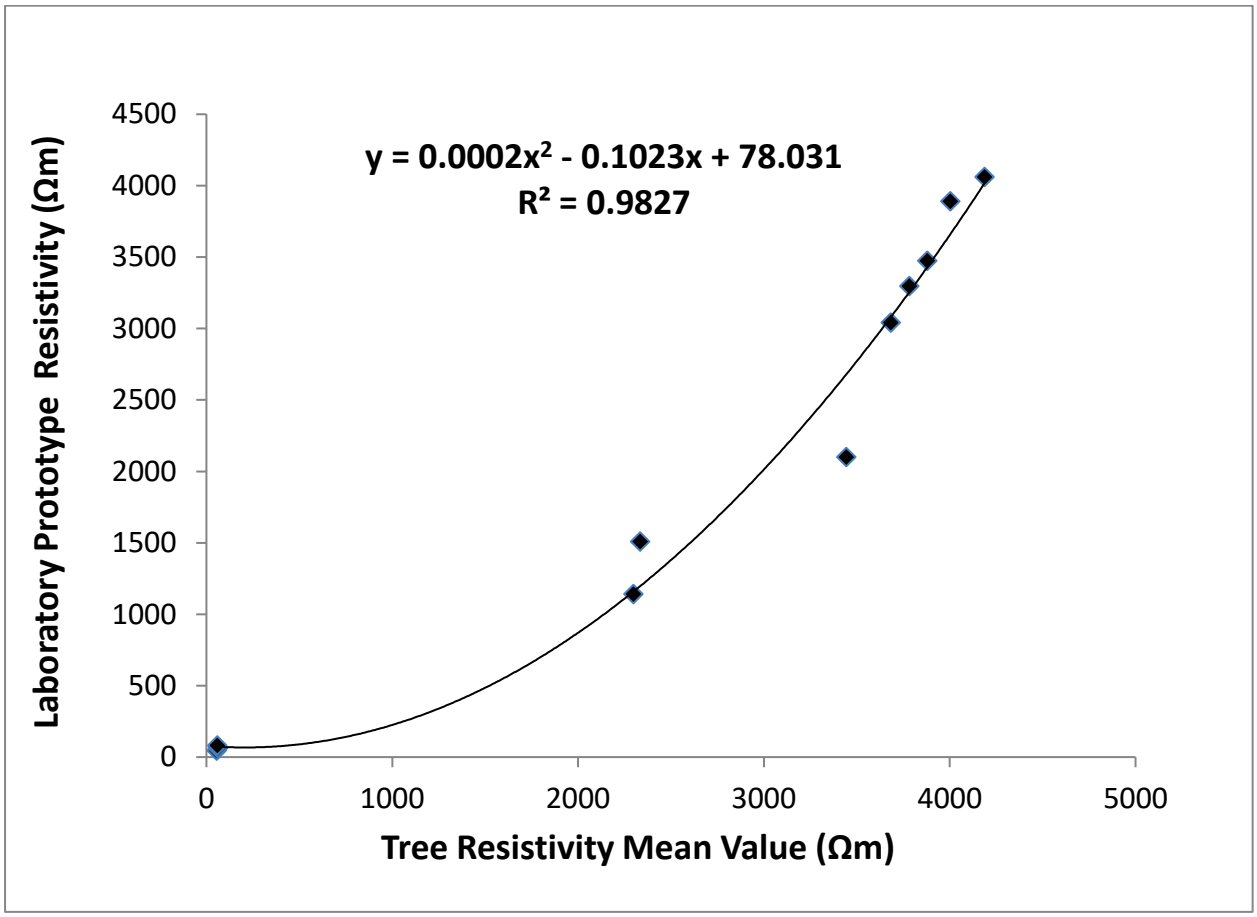

Fig. 4.7. Resistivity of laboratory prototype versus mean resistivity of candle trees

Table 4.2. Resistivity values of the healthy and decayed cambium of a candle tree

AB/2[a] (cm)	MN[b] (cm)	Resistivity (Ωm)			
		Healthy Cambium		Decayed Cambium	
		Side A	Side B	Side A	Side B
4	4	65	51	13	12
6	4	77	62	13	12
8	6	68	57	14	14
10	6	70	52	15	15

[a]Current electrode half separation
[b]Potential electrode separation

Stem diameter of the tree: 40.5 cm
Length of the healthy part: 21 cm
Decay length: 20 cm
Decay diameter: 6 cm

Table 4.3. Resistivity values of the healthy and hollowed xylem of a candle tree

AB/2[a] (cm)	MN[b] (cm)	Resistivity (Ωm) Hollowed Xylem		Resistivity (Ωm) Healthy Xylem	
		Side A	Side B	Side A	Side B
4	4	5622	5732	2144	1880
6	4	6032	6801	1991	1915
8	4	7890	5623	2969	3266
10	6	8606	6610	2941	3117
12	6	9592	7265	3042	3029
14	6	10573	8314	2997	3114

[a]Current electrode half separation
[b]Potential electrode separation

Hollow length: 28 cm
Hollow diameter: 14 cm
Length of the healthy part: 21 cm

(a)

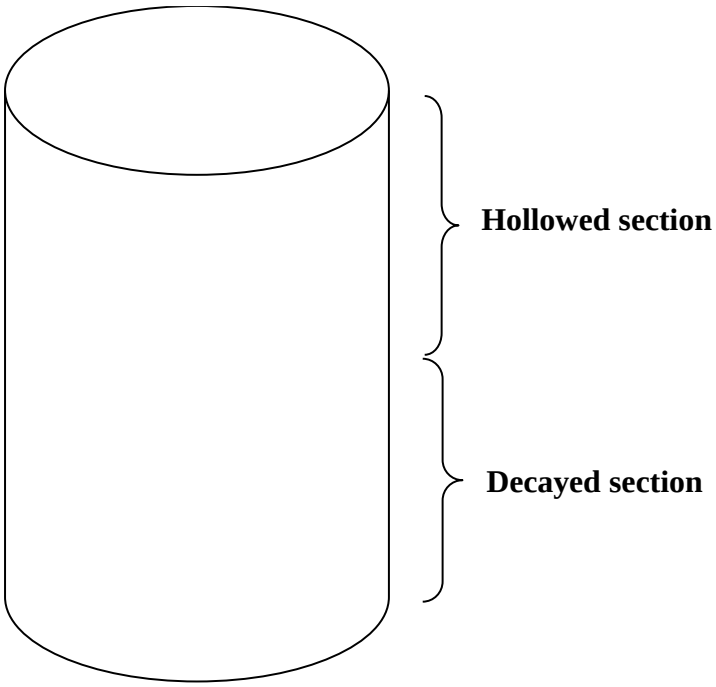

(b)

Fig. 4.8. A decayed candle tree with hollow (a) the freshly-cut tree (b) a schematic diagram showing the hollowed and decayed sections of the tree

Table 4.4. Resistivity values of a hollowed candle tree and healthy candle tree

AB/2[a] (cm)	MN[b] (cm)	Resistivity (Ωm)			
		Healthy Tree		Hollowed Tree	
		Side A	Side B	Side A	Side B
4	4	65	51	177	147
6	4	77	62	204	192
8	4	68	57	214	1565
10	4	2330	52	229	1779
12	4	2144	1880	234	8159
14	6	1991	1915	11928	8475
16	6	2969	3266	12144	9855
18	6	2941	3116	12222	10473
20	6	3042	3029	12959	11321
22	6	2997	3114	13679	12485

[a]Current electrode half separation
[b]Potential electrode separation

Stem diameter of healthy tree: 40.5 cm
Stem diameter of hollowed tree: 41.5 cm

Fig. 4.9. A freshly-cut candle tree with hollow from end to end

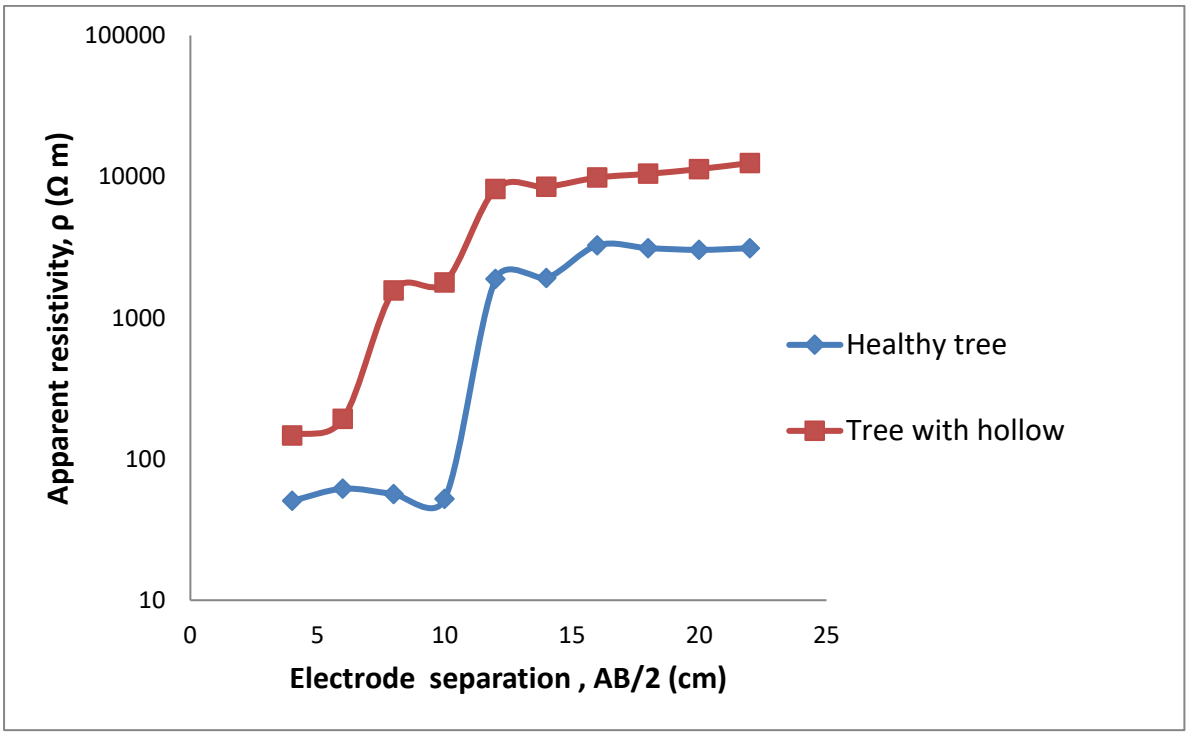

Fig. 4.10. Resistivity plots of a candle tree with hollow (Side B) and a healthy candle tree (Side B)

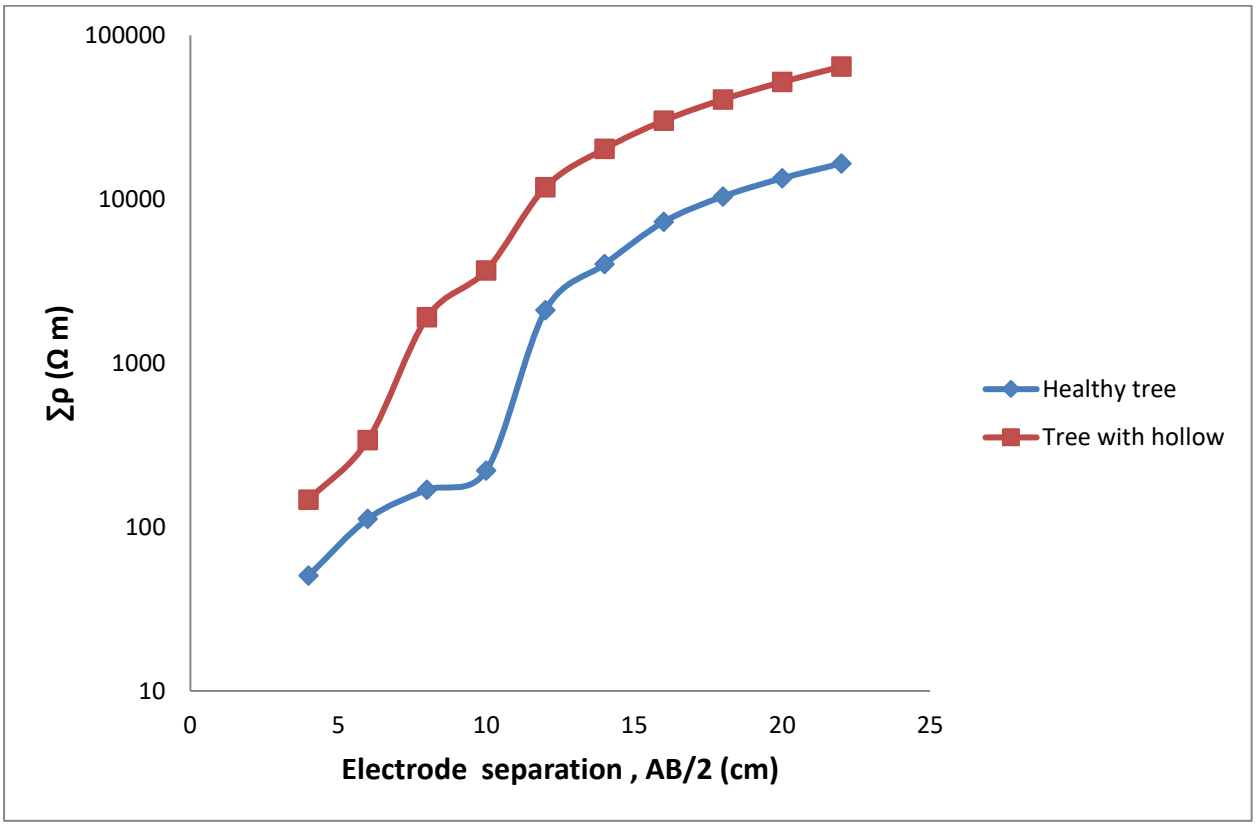

Fig. 4.11. Cumulative resistivity plots of a candle tree with hollow (Side B) and a healthy candle tree (Side B)

Table 4.5. Resistivity values of selected candle trees located at Archaeology and Anthropology Department, University of Ibadan

AB/2[a] (cm)	MN[b] (cm)	Resistivity (Ωm)							
		Tree 1	**Tree 2**	**Tree 3**	**Tree 4**	**Tree 5**	**Tree 6**	**Tree 7**	**Tree 8**
4	4	46	61	51	61	57	48	46	61
6	4	40	70	62	77	83	49	40	70
8	4	46	71	57	74	87	56	46	71
10	4	45	68	52	71	88	2156	45	68
12	4	1847	2705	1880	2760	**281**[c]	2045	1847	2705
14	4	1855	2775	1915	2790	**282**[c]	1945	1855	2775
16	6	2989	4077	3266	3444	**262**[c]	3167	2989	4077
18	6	3116	4046	3116	4448	**479**[c]	3066	3116	4046
20	6	3266	4168	3029	4665	**755**[c]	3141	3266	4168
22	6	3502	4109	3114	4788	**1054**[c]	3257	3502	4109
24	6	3684	4191	3154	4987	4066	3284	3684	4191
26	6	3874	4338	3278	5257	4829	3441	3874	4338
Tree Diameter		**54.4 cm**	**54.5 cm**	**50.4 cm**	**50.4 cm**	**59.2 cm**	**52.1 cm**	**50.8 cm**	**56.5 cm**

[a]Current electrode half separation
[b]Potential electrode separation
[c]Detection point of wood decay

Tree Health Status
Wood decay detected in Tree 5
Trees 1 – 4 and 6 – 8 were healthy trees

Table 4.6. Resistivity values of selected candle trees located at Physics Department, University of Ibadan

AB/2[a] (cm)	MN[b] (cm)	Resistivity (Ωm)					
		Tree 9	**Tree 10**	**Tree 11**	**Tree 12**	**Tree 13**	**Tree 14**
4	4	**7781[d]**	156	159	179	209	215
6	4	**15627[d]**	90	172	185	216	221
8	4	**15155[d]**	108	194	201	231	236
10	4	6802	4016	5215	5339	5740	5761
12	4	9896	**2230[c]**	7131	7331	7731	7752
14	4	6846	**2258[c]**	8155	8356	8756	8777
16	6	4948	**2307[c]**	8277	8477	8878	8899
18	6	10090	**2295[c]**	9307	9507	9907	9928
20	6	9517	**2256[c]**	10330	10530	10930	10951
22	6	14806	**2190[c]**	12343	12544	12944	12965
24	6	15502	**2214[c]**	14359	14559	14959	14980
26	6	16254	**3747[c]**	15384	15585	15985	16006
Tree Diameter		**90.8 cm**	**92.5 cm**	**91.3 cm**	**92.8 cm**	**100.1 cm**	**100.5 cm**

[a]Current electrode half separation
[b]Potential electrode separation
[c]Detection point of wood decay
[d]Detection point of hollow or cavity

Tree Health Status
Hollow or cavity detected in Tree 9
Wood decay detected in Tree 10
Trees 11 – 14 were healthy trees

Table 4.7. Resistivity values of selected candle trees located at Chemistry Department, University of Ibadan

AB/2[a] (cm)	MN[b] (cm)	Resistivity (Ωm)			
		Tree 15	**Tree 16**	**Tree 17**	**Tree 18**
4	4	204	220	231	**992[d]**
6	4	211	227	237	**1019[d]**
8	4	226	242	253	**1082[d]**
10	4	5560	5781	5822	**1190[c]**
12	4	7552	7773	7814	**1597[c]**
14	4	8577	8798	8838	**1806[c]**
16	6	8698	8919	8960	**1831[c]**
18	6	9728	9949	9989	**2041[c]**
20	6	10751	10972	11012	**2250[c]**
22	6	12765	12986	13026	**2661[c]**
24	6	14780	15001	15041	**3072[c]**
26	6	15806	16027	16067	**3281[c]**
Tree Diameter		**98.9 cm**	**100.9 cm**	**109.8 cm**	**110.4 cm**

[a]Current electrode half separation
[b]Potential electrode separation
[c]Detection point of wood decay
[d]Detection point of hollow or cavity

Tree Health Status
Wood decay and hollow or cavity detected in Tree 18
Trees 15 – 17 were healthy trees

Table 4.8. Resistivity values of selected candle trees located at Microbiology Department, University of Ibadan

AB/2[a] (cm)	MN[b] (cm)	Resistivity (Ωm)					
		Tree 19	**Tree 20**	**Tree 21**	**Tree 22**	**Tree 23**	**Tree 24**
4	4	127	136	**1125[d]**	230	169	155
6	4	153	162	**1157[d]**	236	195	181
8	4	157	165	**1232[d]**	**50[c]**	198	185
10	4	159	167	5772	**1178[c]**	2565	186
12	4	2339	2355	7763	**1577[c]**	4768	3070
14	4	2345	2360	8788	**1782[c]**	4774	3075
16	6	2239	2254	8910	**1806[c]**	4668	2969
18	6	3411	3426	9939	**2012[c]**	5840	4141
20	6	4896	4912	10962	11083	7325	5626
22	6	6515	6530	12976	13097	8944	7245
24	6	8953	8969	14991	15112	11382	9683
26	6	10480	10496	16017	16137	12909	11211
Tree Diameter		**70.6 cm**	**70.9 cm**	**105.95 cm**	**107.3 cm**	**82.5 cm**	**76.8 cm**

[a]Current electrode half separation
[b]Potential electrode separation
[c]Detection point of wood decay
[d]Detection point of hollow or cavity

Tree Health Status
Wood decay detected in Tree 22
Cavity or hollow detected in Tree 21
Trees 19, 20, 23 and 24 were healthy trees

Table 4.9. Resistivity values of selected candle trees located at Faculty of Social Sciences, University of Ibadan

AB/2[a] (cm)	MN[b] (cm)	Resistivity (Ωm)							
		Tree 25	**Tree 26**	**Tree 27**	**Tree 28**	**Tree 29**	**Tree 30**	**Tree 31**	**Tree 32**
4	4	36	31	30	**463[d]**	114	97	118	110
6	4	30	40	41	**575[d]**	140	123	144	136
8	4	36	40	36	**591[d]**	144	127	148	140
10	4	35	39	32	**598[d]**	145	129	149	141
12	4	1247	1205	1380	**9321[d]**	2268	2067	2168	2189
14	4	1254	1274	1415	**9345[d]**	2274	2073	2173	2194
16	6	2388	2577	2766	**8890[d]**	2168	1967	2067	2088
18	6	2516	2546	2616	**13927[d]**	3339	3139	3239	3260
20	6	2665	2667	2829	4725	4825	4624	4724	4745
22	6	2902	2609	2914	6343	6443	6243	6343	6364
24	6	3083	2991	3054	8782	8882	8681	8782	8803
26	6	3273	3038	3078	10309	10409	10209	10309	10330
Tree Diameter		**45.2 cm**	**44.8 cm**	**48.2 cm**	**64.5 cm**	**69.8 cm**	**62.1 cm**	**65.2 cm**	**64.7 cm**

[a]Current electrode half separation
[b]Potential electrode separation
[d]Detection point of hollow or cavity

Tree Health Status

Hollow or cavity detected in Tree 28
Trees 25 – 27, 29 – 32 were healthy trees

Table 4.10. Resistivity values of selected candle trees located at Botany Department, University of Ibadan

AB/2[a] (cm)	MN[b] (cm)	Resistivity (Ωm)							
		Tree 33	**Tree 34**	**Tree 35**	**Tree 36**	**Tree 37**	**Tree 38**	**Tree 39**	**Tree 40**
4	4	**515[d]**	124	134	175	155	165	172	178
6	4	**620[d]**	150	161	201	181	191	185	191
8	4	**635[d]**	154	164	205	185	195	207	213
10	4	**641[d]**	155	166	2755	2191	2314	5739	6237
12	4	**8791[d]**	2318	2369	4958	4395	4518	7655	8153
14	4	2203	2324	2375	4964	4400	4523	8680	9178
16	6	2097	2218	2269	4858	4294	4417	8801	9300
18	6	**659[c]**	3390	3440	6029	5466	5589	9831	10329
20	6	**959[c]**	4876	4926	7515	6951	7075	10854	11352
22	6	**1285[c]**	6494	6544	9133	8570	8693	12868	13366
24	6	**1777[c]**	8933	8983	11572	11008	11132	14883	15381
26	6	**2084[c]**	10460	10510	13099	12535	12659	15909	16407
Tree Diameter		**66.3 cm**	**70.2 cm**	**85.1 cm**	**85.1 cm**	**79.8 cm**	**80.8 cm**	**89.2 cm**	**90.2 cm**

[a]Current electrode half separation
[b]Potential electrode separation
[c]Detection point of wood decay
[d]Detection point of hollow or cavity

Tree Health Status

Wood decay and hollow detected in Tree 33
Trees 34 – 40 were healthy trees

Table 4.11. Resistivity values of four healthy almond trees with similar diameter located at Microbiology and Mathematics Departments, University of Ibadan

AB/2[a] (cm)	MN[b] (cm)	Resistivity (Ωm)					
		Tree 1	Tree 2	Tree 3	Tree 4	Mean Value	Laboratory Prototype
4	4	75	52	96	132	89	81
6	4	95	78	131	135	110	128
8	4	114	91	149	113	117	135
10	4	106	85	164	136	123	142
12	4	101	86	163	115	116	153
14	4	145	87	170	120	130	162
16	6	147	125	275	178	181	249
18	6	7339	6484	6269	5417	6377	5826
20	6	7216	6749	6579	5835	6595	6158
22	6	7125	6710	6816	6153	6701	6425
24	6	6739	6604	6964	6487	6699	6578
26	6	7020	6545	7011	6764	6835	6816

[a]Current electrode half separation
[b]Potential electrode separation

Trees 1 and 2 are of diameter 52.50 cm and located at Microbiology Dept. U.I.
Trees 3 and 4 are of diameter 50.89 cm and located at Mathematics Dept. U.I.

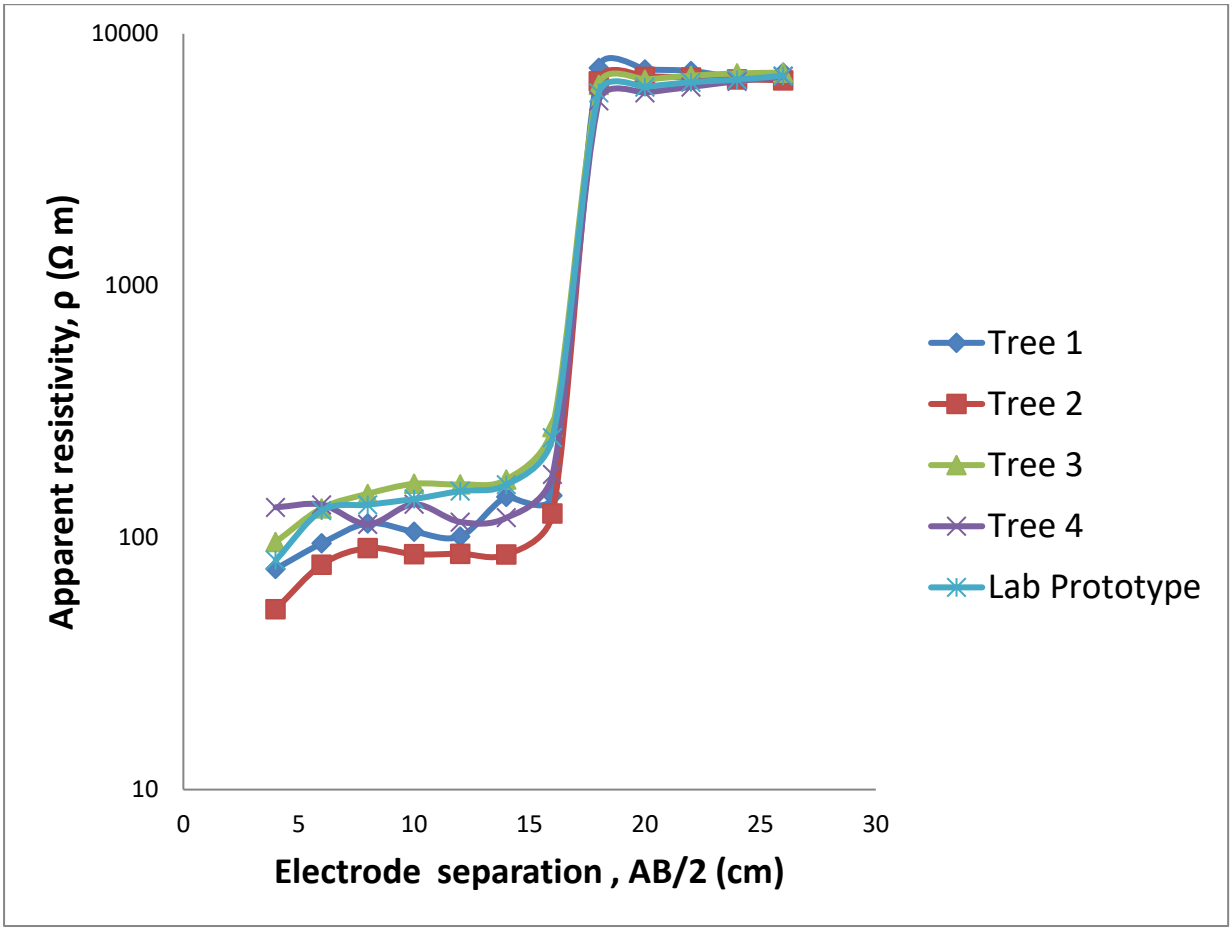

Fig. 4.12. Resistivity plots of almond trees of similar diameter and their replica

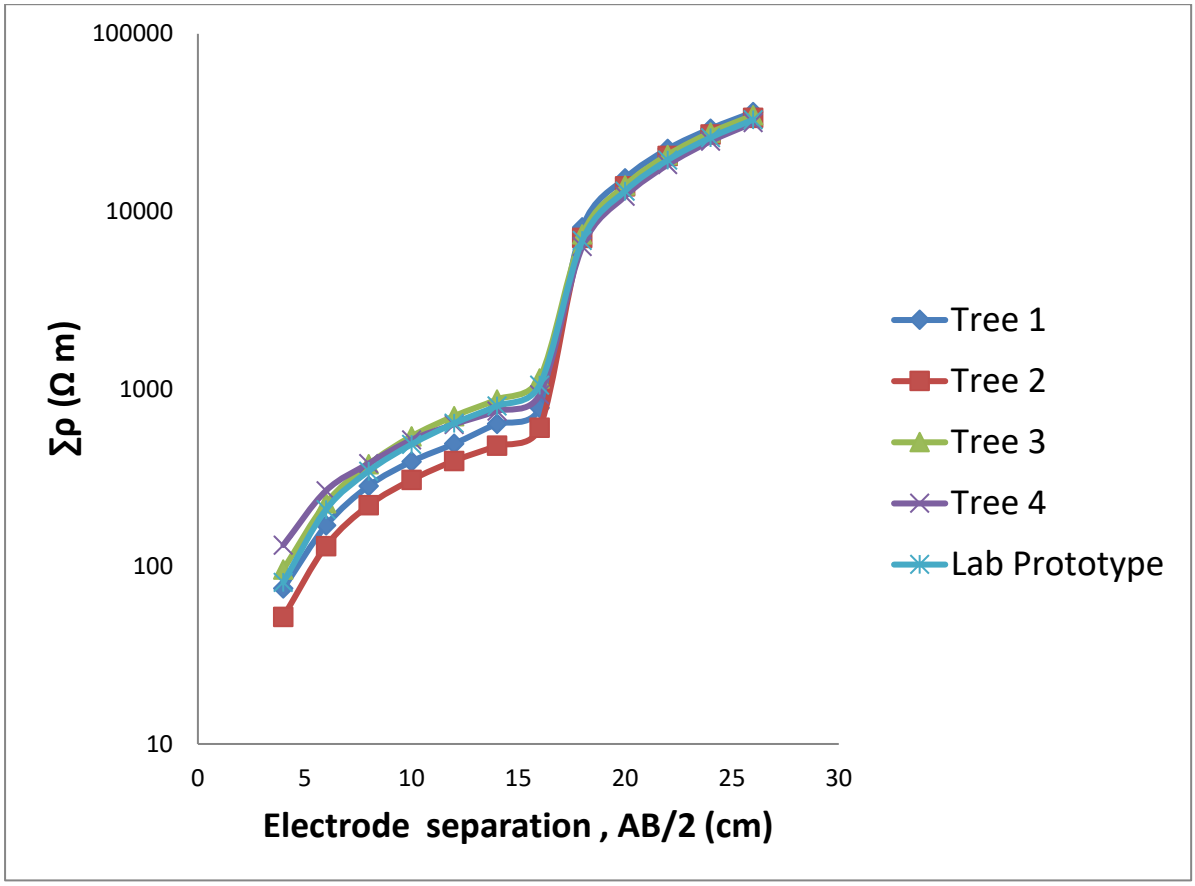

Fig. 4.13. Cumulative resistivity plots of almond trees of similar diameter and their replica

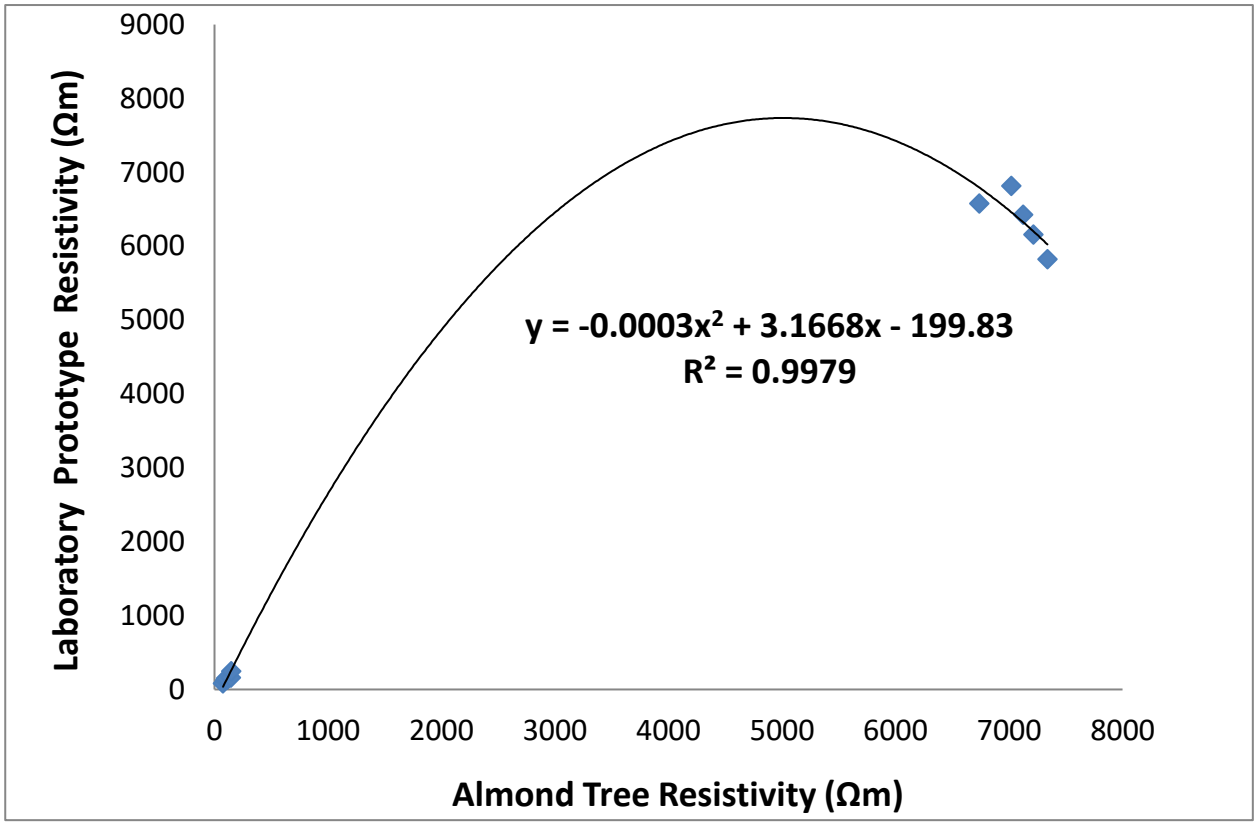

Fig. 4.14. Resistivity of laboratory prototype versus resistivity of almond tree 1

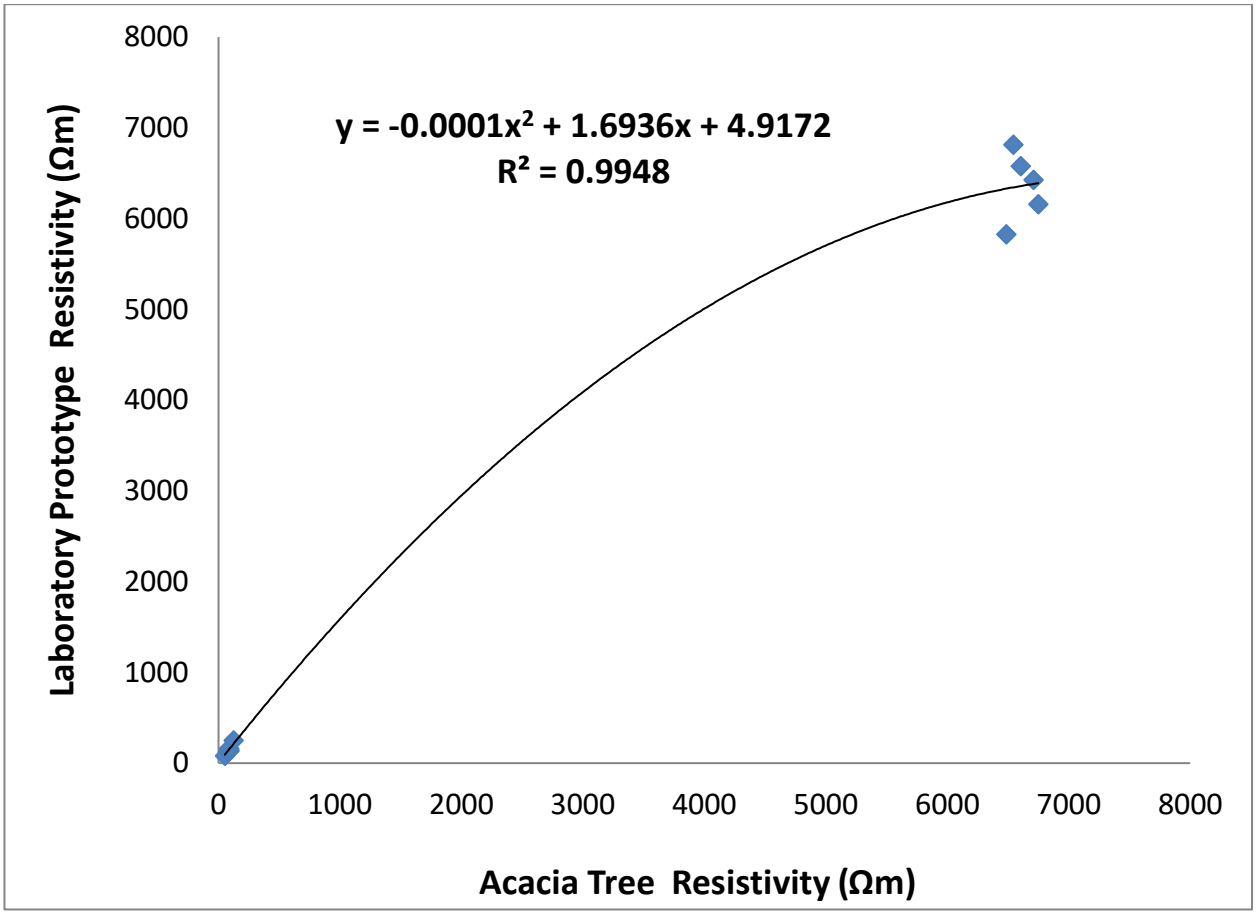

Fig. 4.15. Resistivity of laboratory prototype versus resistivity of almond tree 2

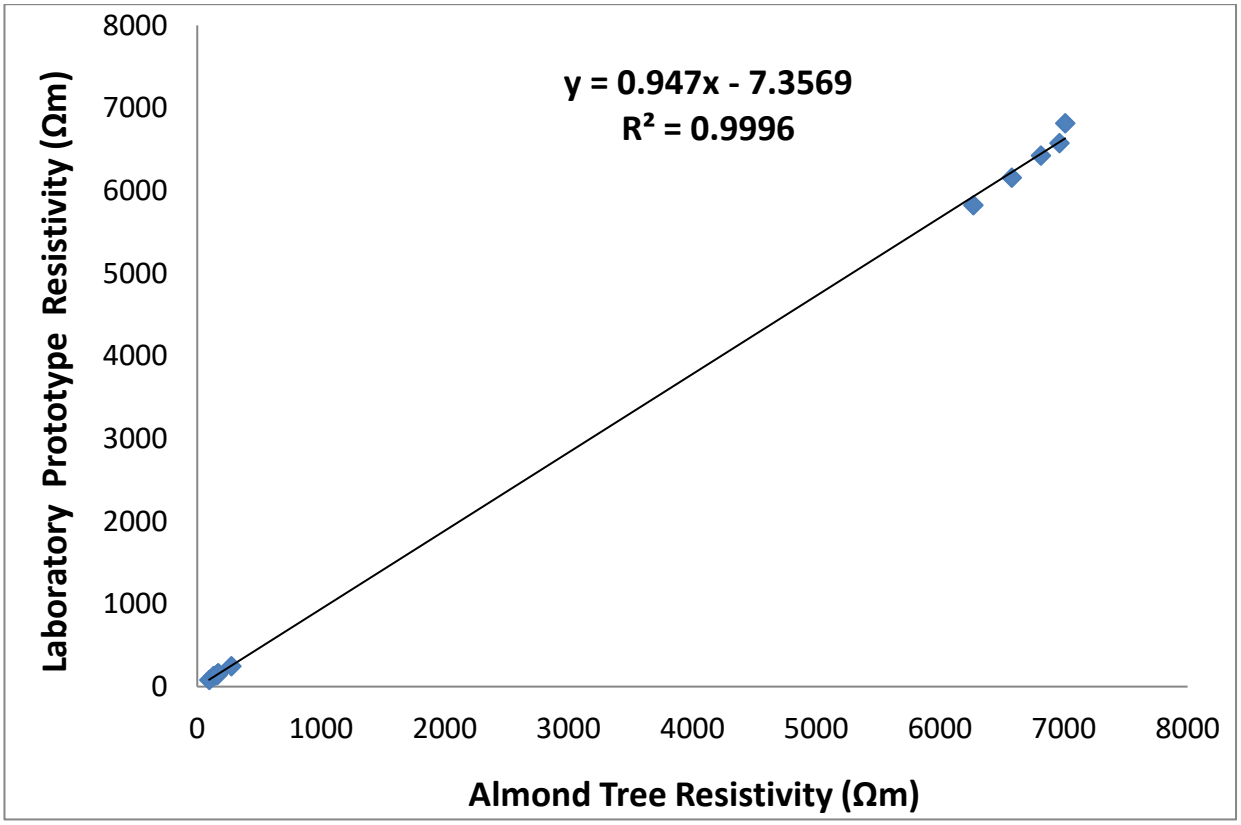

Fig. 4.16. Resistivity of laboratory prototype versus resistivity of almond tree 3

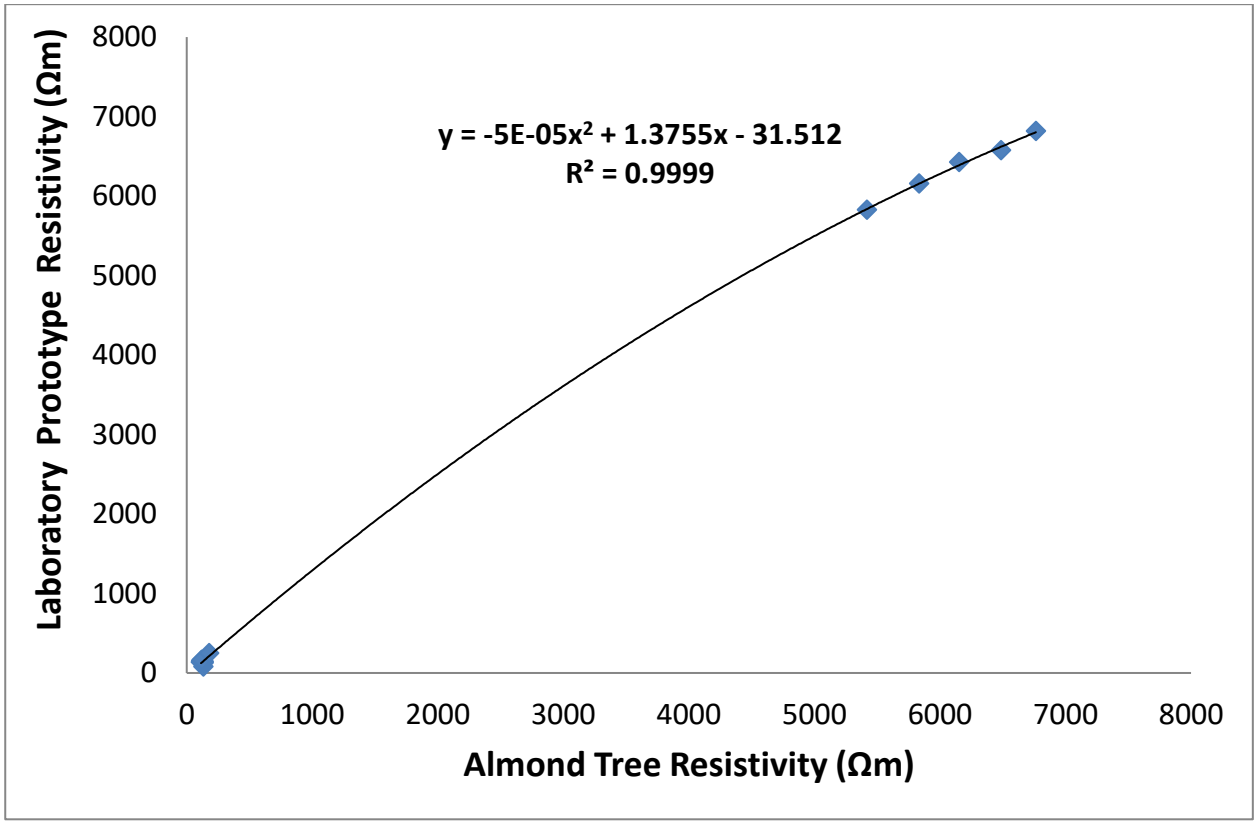

Fig. 4.17. Resistivity of laboratory prototype versus resistivity of almond tree 4

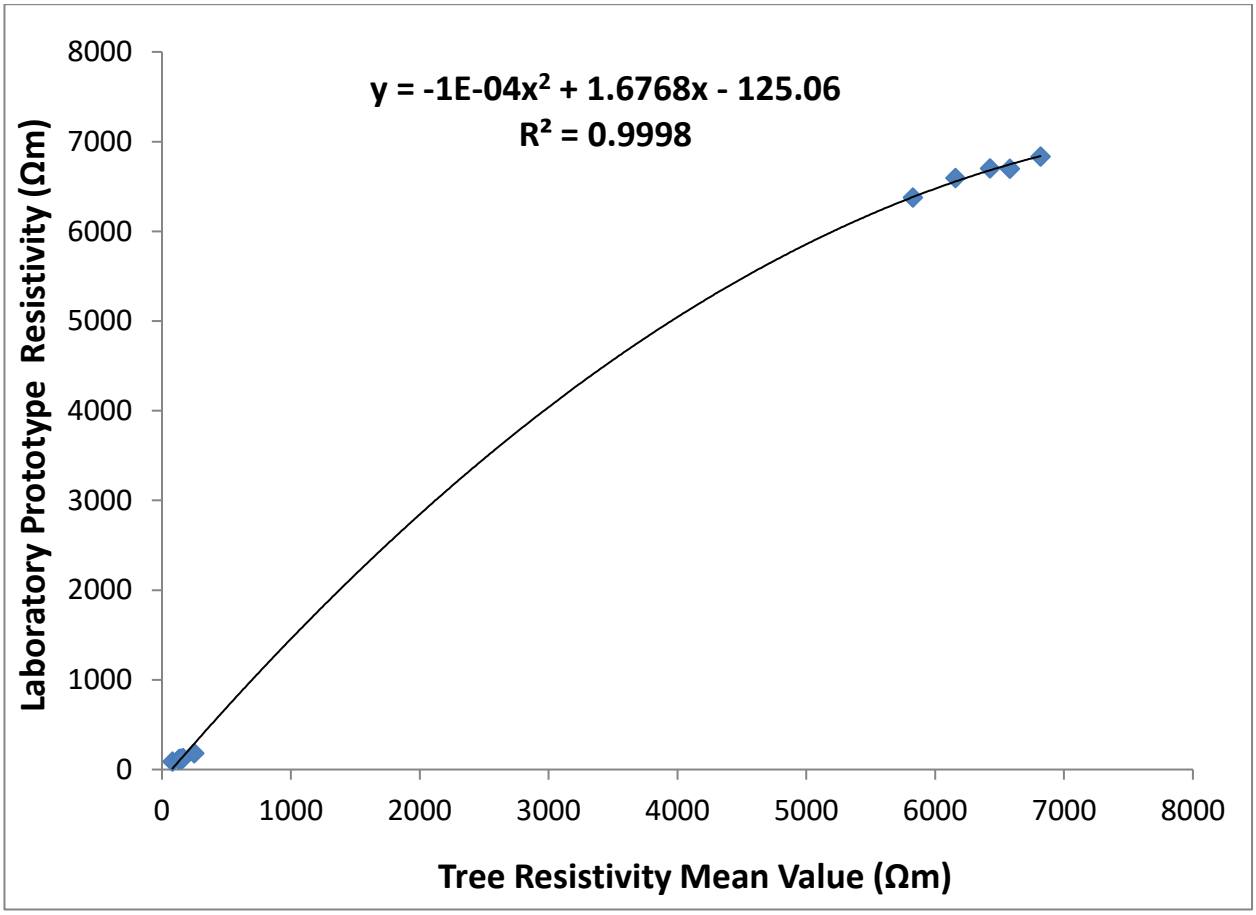

Fig. 4.18. Resistivity of laboratory prototype versus mean resistivity of almond trees

Table 4.12. Resistivity values of a healthy almond tree and a decayed almond tree with hollow

AB/2[a] (cm)	MN[b] (cm)	Resistivity (Ωm)	
		Healthy tree	Decayed tree with hollow
4	4	134	13
6	4	184	14
8	4	209	16
10	4	231	17
12	4	154	16
14	4	160	12
16	6	4038	11228
18	6	4072	12101
20	6	3950	13490
22	6	3725	14538
24	6	3621	10243
26	6	3742	11976

[a]Current electrode half separation
[b]Potential electrode separation

Stem diameter of the tree: 45 cm
Decay diameter: 10.2 cm
Decay length: 25 cm
Hollow length: 27cm
Hollow diameter: 10 cm

(a)

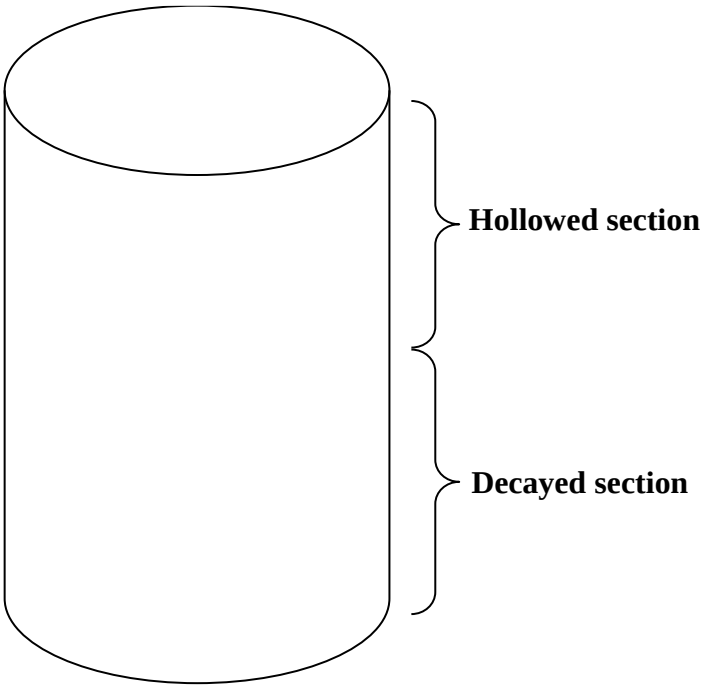

(b)

Fig. 4.19. A decayed almond tree with hollow (a) the freshly-cut tree (b) a schematic diagram showing the hollowed and decayed sections of the tree

Table 4.13. Resistivity values of selected almond trees located at Microbiology Department, University of Ibadan

AB/2[a] (cm)	MN[b] (cm)	Resistivity (Ωm)							
		Tree 1	**Tree 2**	**Tree 3**	**Tree 4**	**Tree 5**	**Tree 6**	**Tree 7**	**Tree 8**
4	4	75	52	88	71	241	348	320	284
6	4	95	78	106	87	265	394	366	330
8	4	114	91	115	95	264	412	383	348
10	4	106	86	120	87	281	420	392	356
12	4	101	86	121	93	273	**2553[c]**	12898	13317
14	4	145	86	172	191	277	**2580[c]**	13025	13420
16	6	147	125	162	262	365	**2615[c]**	13190	13586
18	6	7339	6484	8068	6359	8142	**2651[c]**	13359	13738
20	6	7216	6749	7682	6345	8160	**2680[c]**	13498	13885
22	6	7125	6710	7728	6220	8190	**2669[c]**	13445	13828
24	6	6739	6604	7458	6469	8307	**2724[c]**	13682	13999
26	6	7020	6545	7442	6650	8437	**2780[c]**	13919	14129
Tree Diameter		**52.5 cm**	**52.5 cm**	**58.6 cm**	**54.1 cm**	**65.2 cm**	**103.4 cm**	**105.7 cm**	**106.2 cm**

[a]Current electrode half separation
[b]Potential electrode separation
[c]Detection point of wood decay

Tree Health Status
Wood decay detected in Tree 6
Trees 1 – 5, 7 and 8 were healthy trees

Table 4.14.. Resistivity values of selected almond trees located at Mathematics Department, University of Ibadan

AB/2[a] (cm)	MN[b] (cm)	Resistivity (Ωm)							
		Tree 9	**Tree 10**	**Tree 11**	**Tree 12**	**Tree 13**	**Tree 14**	**Tree 15**	**Tree 16**
4	4	96	132	104	80	95	107	144	96
6	4	131	135	128	99	127	117	117	131
8	4	149	113	126	114	141	111	111	149
10	4	164	136	144	169	142	113	111	140
12	4	163	115	135	156	137	111	152	151
14	4	170	120	139	323	240	241	122	152
16	6	275	178	228	173	358	239	187	4037
18	6	6269	5417	7242	7312	3493	3672	3551	4072
20	6	6579	5835	7260	7439	3390	3809	3786	3950
22	6	6816	6153	7289	7603	3265	3931	4002	3725
24	6	6964	6487	7406	7772	3288	3488	3738	3621
26	6	7011	6764	7536	7911	3214	3364	3764	3742
Tree Diameter		**50.9 cm**	**50.9 cm**	**59.3 cm**	**63.2 cm**	**42.1 cm**	**47.4 cm**	**48.4 cm**	**48.5 cm**

[a]Current electrode half separation
[b]Potential electrode separation

Tree Health Status
Trees 9 – 16 were healthy trees

Table 4.15. Resistivity values of selected almond trees located at Zoology Department, University of Ibadan

AB/2[a] (cm)	MN[b] (cm)	Resistivity (Ωm)							
		Tree 17	**Tree 18**	**Tree 19**	**Tree 20**	**Tree 21**	**Tree 22**	**Tree 23**	**Tree 24**
4	4	93	124	332	243	318	266	295	336
6	4	139	103	**1121[d]**	290	364	312	341	382
8	4	157	114	**1300[d]**	307	382	330	359	399
10	4	165	**1066[d]**	**1407[d]**	315	390	338	367	408
12	4	167	**1704[d]**	**1210[d]**	317	392	340	**66[c]**	410
14	4	172	**1458[d]**	**1506[d]**	322	397	345	**67[c]**	539
16	6	241	**1890[d]**	**1268[d]**	392	467	414	**1709[c]**	10866
18	6	7522	7472	312	8072	852	8470	**1732[c]**	11030
20	6	7649	7502	320	8199	8649	8597	**1761[c]**	11199
22	6	7813	7598	377	8364	8813	8761	**1791[c]**	11339
24	6	7982	7685	430	8532	8983	8930	**1816[c]**	11286
26	6	8121	7796	502	8672	9122	9070	**1964[c]**	1051
Tree Diameter		**65.2 cm**	**62.8 cm**	**67.5 cm**	**70.2 cm**	**75.3 cm**	**74.2 cm**	**88.0 cm**	**90.0 cm**

[a]Current electrode half separation
[b]Potential electrode separation
[c]Detection point of wood decay
[d]Detection point of hollow or cavity

Tree Health Status

Cavity or hollow detected in Trees 18 and 19
Wood decay detected in Tree 23
Trees 17, 20, 21, 22 and 24 were healthy trees

Table 4.16. Resistivity values of selected almond trees located at Faculty of Social Sciences, University of Ibadan

AB/2[a] (cm)	MN[b] (cm)	Resistivity (Ωm)					
		Tree 25	**Tree 26**	**Tree 27**	**Tree 28**	**Tree 29**	**Tree 30**
4	4	113	294	143	269	311	361
6	4	159	341	189	315	357	407
8	4	177	358	207	333	375	425
10	4	185	366	215	341	383	433
12	4	187	368	217	343	385	14051
14	4	192	373	222	348	390	14107
16	6	262	8572	292	8450	8862	14256
18	6	**1510[c]**	8699	8202	8577	8989	14399
20	6	**1536[c]**	8864	8329	8742	9153	14545
22	6	**1569[c]**	9033	8493	8910	9322	14483
24	6	**1603[c]**	9172	8662	9050	9461	14584
26	6	**1631[c]**	10254	8802	9195	9409	14785
Tree Diameter		**68.9 cm**	**60.2 cm**	**79.8 cm**	**66.8 cm**	**78.5 cm**	**80.9 cm**

[a]Current electrode half separation
[b]Potential electrode separation
[c]Detection point of wood decay

Tree Health Status
Wood decay detected in Tree 25
Trees 26 – 30 were healthy trees

Table 4.17. Resistivity values of selected almond trees located at Botany Department, University of Ibadan

AB/2[a] (cm)	MN[b] (cm)	Resistivity (Ωm)					
		Tree 31	**Tree 32**	**Tree 33**	**Tree 34**	**Tree 35**	**Tree 36**
4	4	321	337	352	**1182[d]**	350	259
6	4	368	383	398	**1343[d]**	396	305
8	4	385	401	416	**1405[d]**	414	322
10	4	393	409	424	**1434[d]**	422	331
12	4	395	411	426	**1441[d]**	424	333
14	4	400	416	10248	10798	11099	338
16	6	9107	9688	10374	10925	11225	407
18	6	9234	9814	10539	11089	11390	8472
20	6	9399	9979	10708	11258	11559	8599
22	6	9568	10148	10847	11398	11698	8764
24	6	9707	10287	10795	11345	11645	8933
26	6	9654	10234	560	11022	1411	9072
Tree Diameter		**82.5 cm**	**83.7 cm**	**89.4 cm**	**90.2 cm**	**95.6 cm**	**72.5 cm**

[a]Current electrode half separation
[b]Potential electrode separation
[d]Detection point of hollow or cavity

Tree Health Status
Cavity or hollow detected in Tree 34
Trees 31 – 33, 35, 36 were healthy trees

Table 4.18. Resistivity values of selected almond trees located at Botany Department, University of Ibadan

AB/2[a] (cm)	MN[b] (cm)	Resistivity (Ωm)			
		Tree 37	**Tree 38**	**Tree 39**	**Tree 40**
4	4	361	342	342	**1087[d]**
6	4	407	388	388	**1239[d]**
8	4	425	405	405	**1297[d]**
10	4	433	414	414	401
12	4	14051	14307	14307	**2820[c]**
14	4	14107	14364	14363	**2845[c]**
16	6	14256	14512	14512	**2878[c]**
18	6	14399	14656	14655	**2912[c]**
20	6	14545	14801	14801	**2940[c]**
22	6	14483	14739	14739	**2929[c]**
24	6	14584	14840	14840	**2981[c]**
26	6	14785	15041	15040	**3033[c]**
Tree Diameter		**98.9 cm**	**108.2 cm**	**109.8 cm**	**110.4 cm**

[a]Current electrode half separation
[b]Potential electrode separation
[c]Detection point of wood decay
[d]Detection point of hollow or cavity

Tree Health Status
Wood decay and hollow detected in Tree 40
Trees 37 – 39 were healthy trees

Table 4.19. Resistivity values of the laboratory prototype with a copper wire lump at 5-cm depth with the centre of the wire lump as the reference point

AB/2[a] (cm)	MN[b] (cm)	Resistivity, ρ (Ωm)	
		With anomaly	Without anomaly
4	4	**11**[c]	45
6	4	**15**[c]	62
8	4	**17**[c]	63
10	4	65	80
12	4	910	1141
14	4	1207	1508
16	6	1853	2101
18	6	2591	3040
20	6	2908	3296
22	6	3168	3474
24	6	3497	3890
26	6	3834	4061

[a]Current electrode half separation
[b]Potential electrode separation
[c]Detection point of the copper wire lump

Table 4.20. Resistivity values of the laboratory prototype with a copper wire lump at 10-cm depth with the centre of the wire lump as the reference point

AB/2[a] (cm)	MN[b] (cm)	Resistivity, ρ(Ωm)	
		With anomaly	Without anomaly
4	4	39	45
6	4	57	62
8	4	60	63
10	4	**22**[c]	80
12	4	**296**[c]	1141
14	4	**386**[c]	1508
16	6	1902	2101
18	6	2652	3040
20	6	2835	3296
22	6	3214	3474
24	6	3572	3890
26	6	3953	4061

[a]Current electrode half separation
[b]Potential electrode separation
[c]Detection point of the copper wire lump

Table 4.21. Resistivity values of the laboratory prototype with a copper wire lump at 15-cm depth with the centre of the wire lump as the reference point

AB/2[a] (cm)	MN[b] (cm)	Resistivity, ρ(Ωm)	
		With anomaly	Without anomaly
4	4	41	45
6	4	56	62
8	4	61	63
10	4	76	80
12	4	1013	1141
14	4	1315	1508
16	6	**521**[c]	2101
18	6	**752**[c]	3040
20	6	**831**[c]	3296
22	6	3120	3474
24	6	3563	3890
26	6	3845	4061

[a]Current electrode half separation
[b]Potential electrode separation
[c]Detection point of the copper wire lump

Table 4.22. Resistivity values of the laboratory prototype with a copper wire lump at 20-cm depth with the centre of the wire lump as the reference point

AB/2[a] (cm)	MN[b] (cm)	Resistivity, ρ (Ωm)	
		With anomaly	Without anomaly
4	4	43	45
6	4	57	62
8	4	61	63
10	4	77	80
12	4	1021	1141
14	4	1321	1508
16	6	1840	2101
18	6	2605	3040
20	6	2801	3296
22	6	**783**[c]	3474
24	6	**887**[c]	3890
26	6	**1010**[c]	4061

[a]Current electrode half separation
[b]Potential electrode separation
[c]Detection point of the copper wire lump

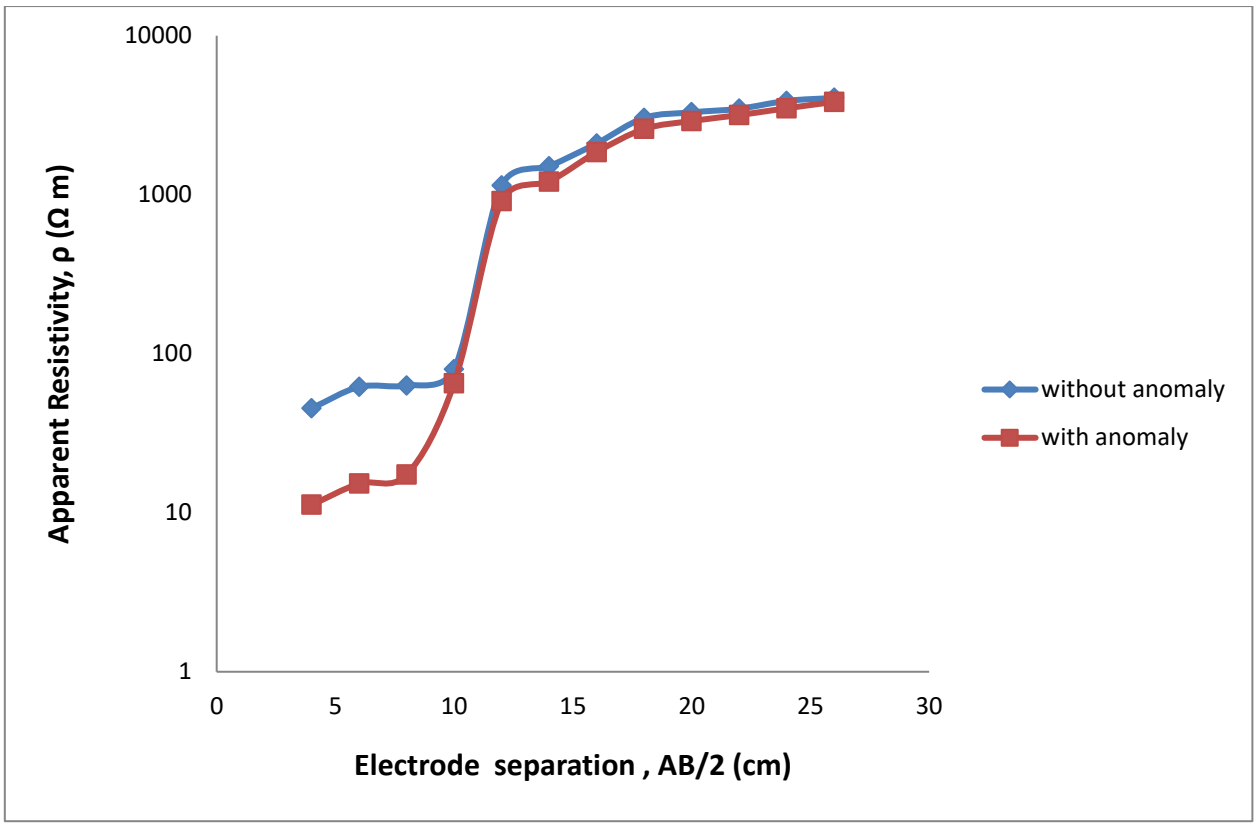

Fig. 4.20. Resistivity plots of the laboratory prototype with a copper wire lump at 5-cm depth

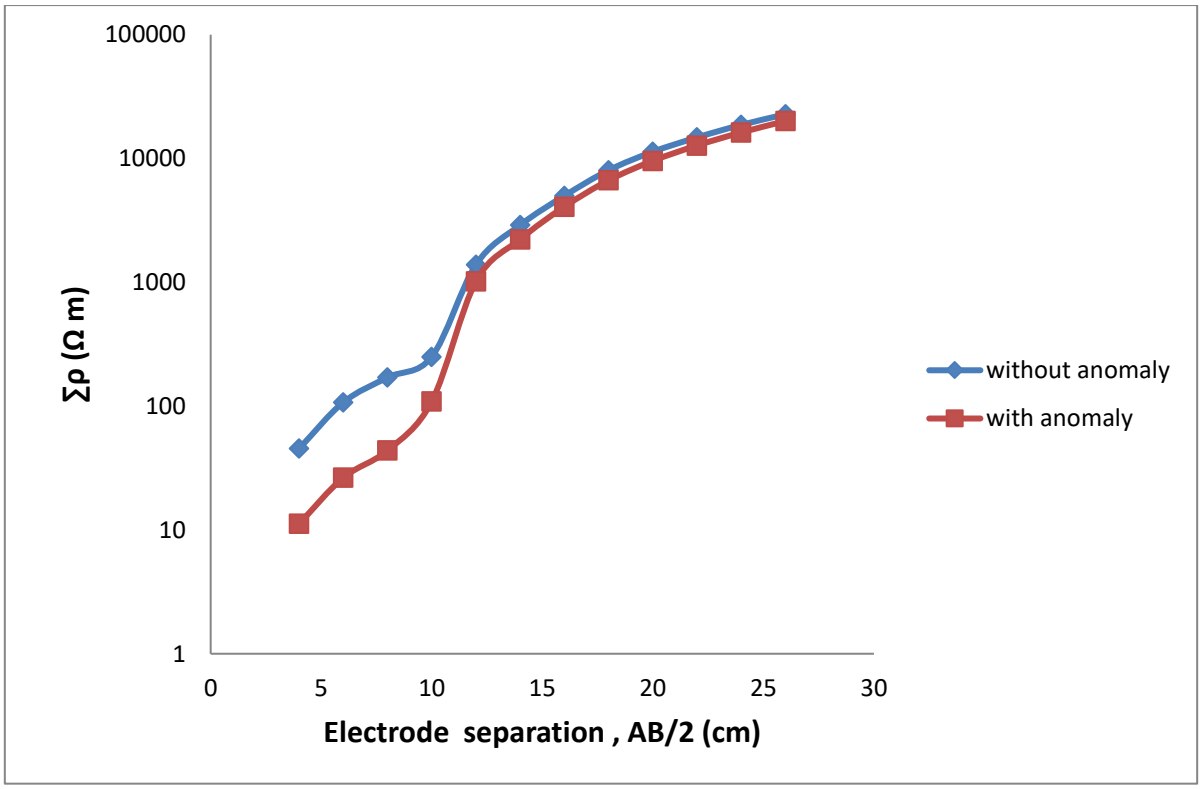

Fig. 4.21. Cumulative resistivity plots of the laboratory prototype with a copper wire lump at 5-cm depth

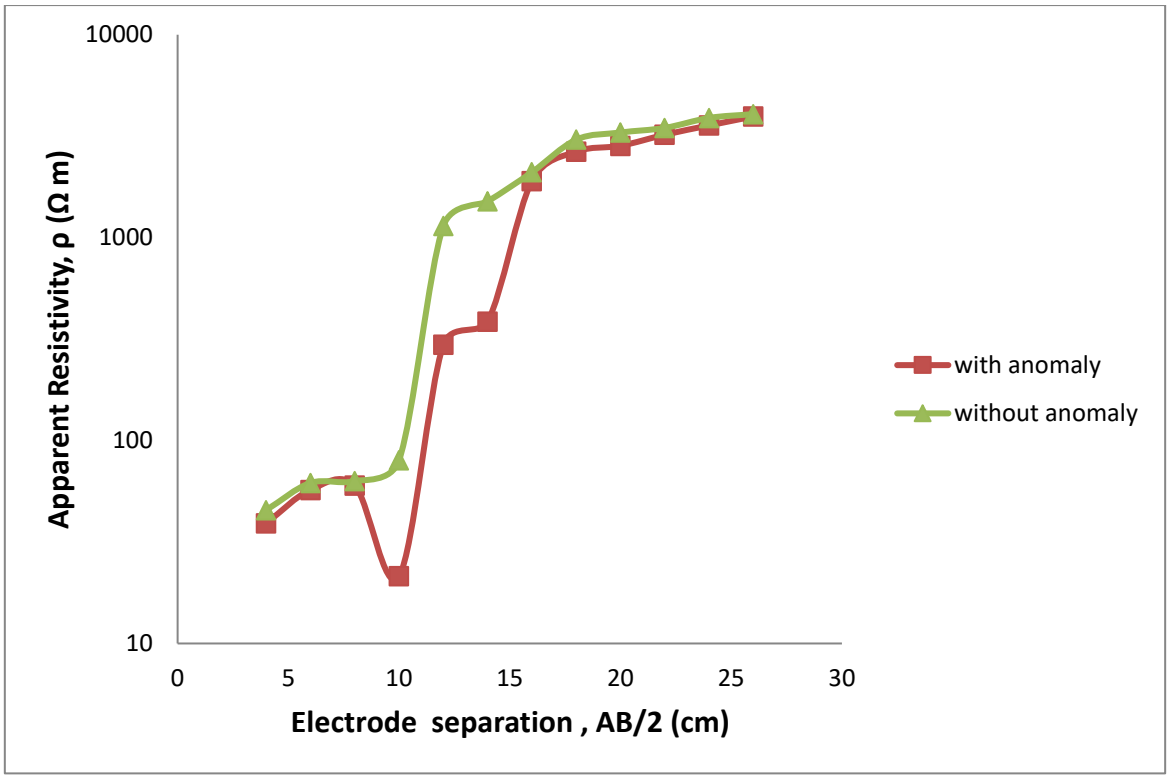

Fig. 4.22. Resistivity plots of the laboratory prototype with a copper wire lump at 10-cm depth

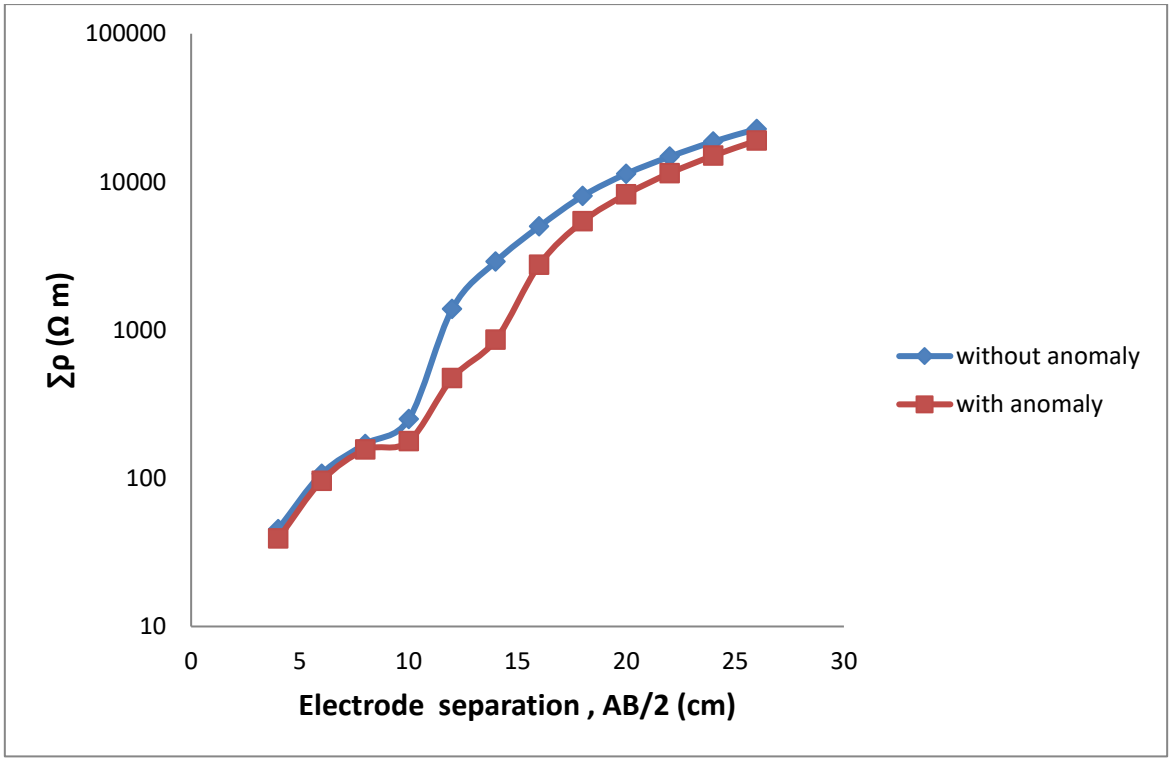

Fig. 4.23. Cumulative resistivity plots of the laboratory prototype with a copper wire lump at 10-cm depth

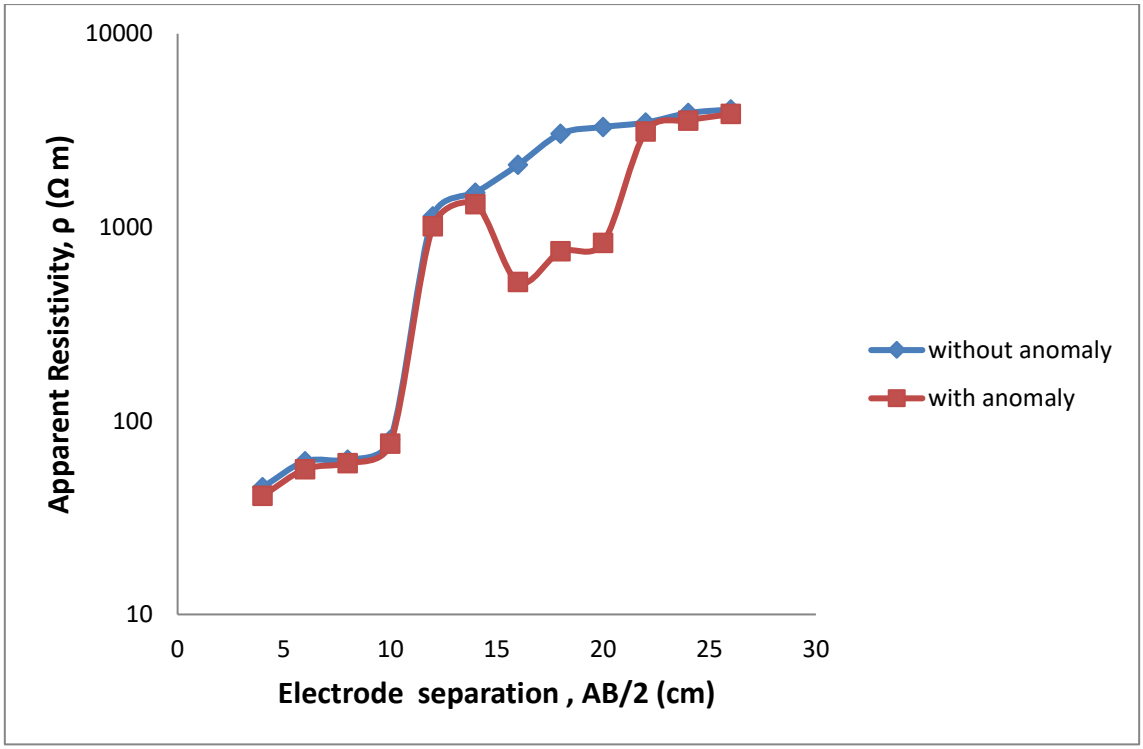

Fig. 4.24. Resistivity plots of the laboratory prototype with a copper wire lump at 15-cm depth

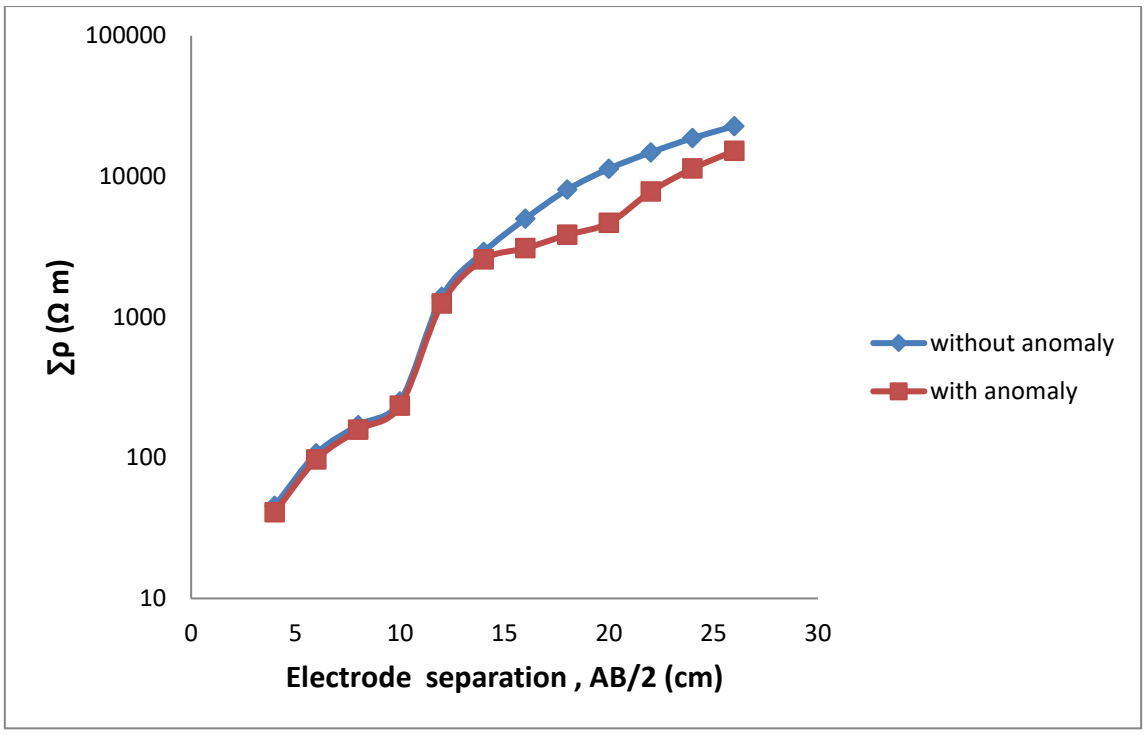

Fig. 4.25. Cumulative resistivity plots of the laboratory prototype with a copper wire lump at 15-cm depth

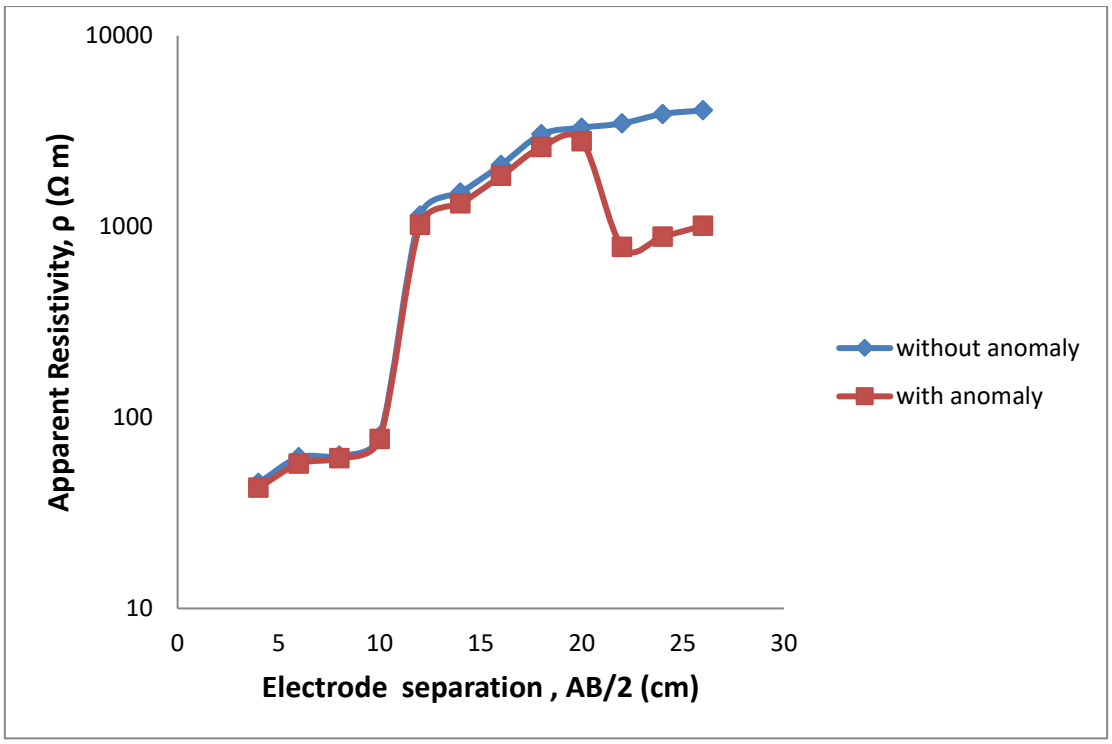

Fig. 4.26. Resistivity plots of the laboratory prototype with a copper wire lump at 20-cm depth

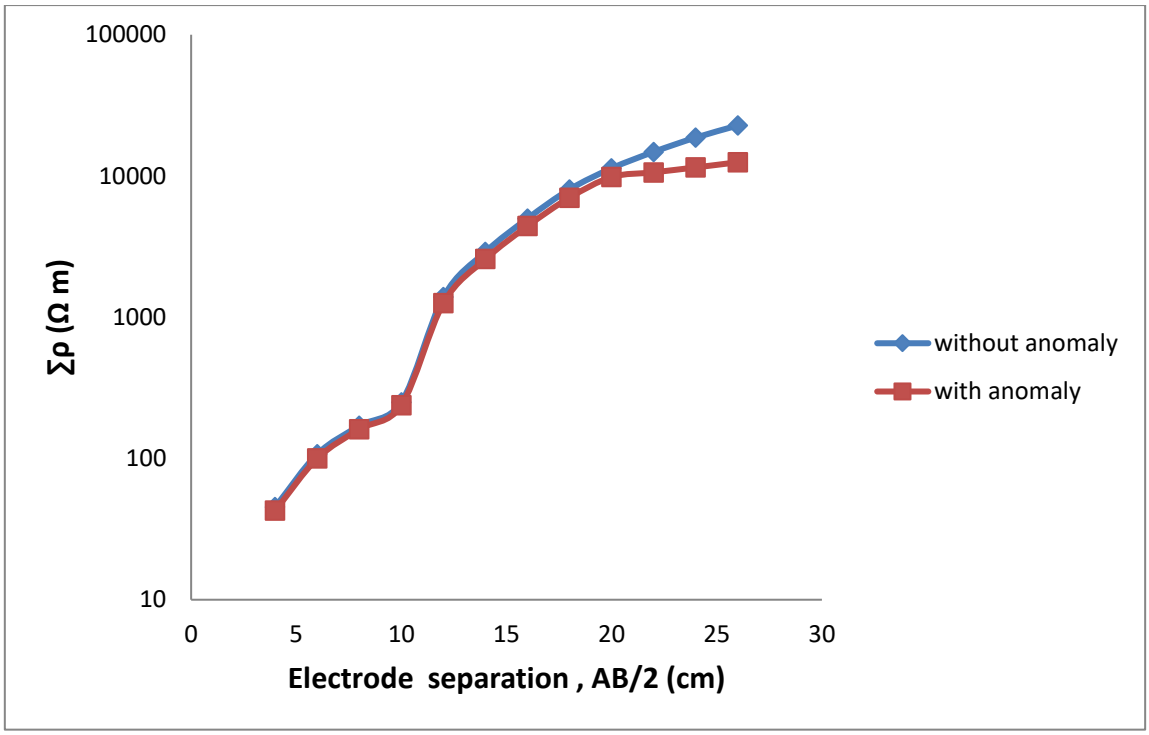

Fig. 4.27. Cumulative resistivity plots of the laboratory prototype with a copper wire lump at 20-cm depth

Table 4.23. Resistivity values of the laboratory prototype with a hollow at 4-cm depth with the centre of the hollow as the reference point

AB/2[a] (cm)	MN[b] (cm)	Resistivity, ρ (Ωm)	
		With anomaly	Without anomaly
4	4	**155**[c]	45
6	4	**206**[c]	62
8	4	**215**[c]	63
10	4	**271**[c]	80
12	4	1250	1141
14	4	1630	1508
16	6	2251	2101
18	6	3152	3040
20	6	3402	3296
22	6	3587	3474
24	6	4002	3890
26	6	4179	4061

[a]Current electrode half separation
[b]Potential electrode separation
[c]Detection point of the modelled hollow

Table 4.24. Resistivity values of the laboratory prototype with a hollow at 12-cm depth with the centre of the hollow as the reference point

AB/2[a] (cm)	MN[b] (cm)	Resistivity, ρ (Ωm)	
		With anomaly	Without anomaly
4	4	57	45
6	4	74	62
8	4	80	63
10	4	93	80
12	4	**3546**[c]	1141
14	4	**4832**[c]	1508
16	6	**6935**[c]	2101
18	6	**10043**[c]	3040
20	6	3413	3296
22	6	3592	3474
24	6	4002	3890
26	6	4185	4062

[a]Current electrode half separation
[b]Potential electrode separation
[c]Detection point of the modelled hollow

Table 4.25. Resistivity values of the laboratory prototype with a hollow at 20-cm depth with the centre of the hollow as the reference point

AB/2[a] (cm)	MN[b] (cm)	Resistivity, ρ(Ωm)	
		With anomaly	Without anomaly
4	4	59	45
6	4	77	62
8	4	85	63
10	4	99	80
12	4	1252	1141
14	4	1641	1508
16	6	2280	2101
18	6	3246	3041
20	6	**10389**[c]	3296
22	6	**11215**[c]	3474
24	6	**12503**[c]	3890
26	6	**12995**[c]	4062

[a]Current electrode half separation
[b]Potential electrode separation
[c]Detection point of the modelled hollow

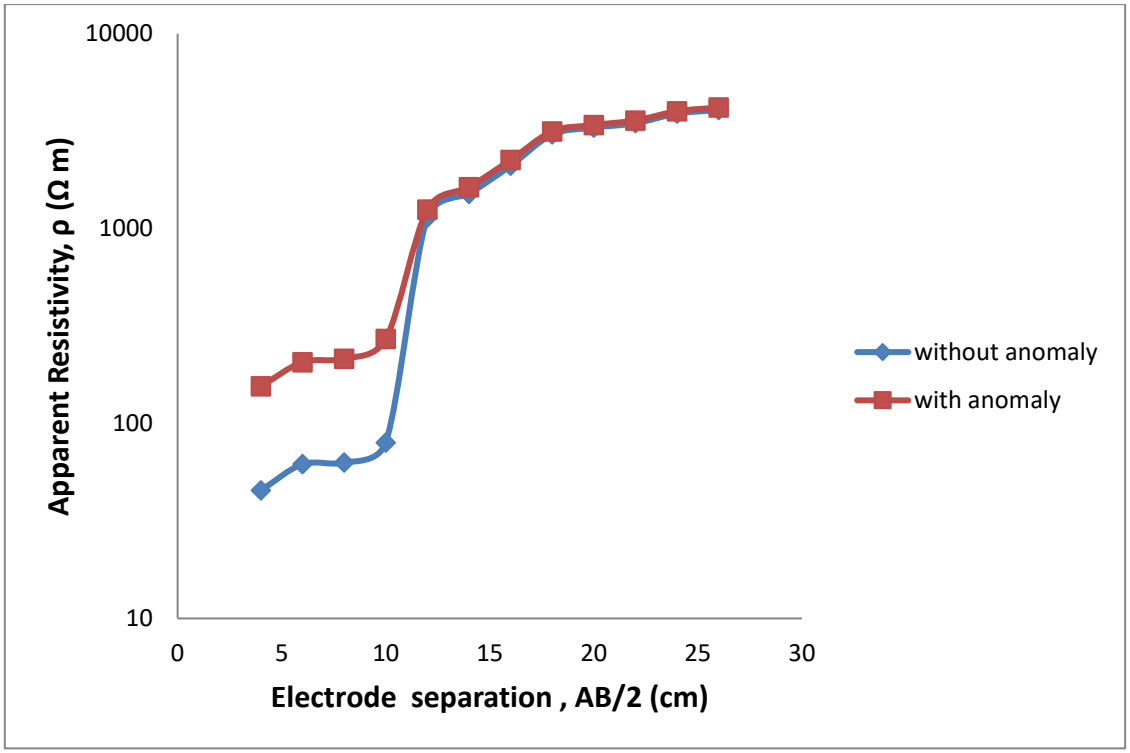

Fig. 4.28. Resistivity plots of the laboratory prototype with a hollow 4-cm depth

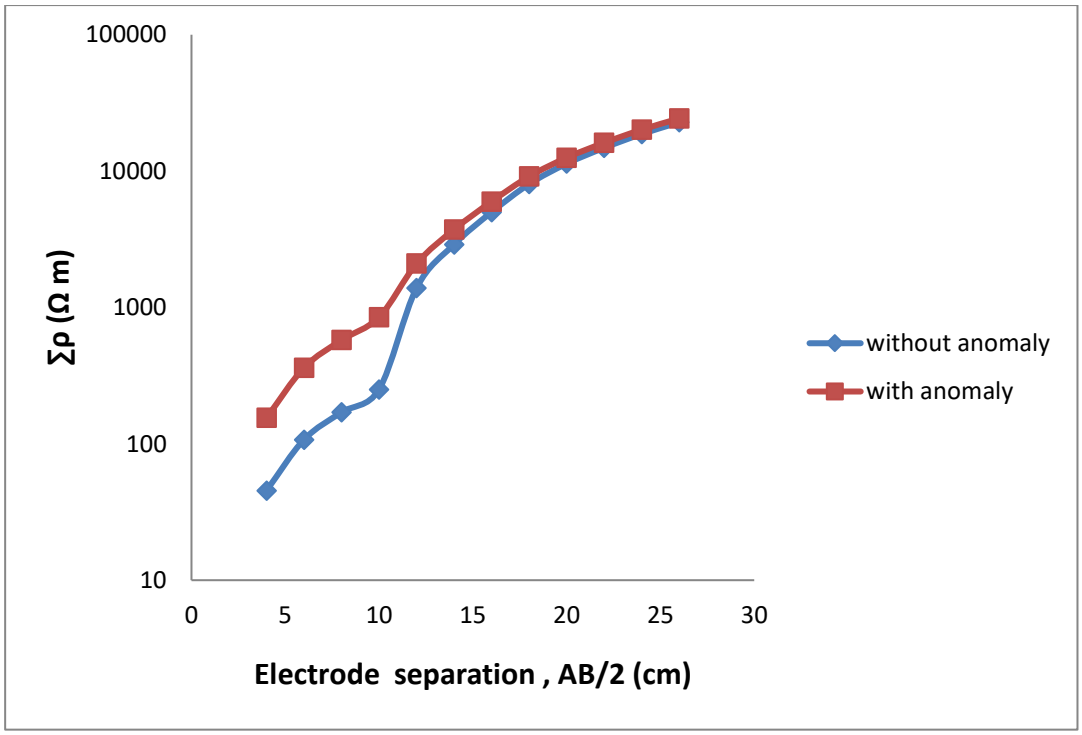

Fig. 4.29. Cumulative resistivity plots of the laboratory prototype with a hollow at 4-cm depth

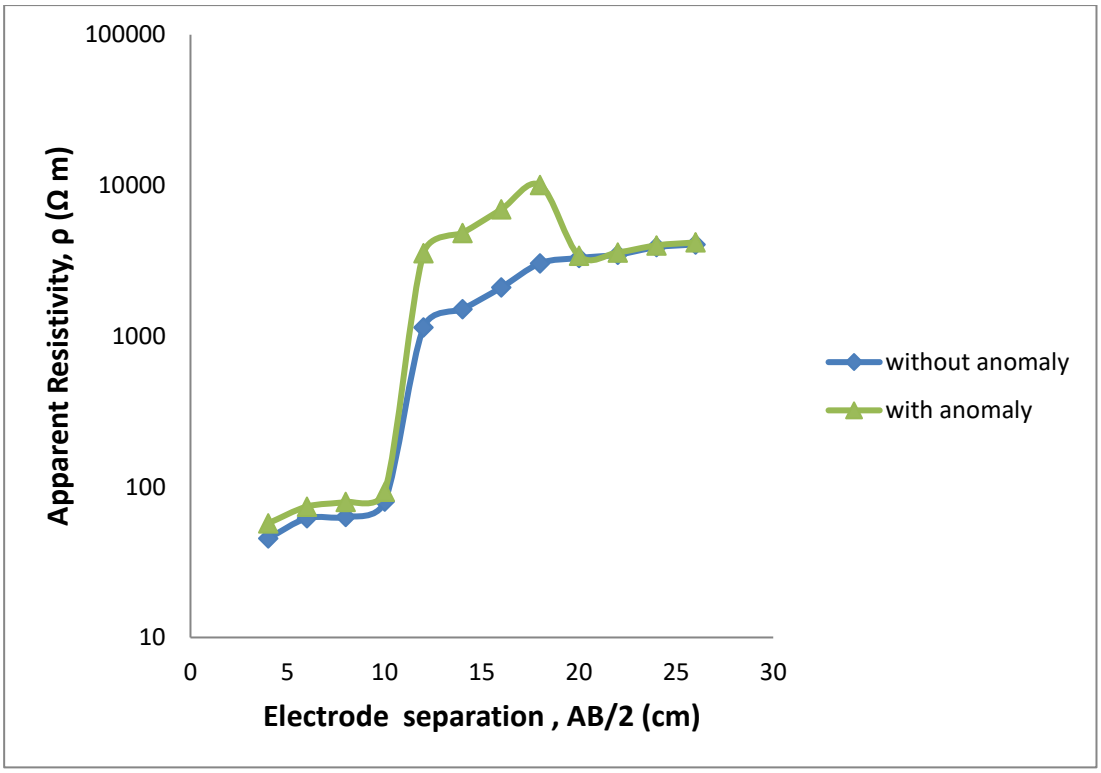

Fig. 4.30. Resistivity plots of the laboratory prototype with a hollow at 12-cm depth

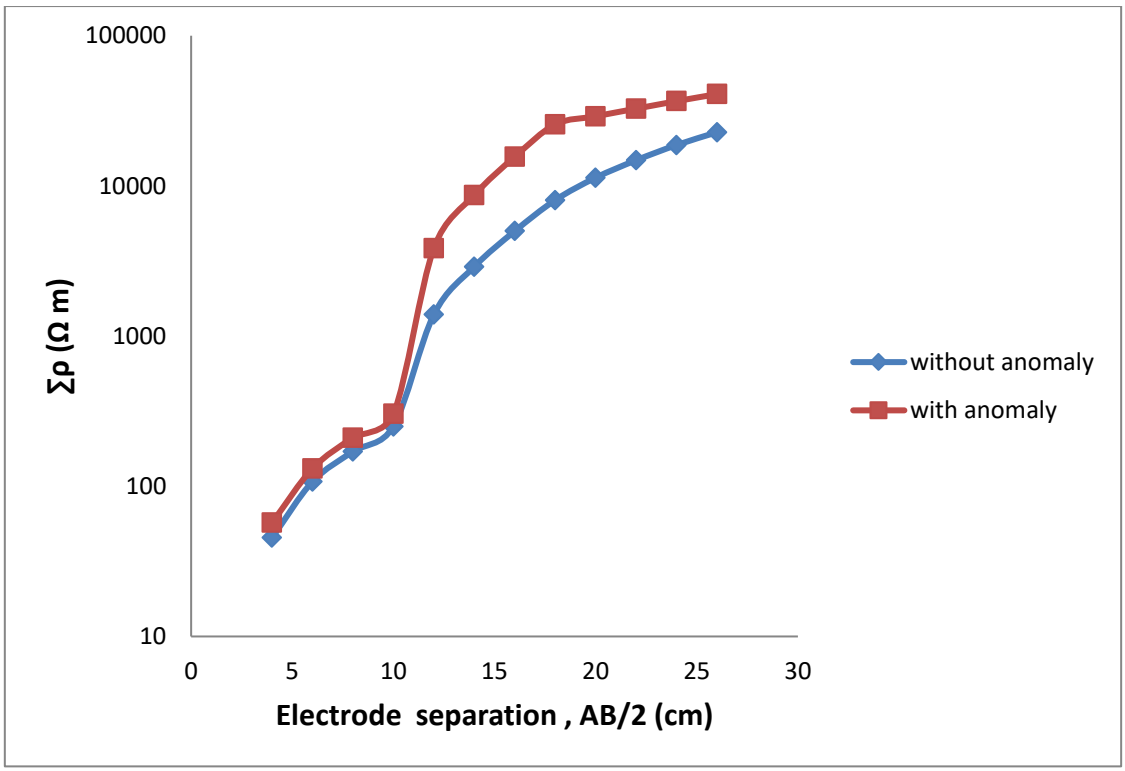

Fig. 4.31. Cumulative resistivity plots of the laboratory prototype with a hollow at 12-cm depth

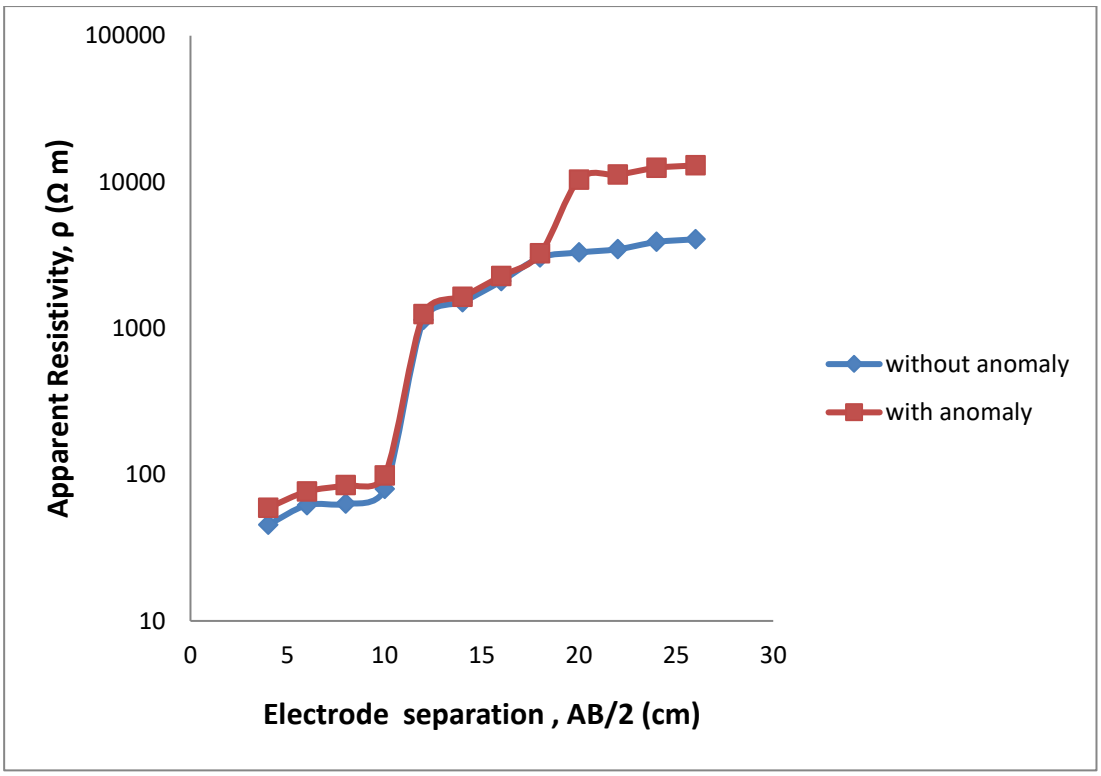

Fig. 4.32. Resistivity plots of the laboratory prototype with a hollow at 20-cm depth

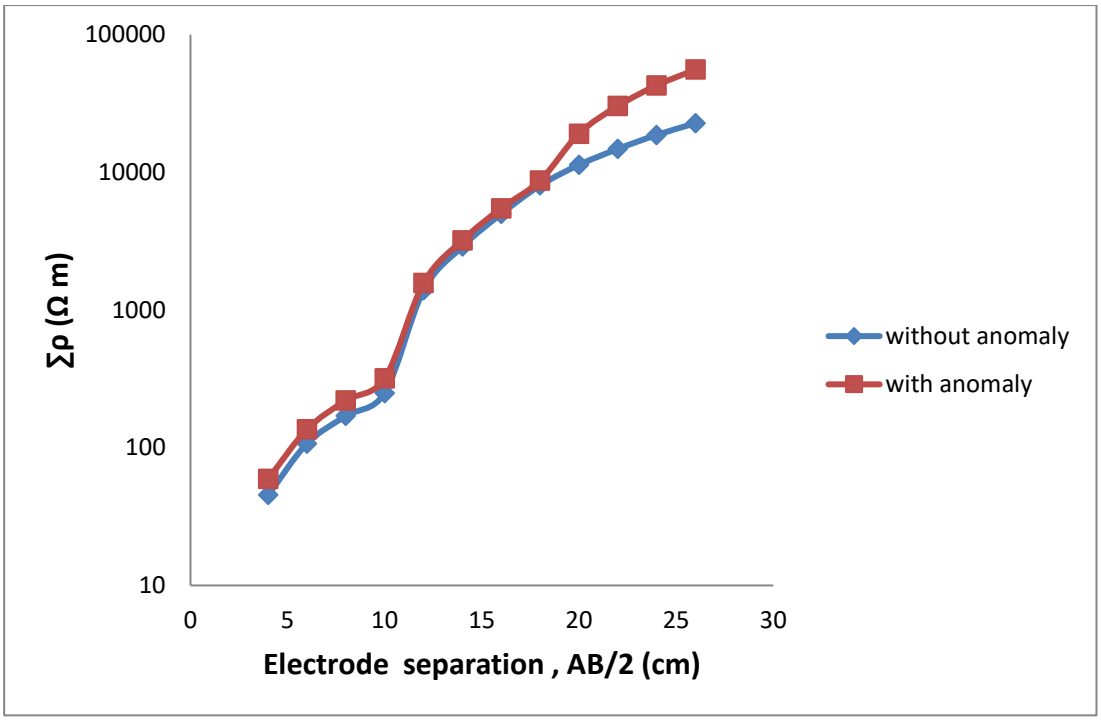

Fig. 4.33. Cumulative resistivity plots of the laboratory prototype with a hollow at 20-cm depth

Table 4.26. Resistivity values of the laboratory prototype with a copper wire lump at 5-cm depth and a hollow at 14.5-cm depth[+]

Current Electrode Half Separation AB/2 (cm)	Potential Electrode Separation MN (cm)	Resistivity, ρ(Ωm)	
		With anomaly	Without anomaly
4	4	**11[c]**	45
6	4	**15[c]**	62
8	4	**16[c]**	63
10	4	**446[d]**	80
12	4	**4653[d]**	1141
14	4	**6372[d]**	1508
16	6	**11563[d]**	2101
18	6	**16704[d]**	3040
20	6	**18132[d]**	3296
22	6	3612	3474
24	6	4001	3890
26	6	4175	4061

[c]Detection point of the copper wire lump
[d]Detection point of the modelled hollow
[+]The centres of the copper wire lump and hollow are the reference points for the depths

Hollow diameter: 14 cm
Hollow length: 20 cm
Length of copper wire lump: 20 cm
Thickness of copper wire lump: 5 cm

Table 4.27. Resistivity values of the laboratory prototype with a hollow at 8-cm depth and a copper wire at 22.5-cm depth[+]

Current Electrode Half Separation AB/2 (cm)	Potential Electrode Separation MN (cm)	Resistivity, ρ(Ωm)	
		With anomaly	Without anomaly
4	4	**255[d]**	45
6	4	**349[d]**	62
8	4	**360[d]**	63
10	4	**463[d]**	80
12	4	**6272[d]**	1141
14	4	**8458[d]**	1508
16	6	2198	2101
18	6	3137	3040
20	6	3402	3296
22	6	**872[c]**	3474
24	6	**979[c]**	3890
26	6	**1023[c]**	4061

[c]Detection point of the copper wire lump
[d]Detection point of the modelled hollow
[+]The centres of the copper wire lump and hollow are the reference points for the depths

Hollow diameter: 14 cm
Hollow length: 20 cm
Length of copper wire lump: 20 cm
Thickness of copper wire lump: 5 cm

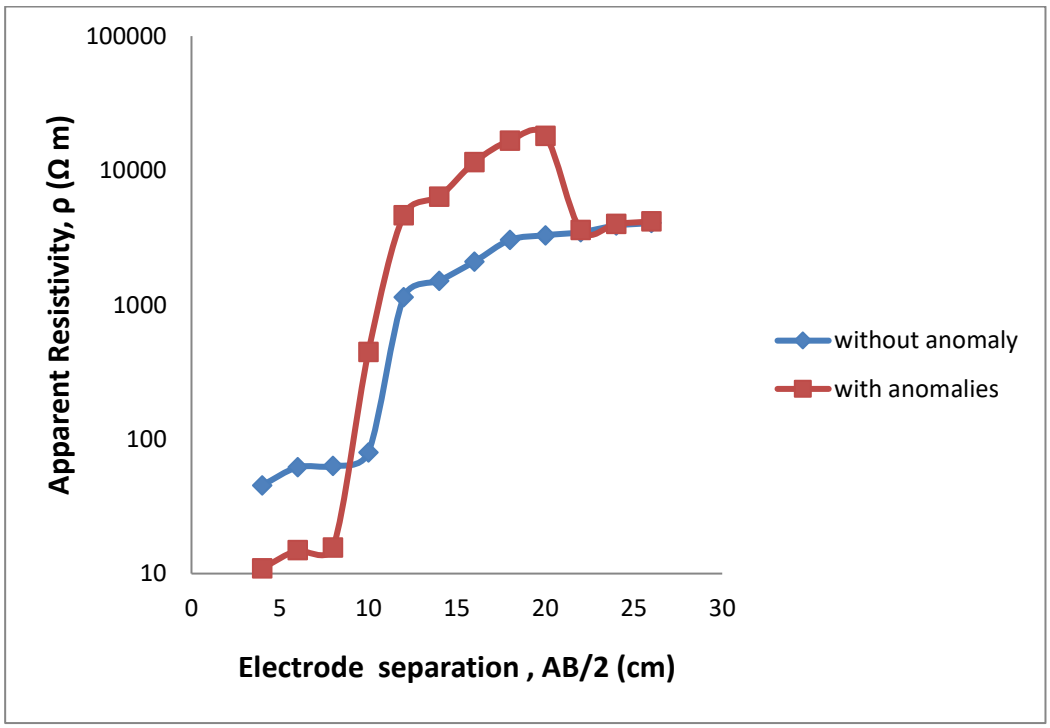

Fig. 4.34. Apparent resistivity plots of the laboratory prototype with a copper wire lump at 5-cm depth and a hollow at 14.5-cm depth

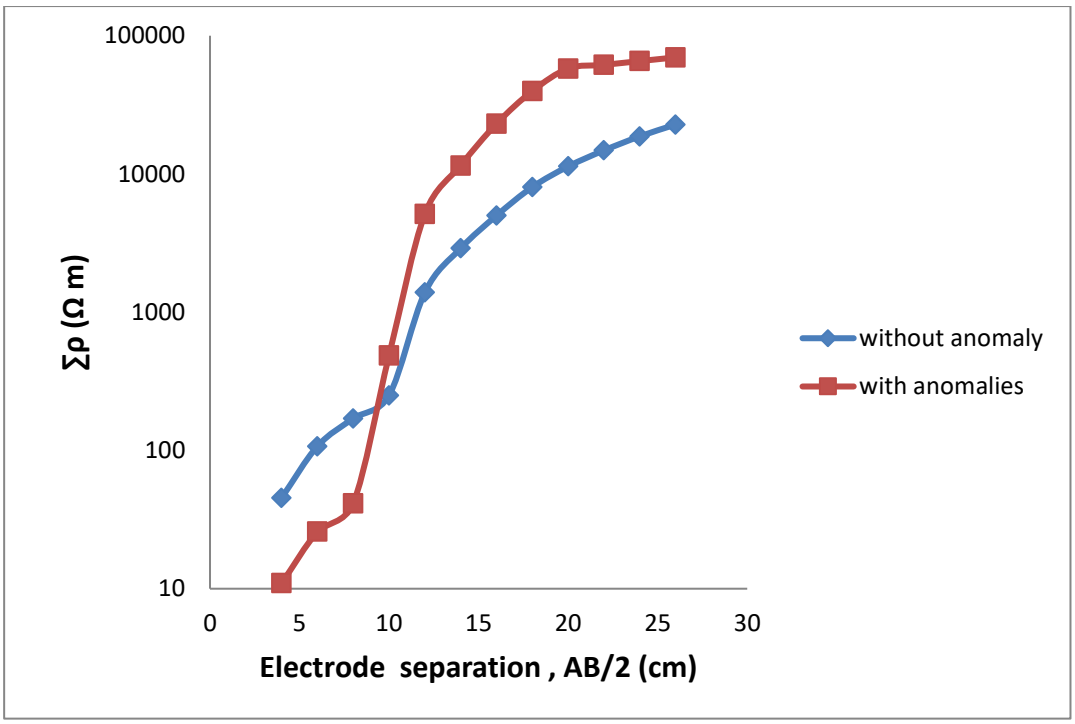

Fig. 4.35. Cumulative resistivity plots of the laboratory prototype with a copper wire at 5-cm depth and a hollow at 14.5-cm depth

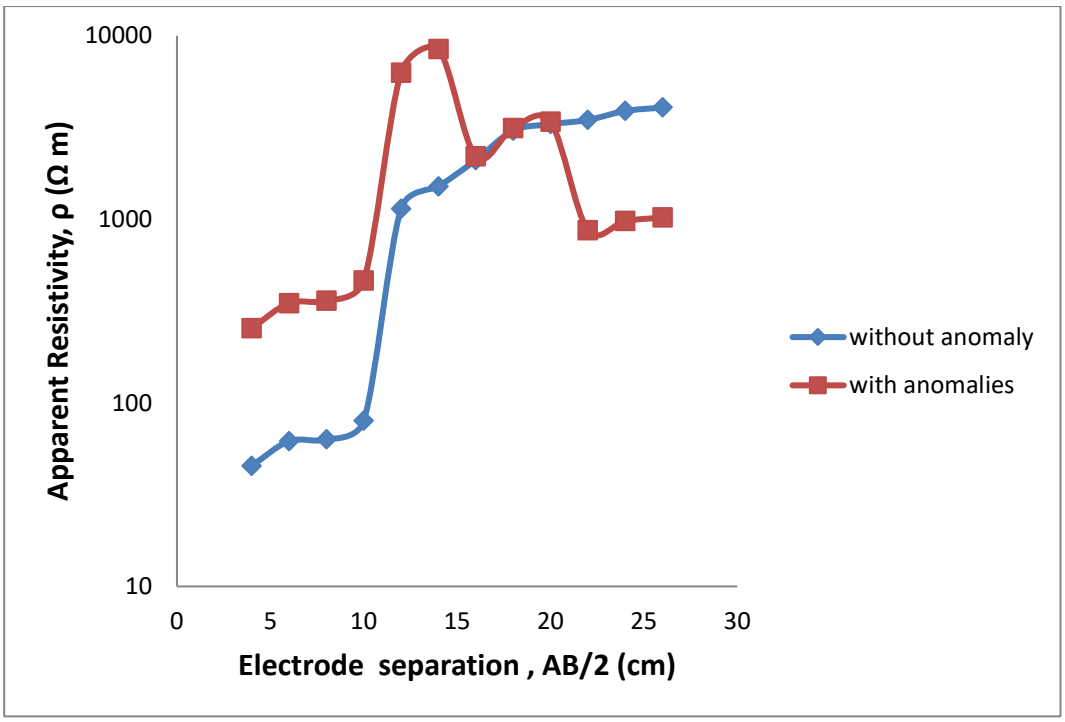

Fig. 4.36. Apparent resistivity plots of the laboratory prototype with a hollow at 8-cm depth and a copper wire lump at 22.5-cm depth

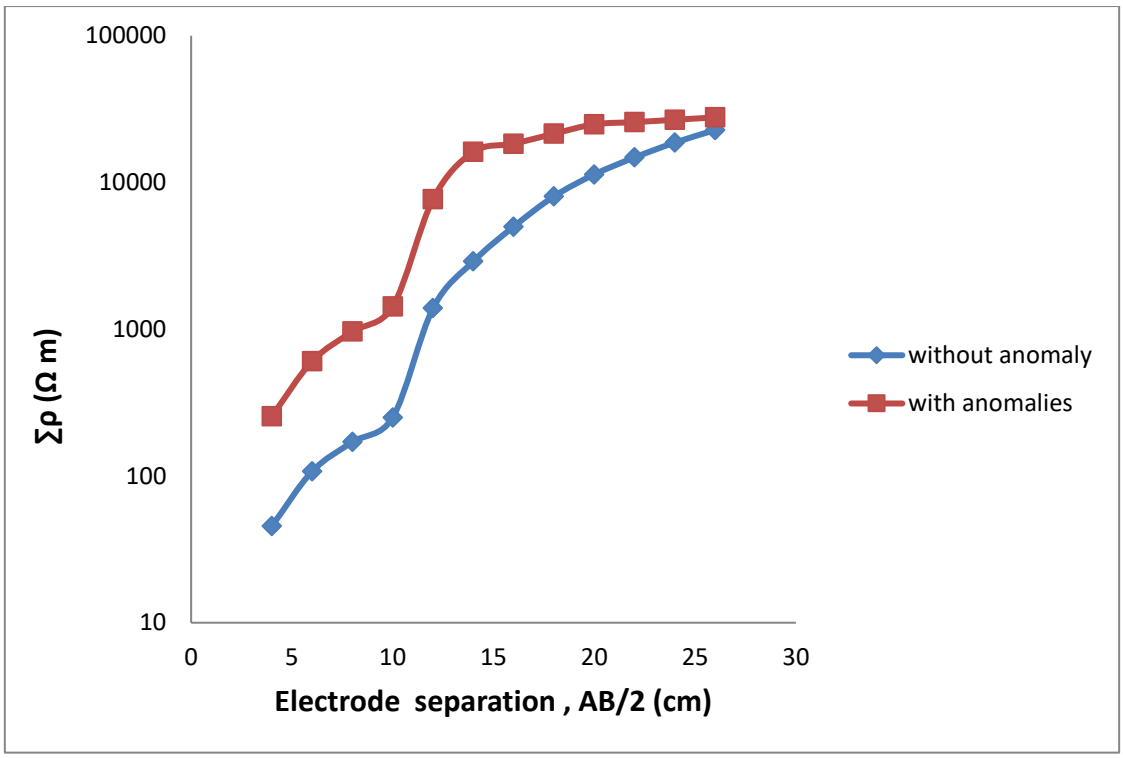

Fig. 4.37. Cumulative resistivity plots of the laboratory prototype with a hollow at 5-cm depth and a copper wire lump at 14.5-cm depth

Table 4.28. Resistivity values of the laboratory prototype with copper wire lumps of length 15 cm and of different thicknesses

AB/2[a] (cm)	MN[b] (cm)	Resistivity, ρ (Ωm)			
		Thickness: 5 cm	8 cm	12 cm	Without anomaly
4	4	**23**[c]	**16**[c]	**13**[c]	81
6	4	**32**[c]	**25**[c]	**20**[c]	128
8	4	**34**[c]	**27**[c]	**22**[c]	135
10	4	131	**28**[c]	**22**[c]	142
12	4	143	140	**24**[c]	153
14	4	155	151	141	162
16	6	241	238	231	249
18	6	5530	5501	5452	5826
20	6	5891	5872	5832	6158
22	6	6136	6119	6081	6425
24	6	6294	6280	6235	6578
26	6	6521	6505	6462	6817

[a]Current electrode half separation
[b]Potential electrode separation
[c]Detection point of the copper wire lump

Table 4.29. Resistivity values of the laboratory prototype with hollows of length 21 cm and of different diameters

AB/2[a] (cm)	MN[b] (cm)	Resistivity, ρ (Ωm)			
		Hollow diameter: 5 cm	**8 cm**	**12 cm**	**Without anomaly**
4	4	**250[c]**	**328[c]**	**458[c]**	81
6	4	**393[c]**	**516[c]**	**720[c]**	128
8	4	**414[c]**	**546[c]**	**753[c]**	135
10	4	**432[c]**	**579[c]**	**798[c]**	142
12	4	196	**618[c]**	**855[c]**	153
14	4	201	227	**914[c]**	162
16	6	276	300	336	249
18	6	5938	5977	6081	5826
20	6	6265	6315	6420	6158
22	6	6532	6599	6697	6425
24	6	6698	6748	6852	6578
26	6	6929	6985	7096	6817

[a]Current electrode half separation
[b]Potential electrode separation
[c]Detection point of the copper wire lump

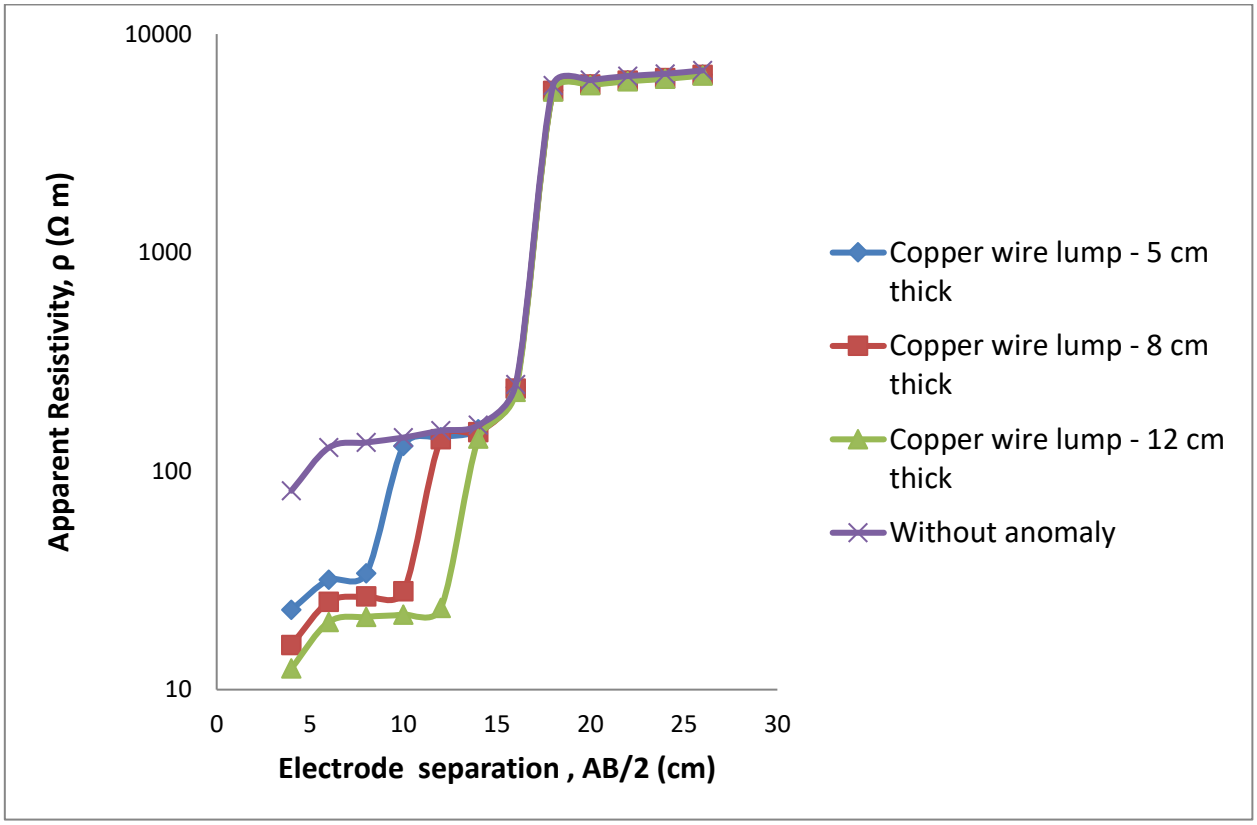

Fig. 4.38. Apparent resistivity plots of the laboratory prototype with copper wire lumps (replicating wood decay) of thicknesses 5 cm, 8 cm and 12 cm inserted at 5-cm, 6.5-cm, and 8.5-cm depths respectively from the centre of the wire lump to the laboratory prototype surface

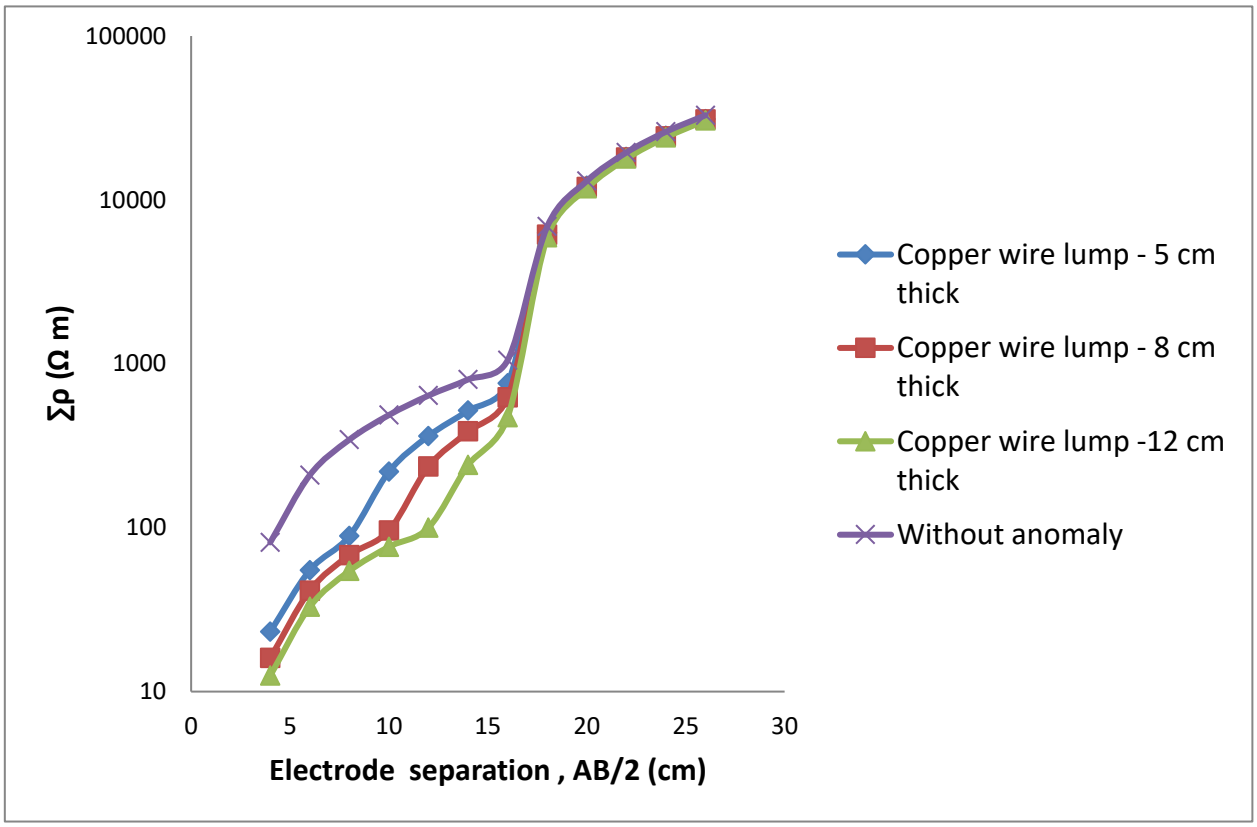

Fig. 4.39. Cumulative resistivity plots of the laboratory prototype with copper wire lumps (replicating wood decay) of thicknesses 5 cm, 8 cm and 12 cm inserted at 5-cm, 6.5-cm, and 8.5-cm depths respectively from the centre of the wire lump to the laboratory prototype surface

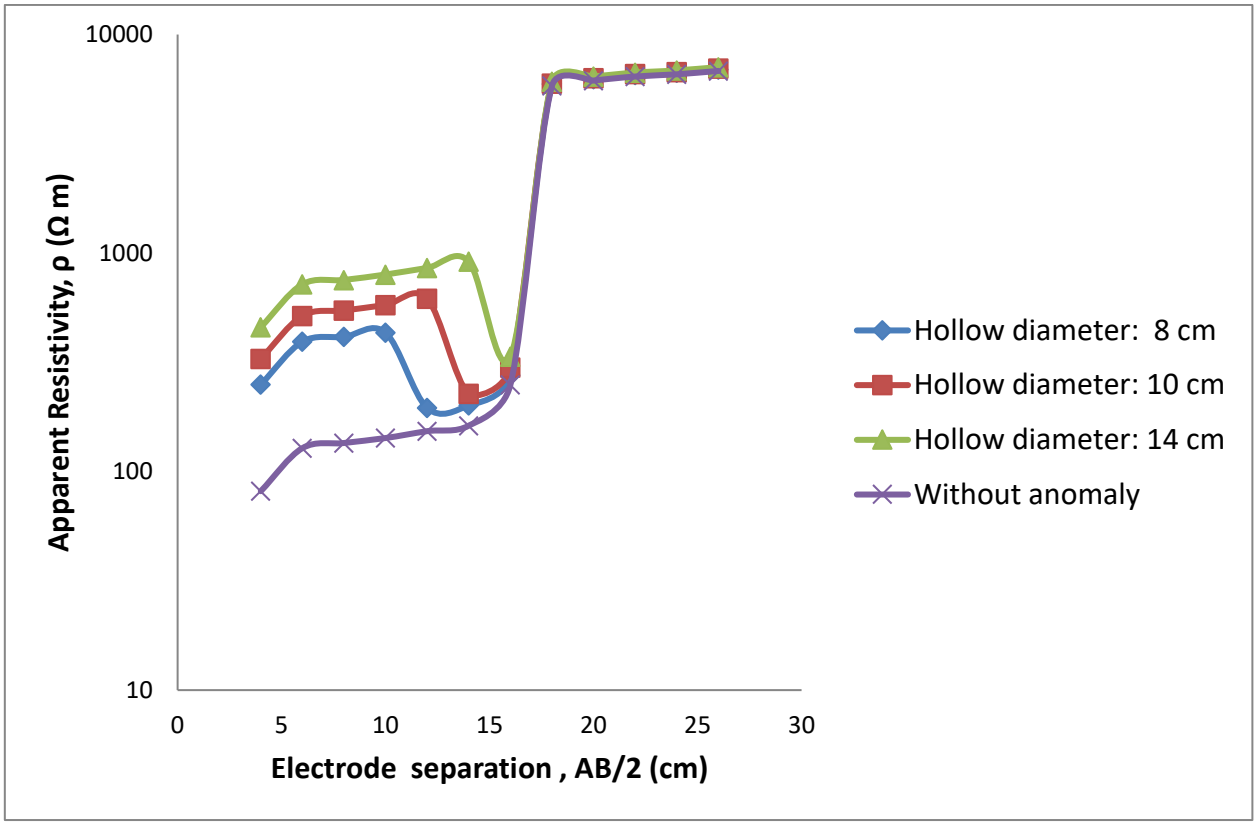

Fig. 4.40. Apparent resistivity plots of the laboratory prototype with hollow of diameters 8 cm, 10 cm and 14 cm inserted at 4-cm, 5-cm, and 7-cm depths respectively from the centre of the hollow to the laboratory prototype surface

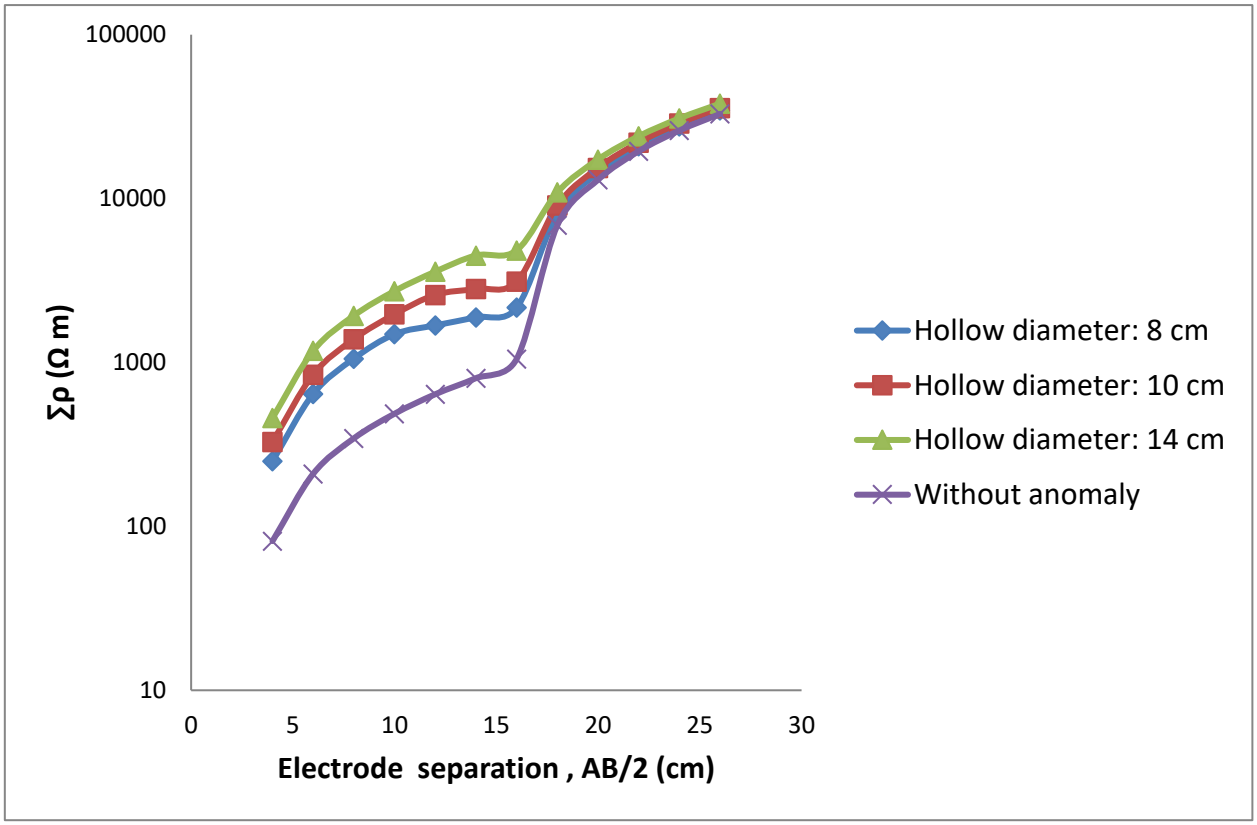

Fig. 4.41. Cumulative resistivity plots of the laboratory prototype with hollow of diameters 8 cm, 10 cm and 14 cm inserted at 4-cm, 5-cm, and 7-cm depths respectively from the centre of the hollow to the laboratory prototype surface

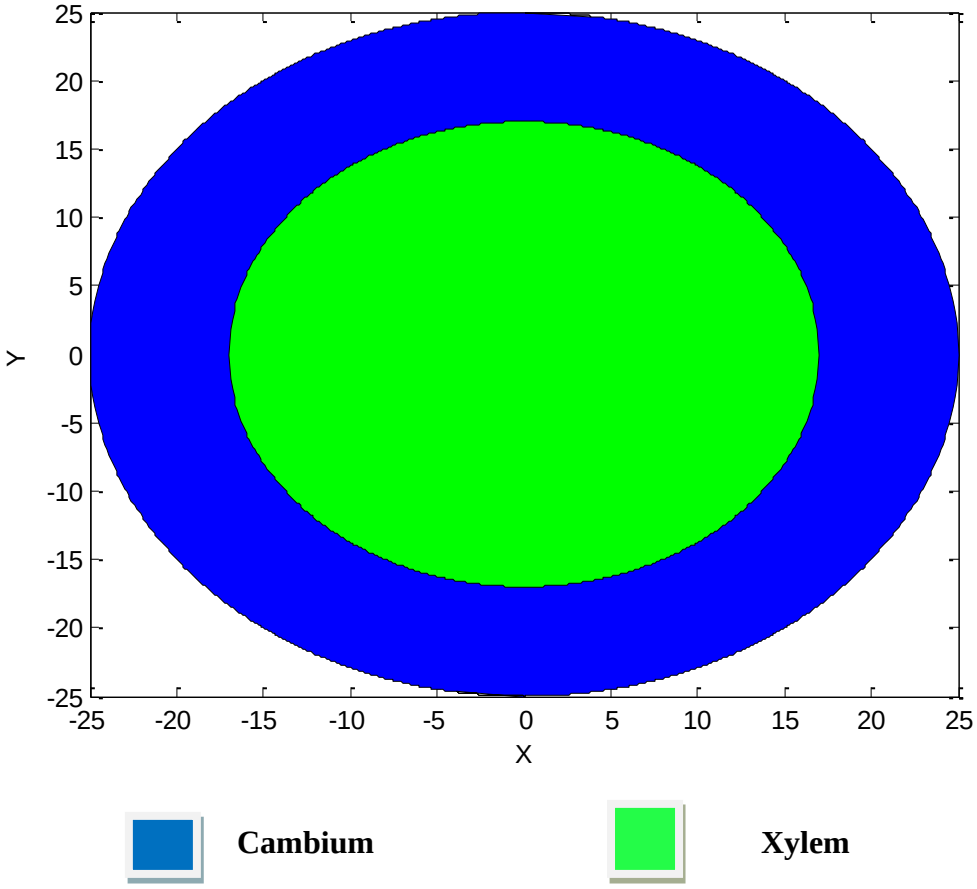

Fig. 4.42. A 2-D image of the cross-section of a healthy tree showing the cambium and xylem

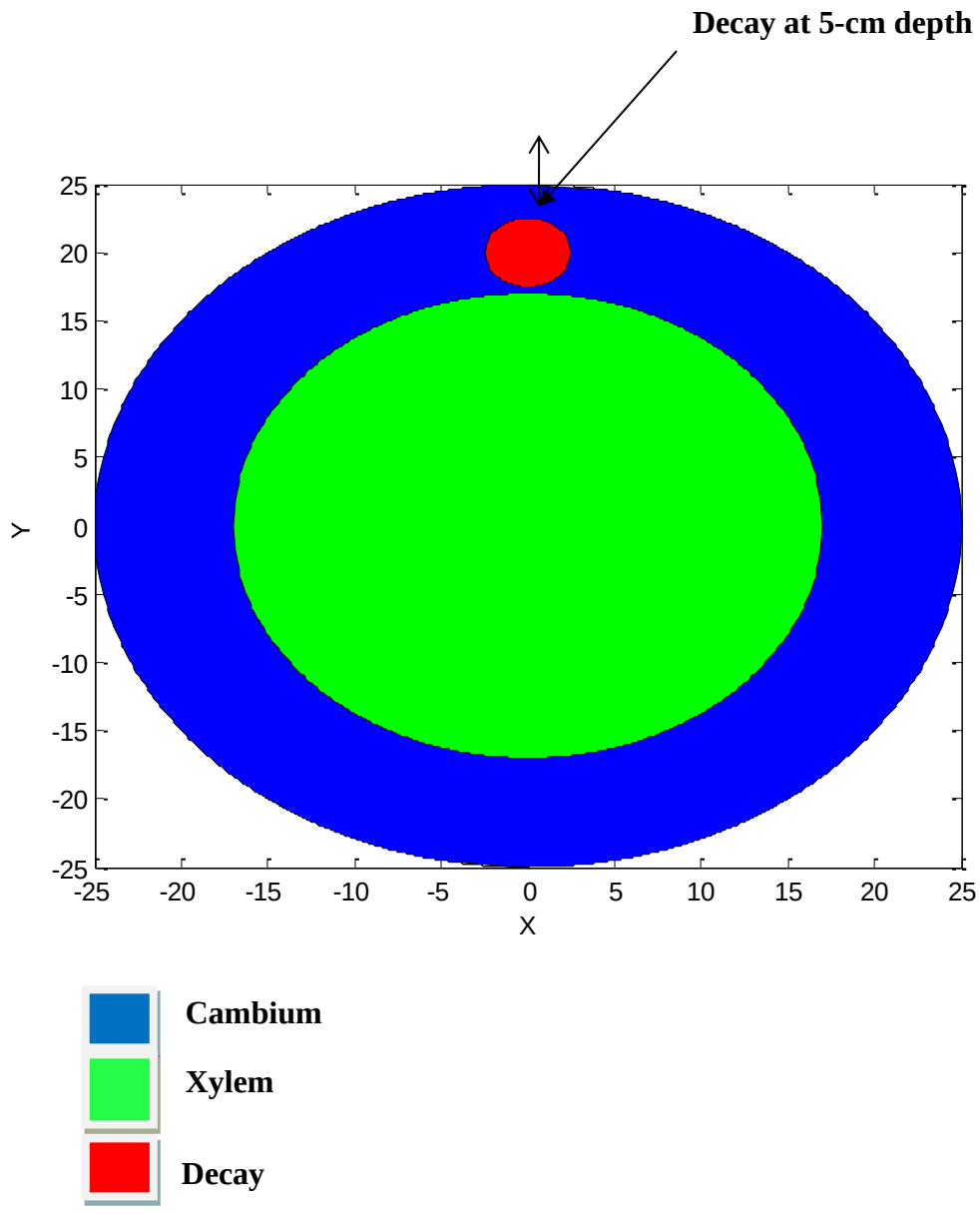

Fig. 4.43. A 2-D image of the cross-section of a decayed tree with wood decay of diameter 5 cm located in the cambium at 5-cm depth with the centre of the decay as the reference point

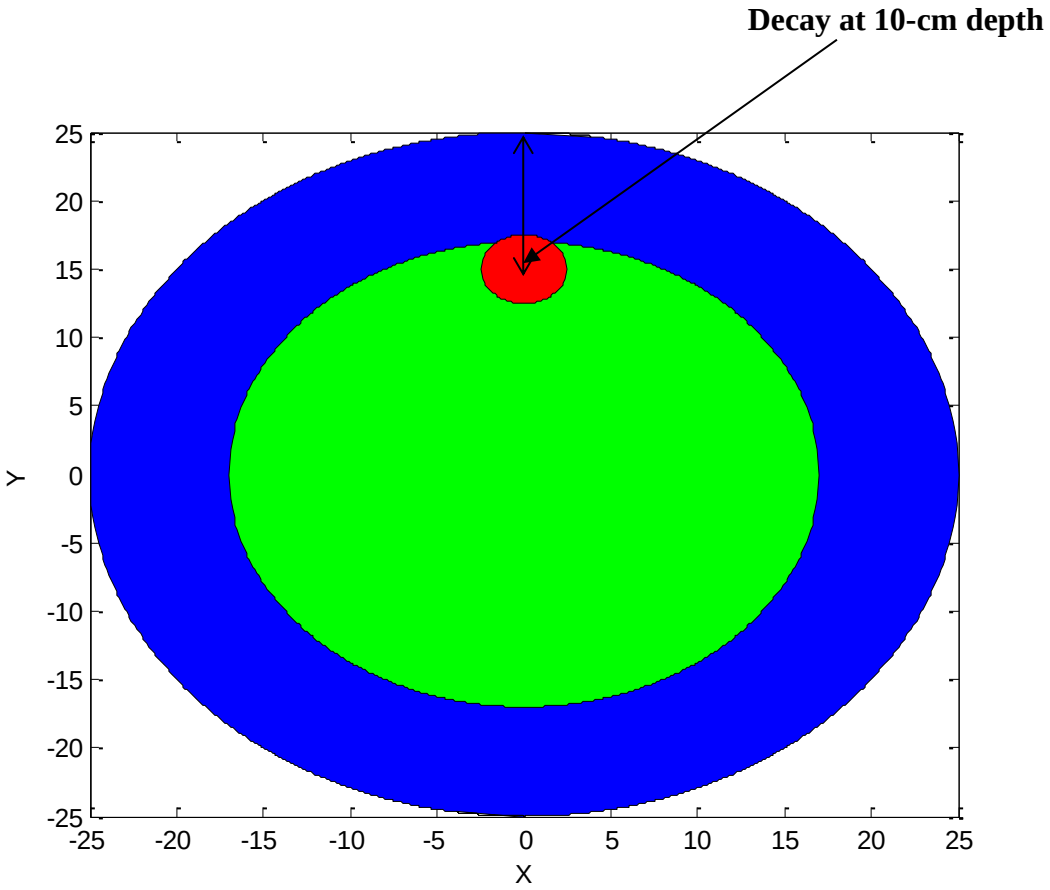

Fig. 4.44. A 2-D image of the cross-section of a decayed tree with wood decay of diameter 5 cm located in both cambium and xylem at 10-cm depth with the centre of the decay as the reference point

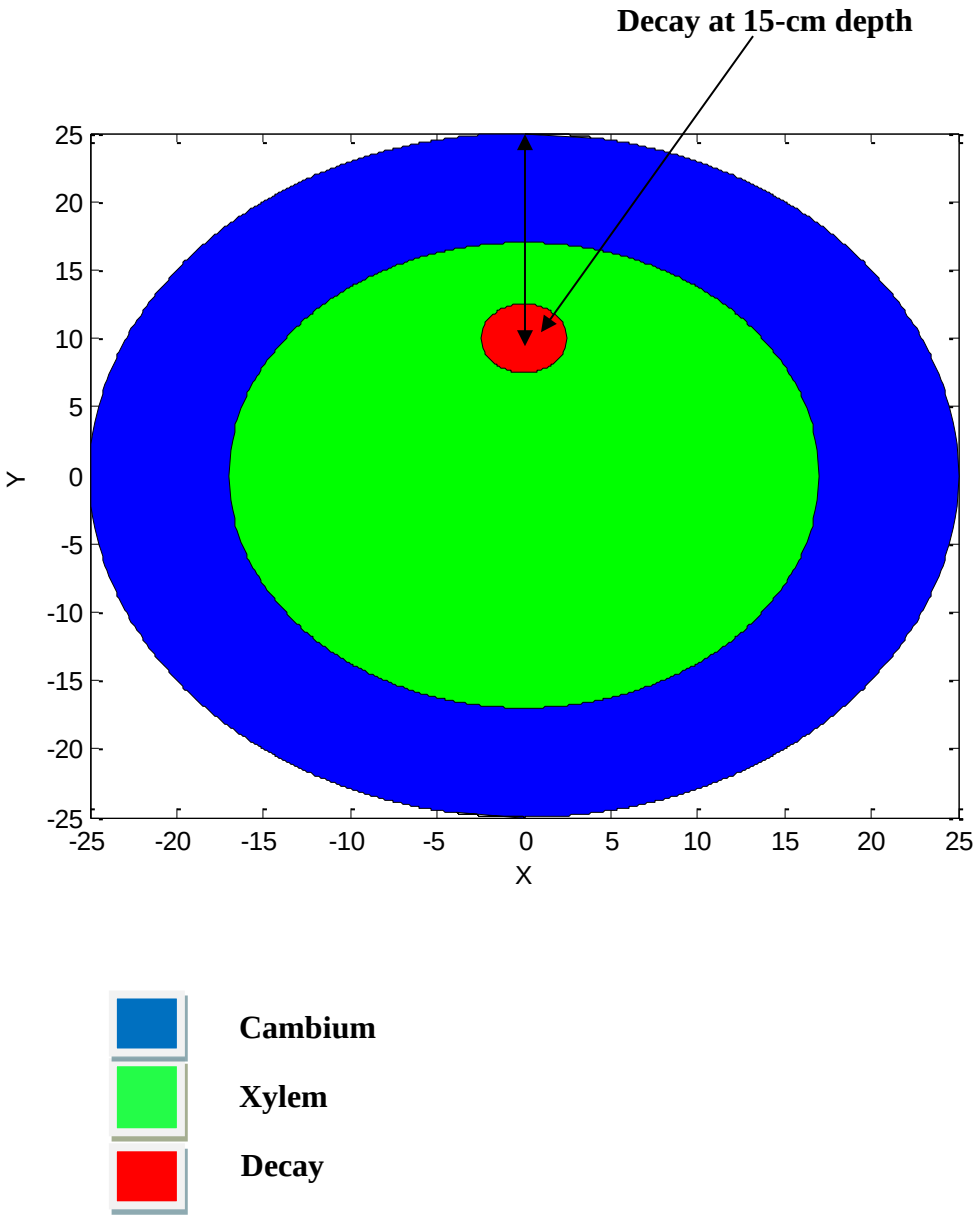

Fig. 4.45. A 2-D image of the cross-section of a decayed tree with wood decay of diameter 5 cm located in the xylem at 15-cm depth with the centre of the decay as the reference point

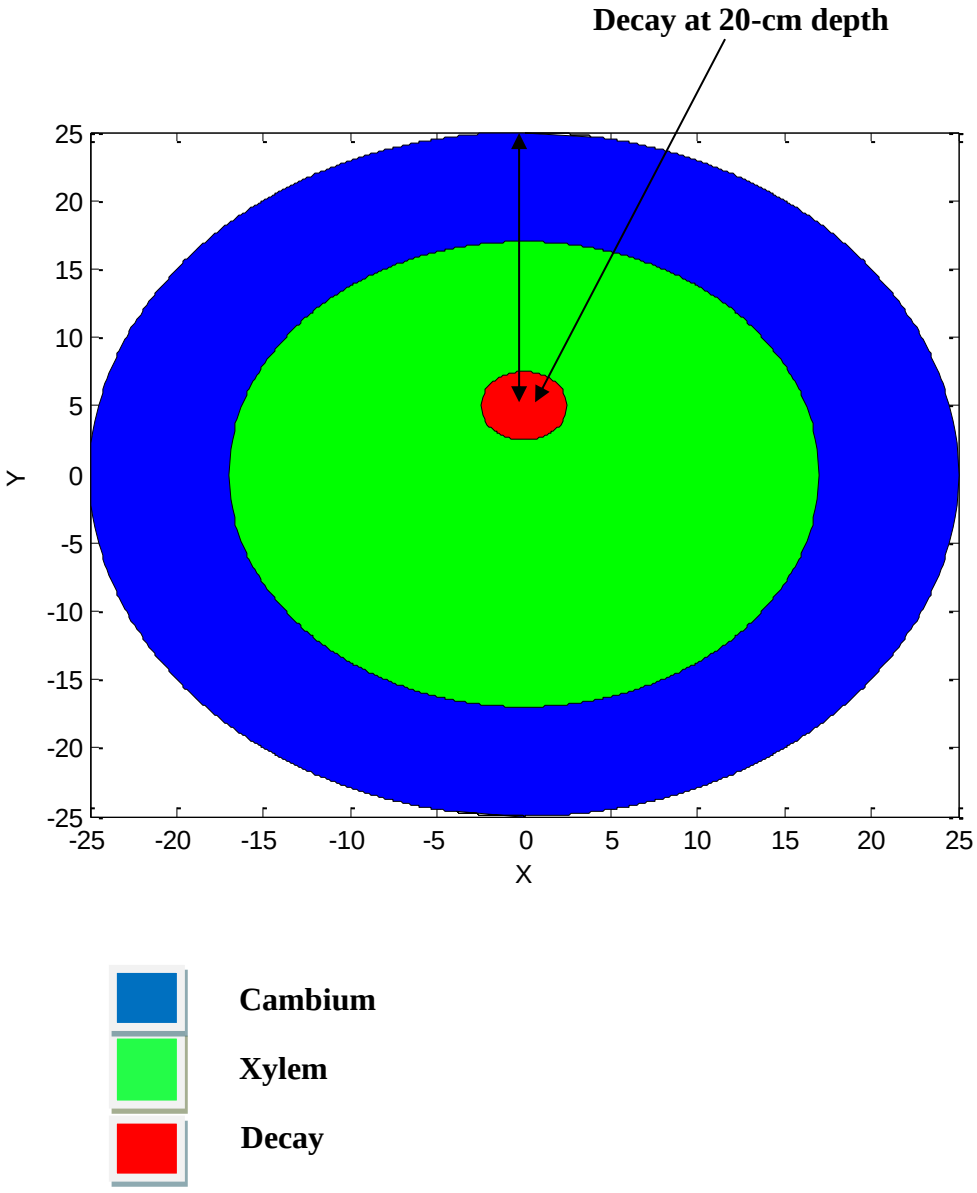

Fig. 4.46. A 2-D image of the cross-section of a decayed tree with wood decay of diameter 5 cm located in the xylem at 20-cm depth with the centre of the decay as the reference point

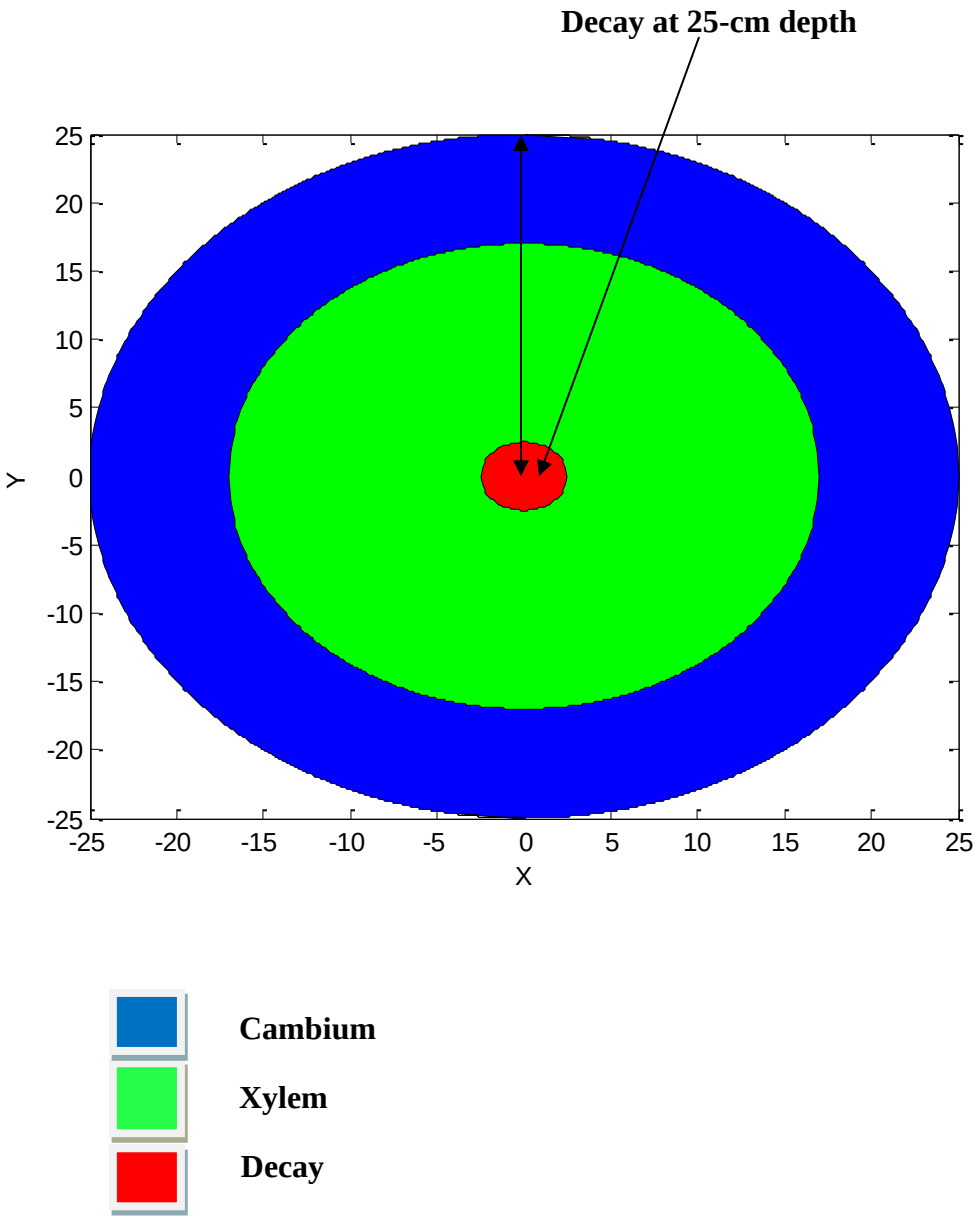

Fig. 4.47. A 2-D image of the cross-section of a decayed tree with wood decay of diameter 5 cm located in the xylem at 25-cm depth with the centre of the decay as the reference point

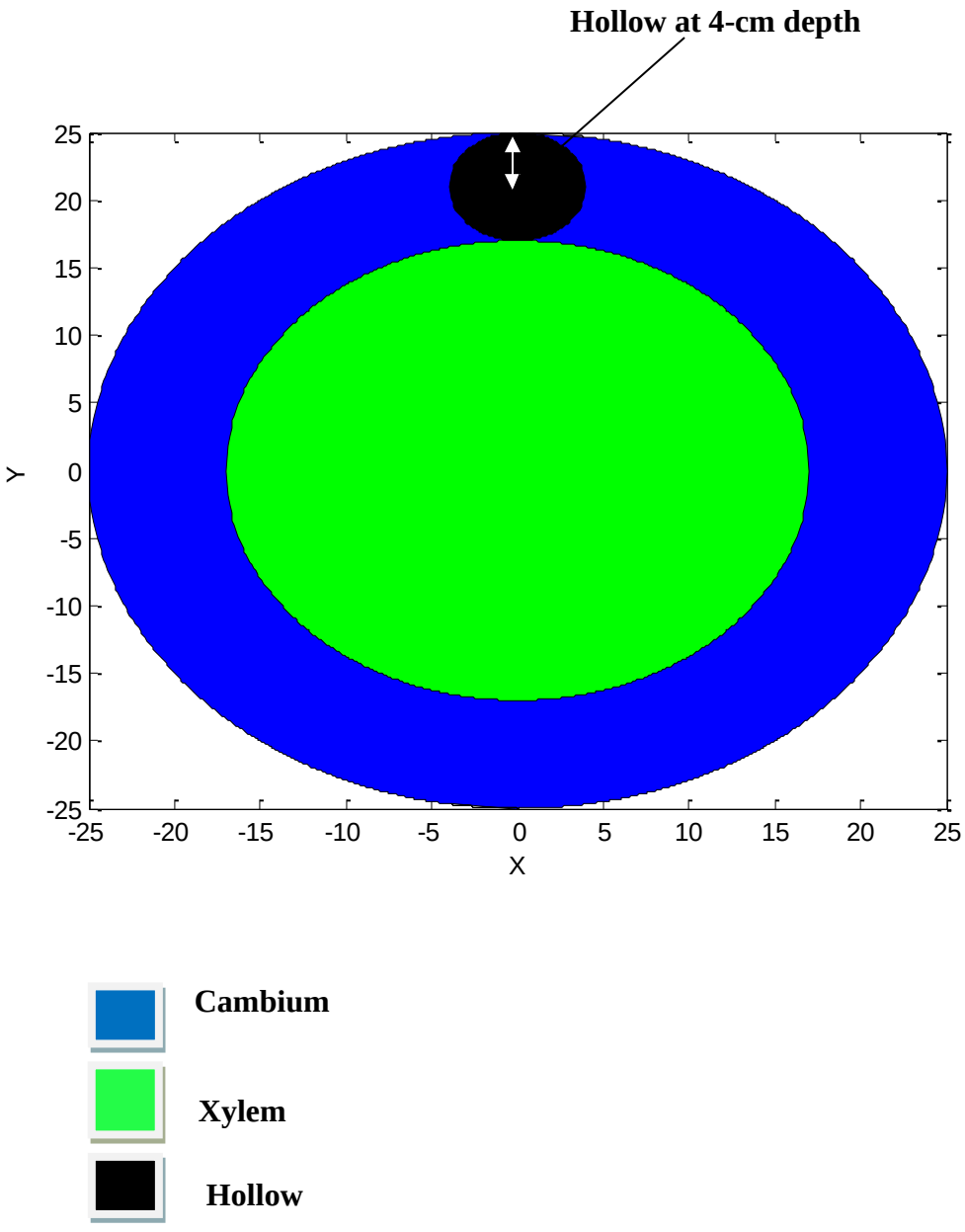

Fig. 4.48. A 2-D image of the cross-section of a tree with a hollow of diameter 8 cm and of length 21 cm located in the cambium at 4-cm depth with the centre of the hollow as the reference point

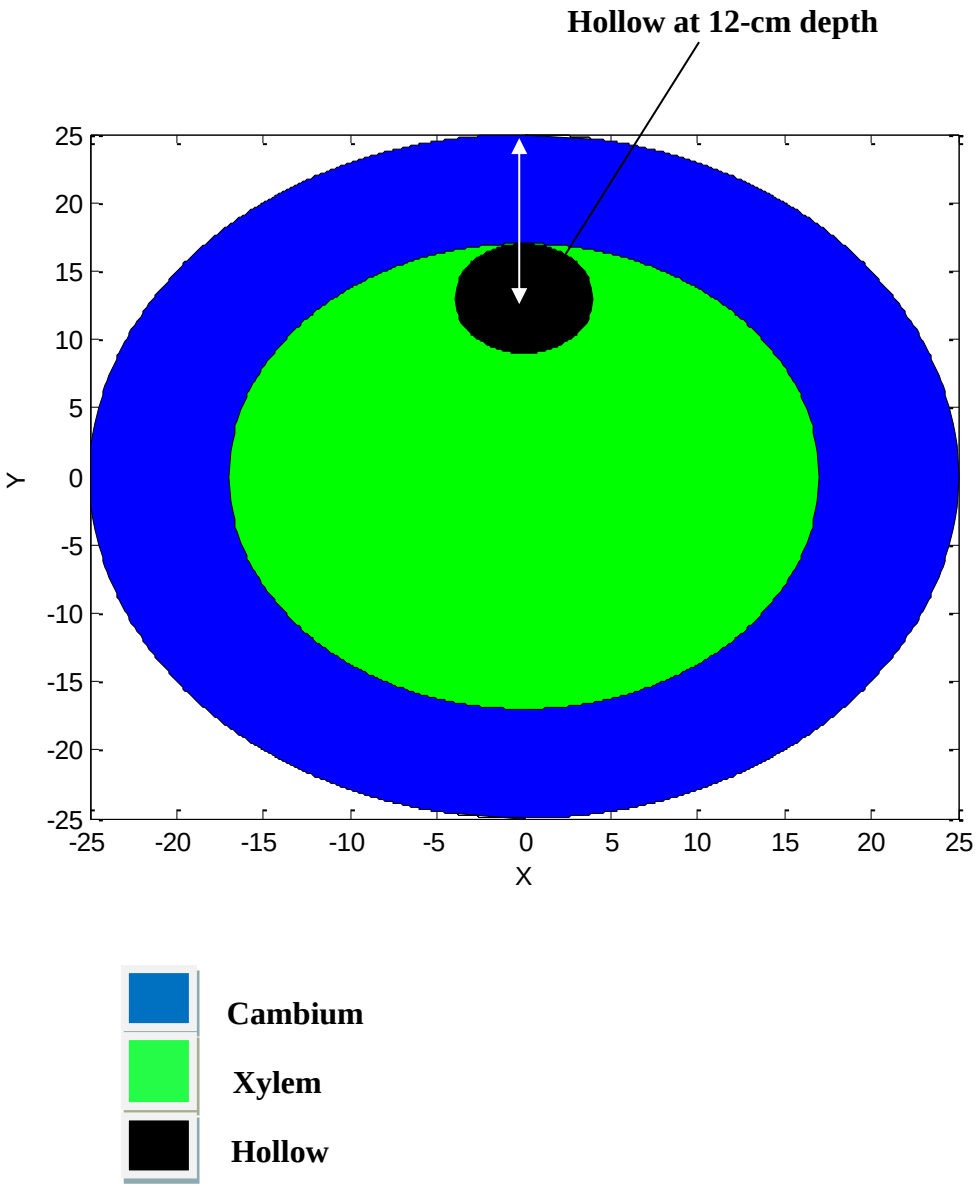

Fig. 4.49. A 2-D image of the cross-section of a tree with a hollow of diameter 8 cm and of length 21 cm located in the xylem at 12-cm depth with the centre of the hollow as the reference point

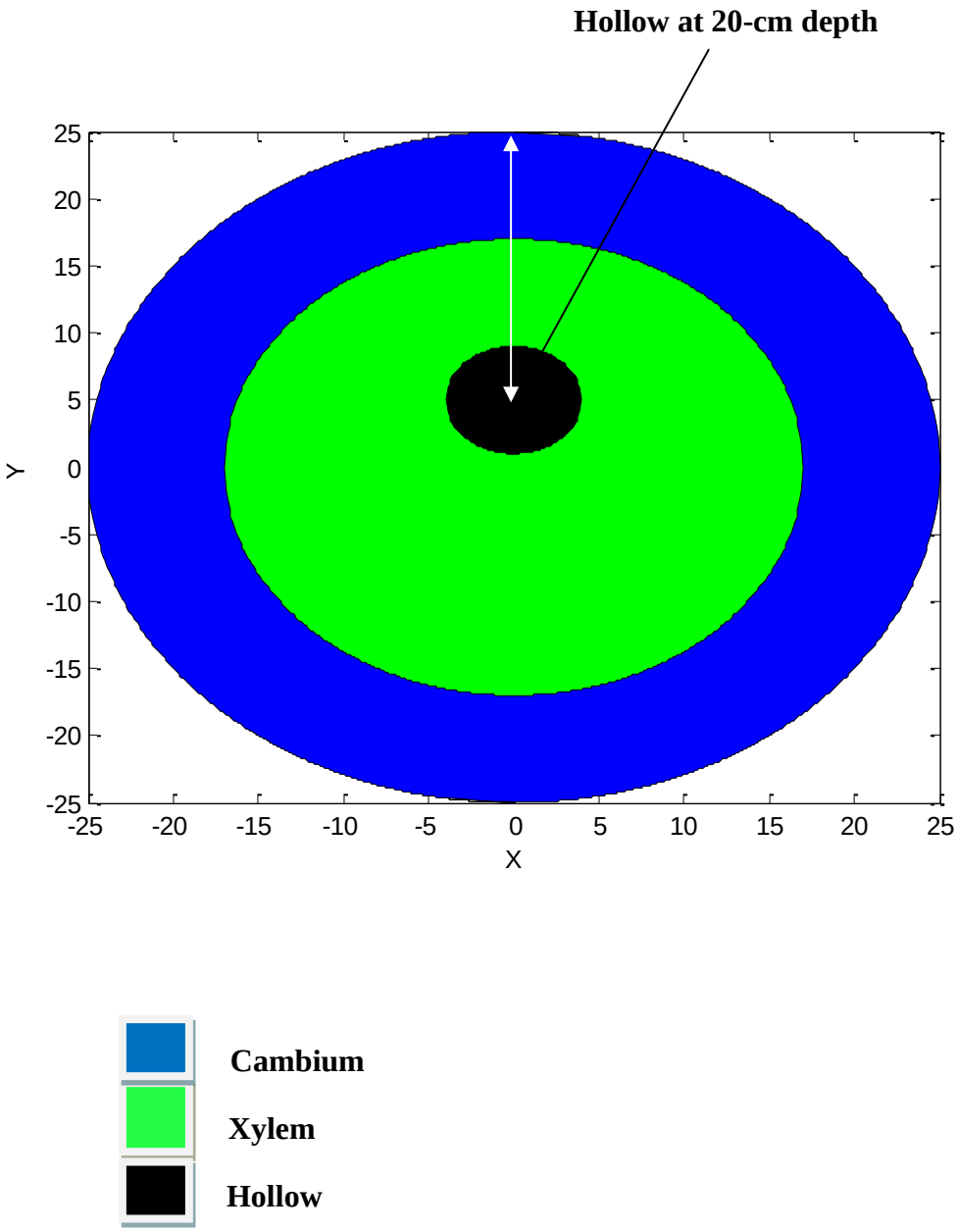

Fig. 4.50. A 2-D image of the cross-section of a tree with a hollow of diameter 8 cm and of length 21 cm located in the xylem at 20-cm depth with the centre of the hollow as the reference point

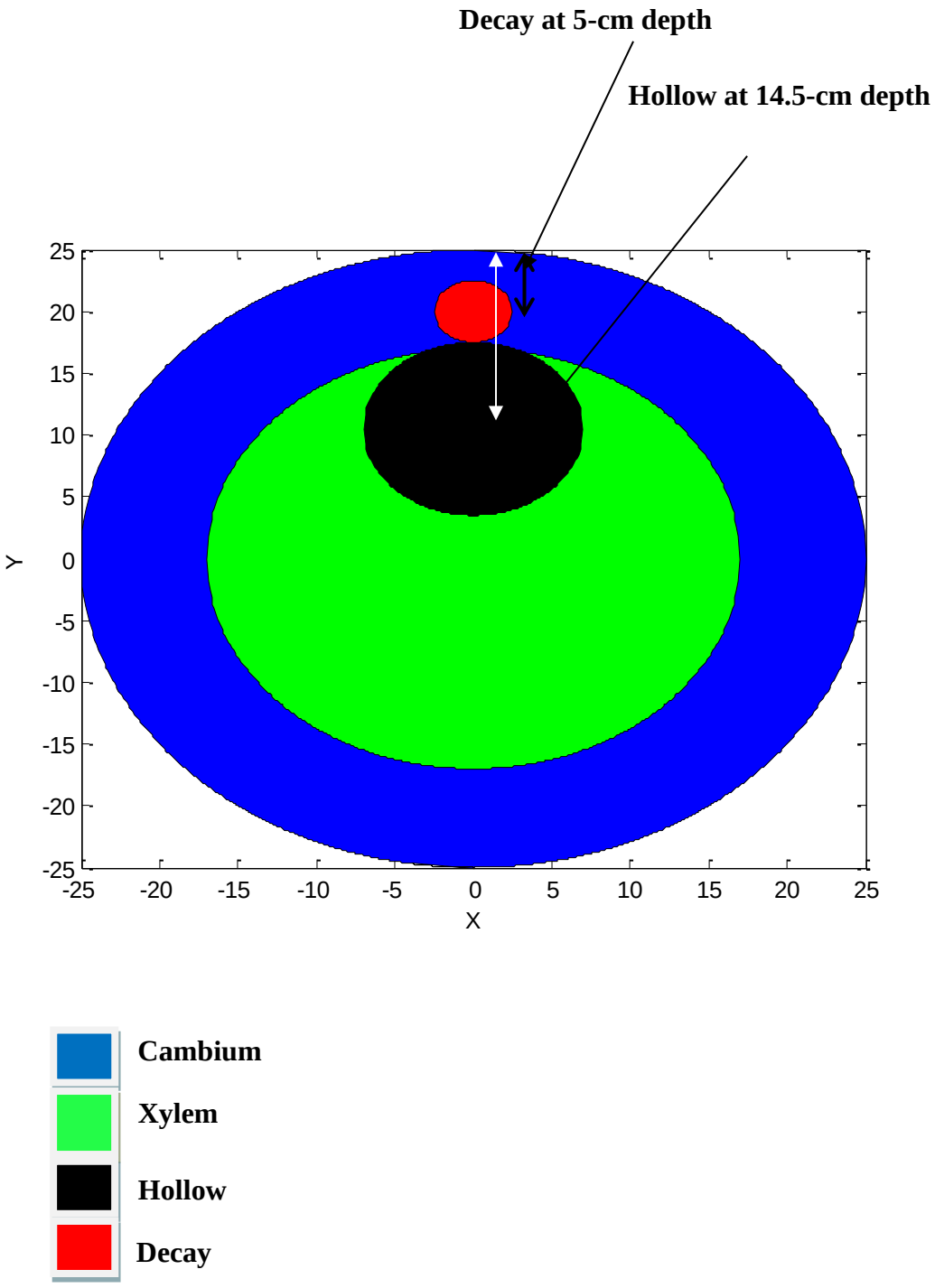

Fig. 4.51. A 2-D image of the cross-section of a tree with wood decay of diameter 5 cm located in the cambium at 5-cm depth and a hollow of diameter 14 cm located in the xylem at 14.5-cm depth

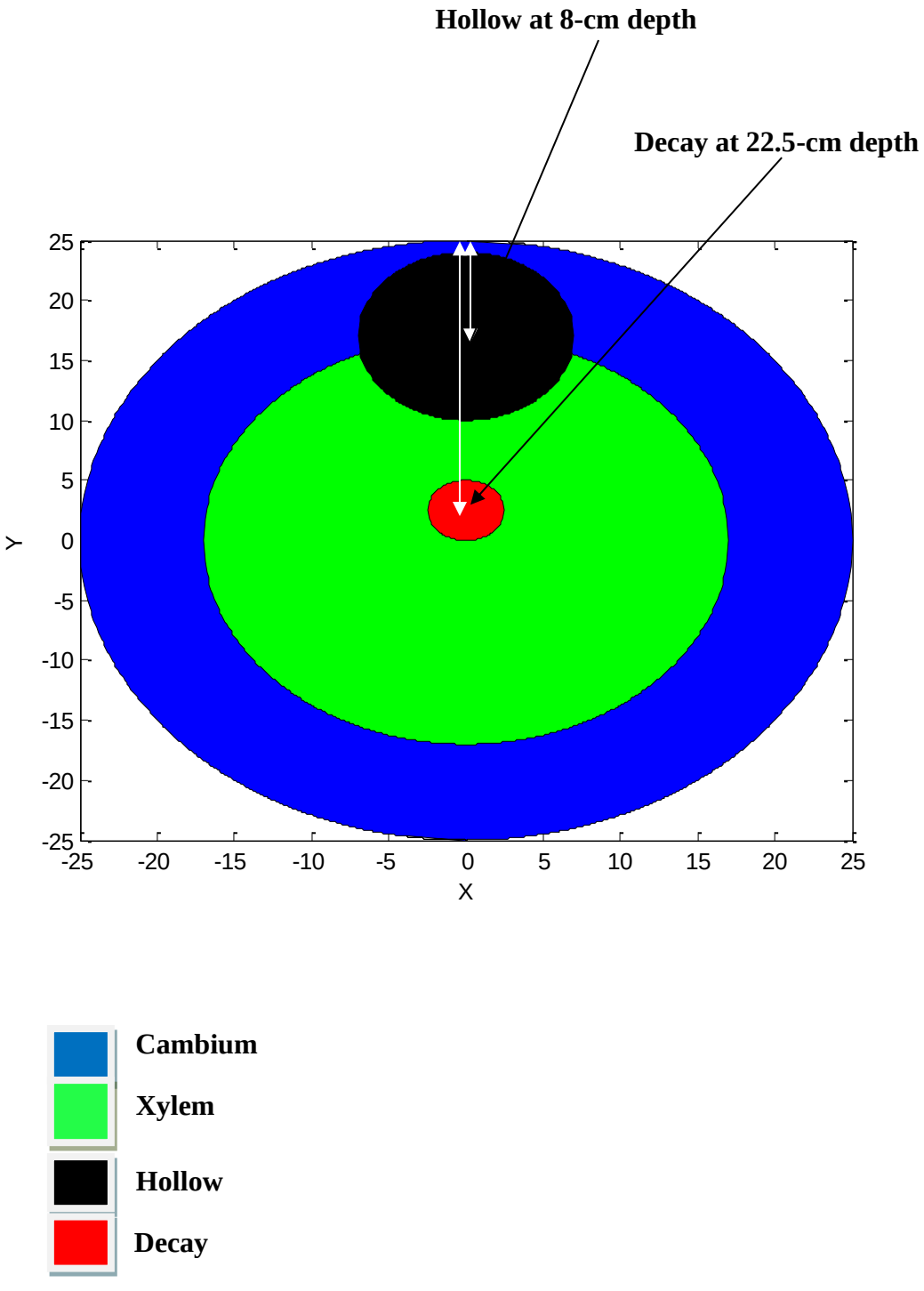

Fig. 4.52. A 2-D image of the cross-section of a tree with a hollow of diameter 14 cm located in both cambium and xylem at 8-cm depth and a wood decay of diameter 5 cm located in the xylem at 22.5-cm depth

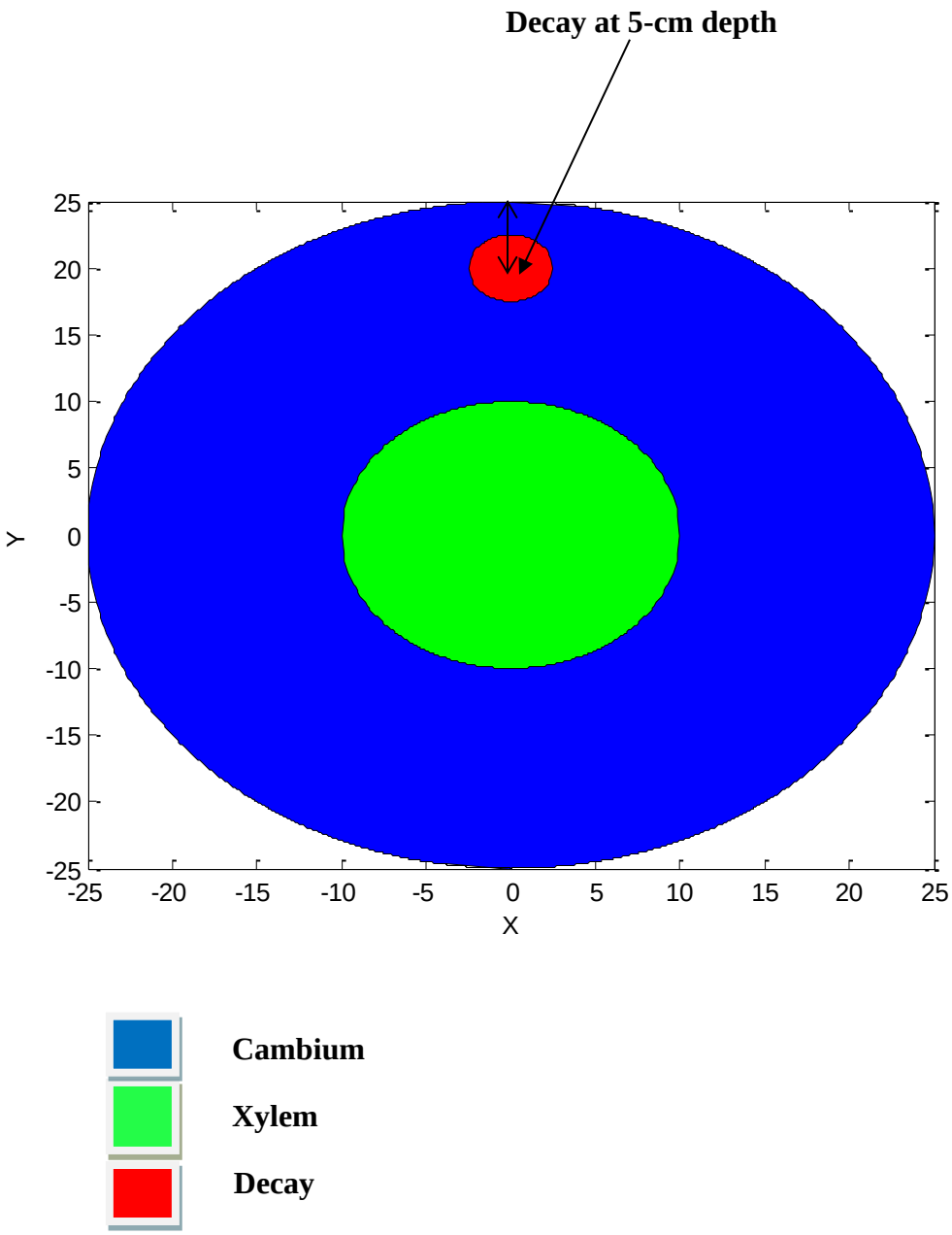

Fig. 4.53. A 2-D image of the cross-section of a decayed tree with wood decay of diameter 5 cm located at 5-cm depth in the cambium with the centre of the decay as the reference point

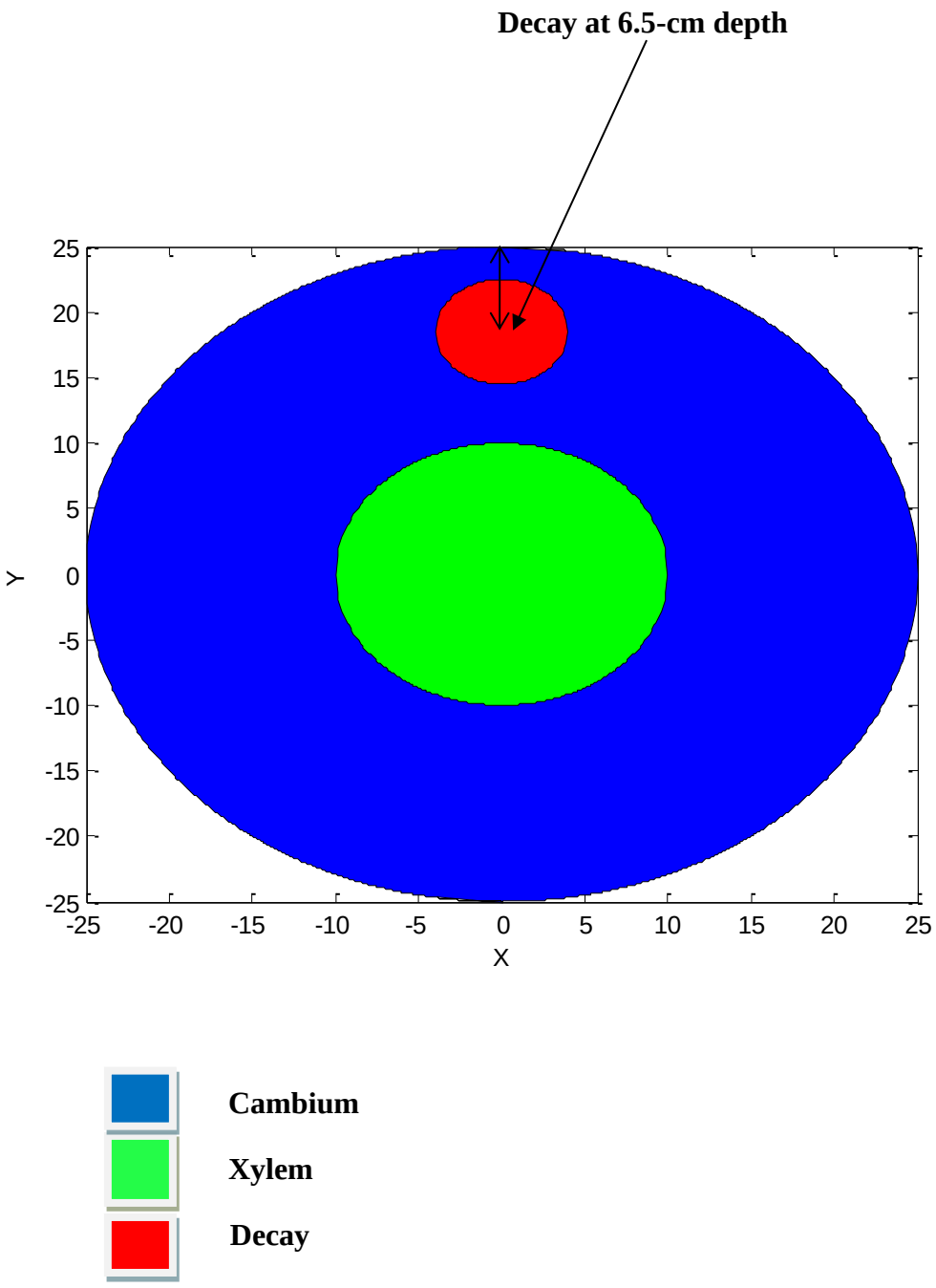

Fig. 4.54. A 2-D image of the cross-section of a decayed tree with wood decay of diameter 8 cm located at 6.5-cm depth in the cambium with the centre of the decay as the reference point

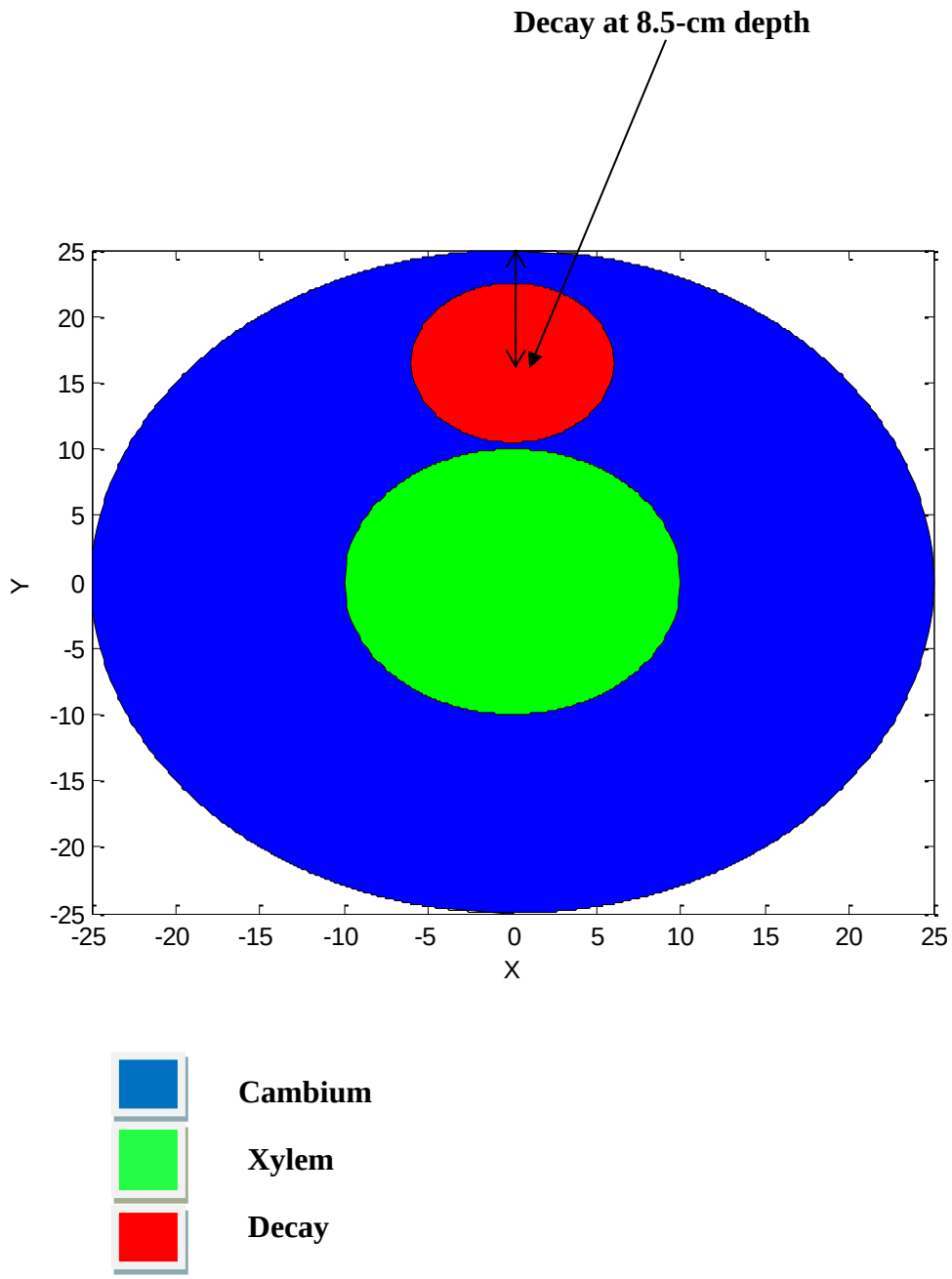

Fig. 4.55. A 2-D image of the cross-section of a decayed tree with wood decay of diameter 12 cm located at 8.5-cm depth in the cambium with the centre of the decay as the reference point

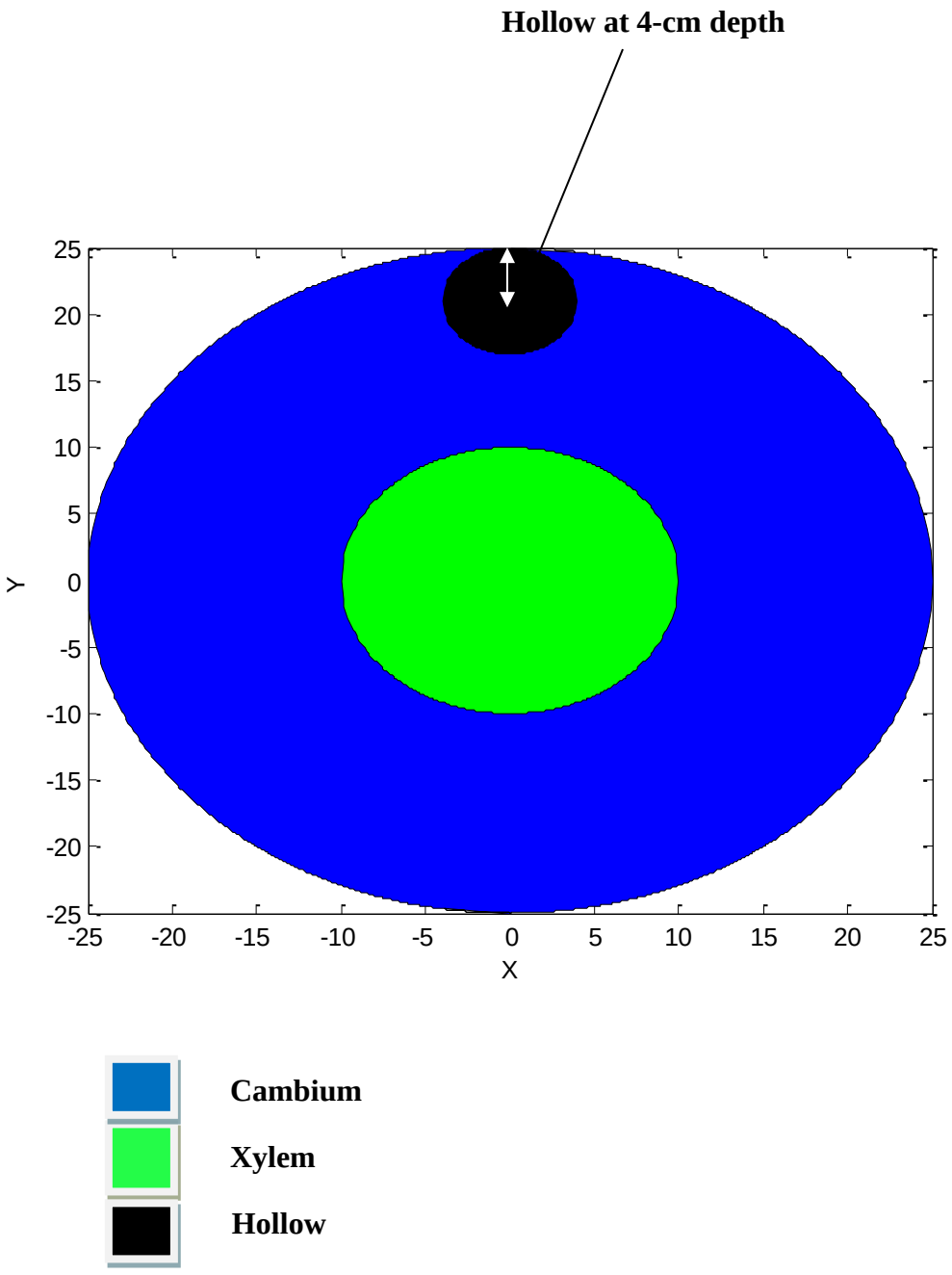

Fig. 4.56. A 2-D image of the cross-section of a tree with a hollow of diameter 8 cm located at 4-cm depth in the cambium with the centre of the hollow as the reference point

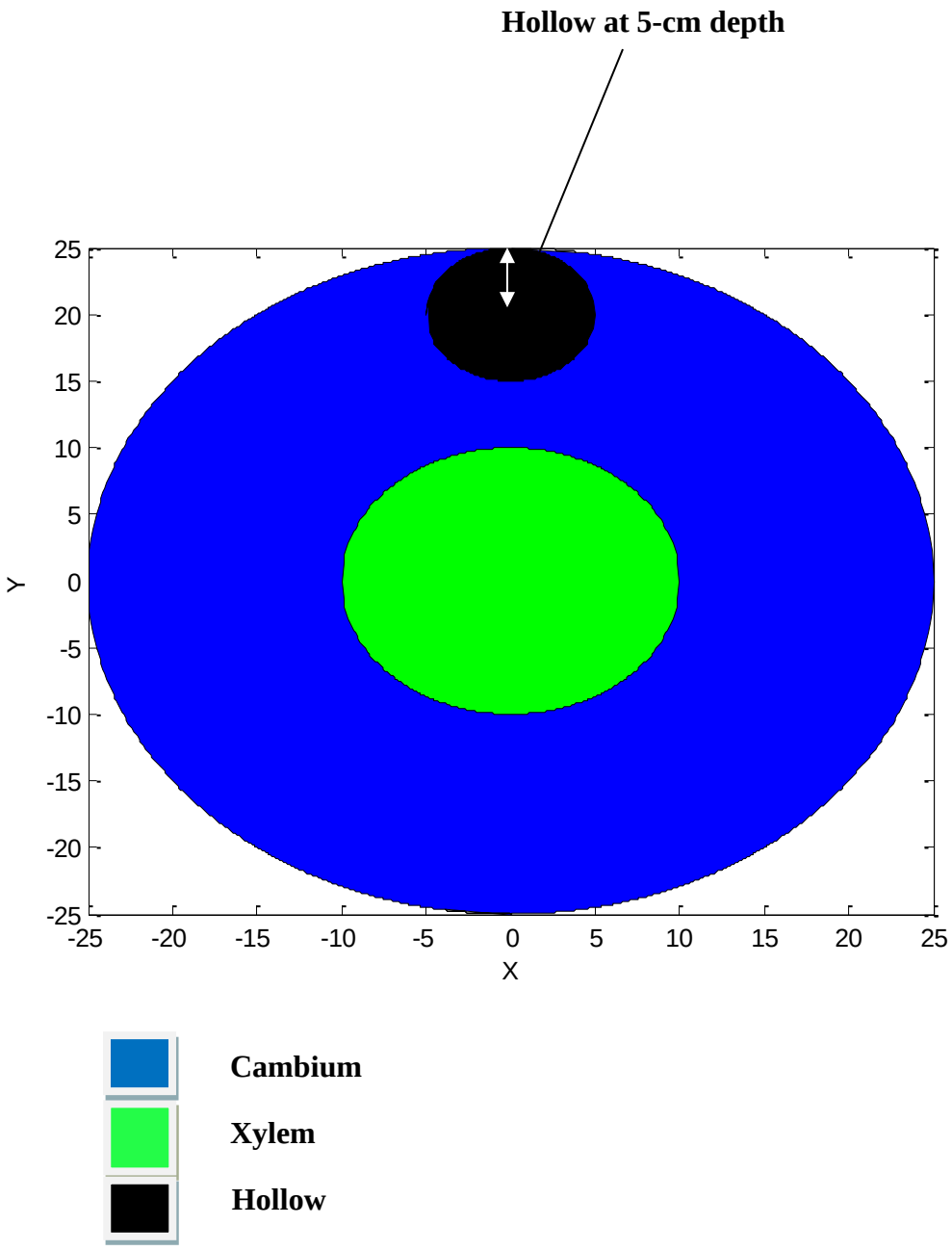

Fig. 4.57. A 2-D image of the cross-section of a tree with a hollow of diameter 10 cm located at 5-cm depth in the cambium with the centre of the hollow as the reference point

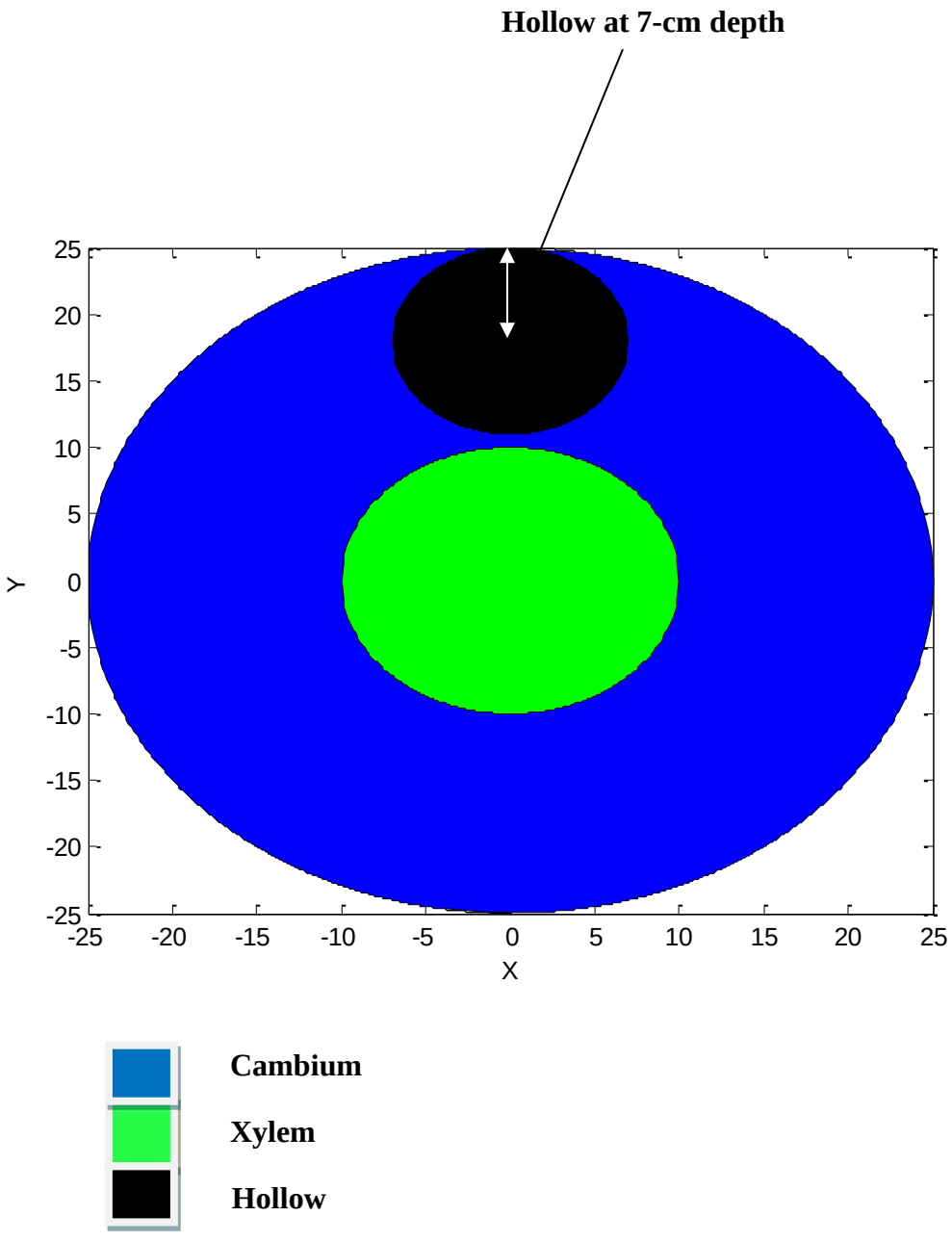

Fig. 4.58. A 2-D image of the cross-section of a tree with a hollow of diameter 14 cm located at 7-cm depth in the cambium with the centre of the hollow as the reference point

4.5 Discussion

In the field results of the healthy candle and almond trees, a rapid increase in resistivity from the cambium to the xylem was observed as shown in Figs. 4.1, 4.2, 4.12 and 4.13. Bieker and Rust (2010) reported the same trend when estimated sapwood and heartwood width in Scots pine (*Pinus sylvestris* L.) trees using Electrical Resistivity Tomography. A steep increase in resistivity between the sapwood and heartwood was clearly displayed by the tomograms. Manyazawale and Ostrofsky (1992) observed a similar trend with the claim that healthy sapwood offers typically lower electrical resistance than heartwood. Guyot *et al*. (2013) reported a noticeable pattern of low resistivities in the stem perimeter and high resistivities in the stem centre of conifers. Thus, the sharp increase in resistivity from the cambium to the xylem implied that the candle and almond trees in Figs. 4.1, 4.2, 4.12 and 4.13 were healthy sound trees.

The resistivities of freshly-cut candle and almond trees with decay and hollow confirmed that wood decay and hollows are characterised by a rapid decrease and increase in resistivity, respectively. This claim is supported by some researchers who reported that a relatively lower resistivity is suggestive of incipient decay (Tattar and Shigo, 1972; Shortle, 1982; Shortle and Ostrofsky, 1983; Shortle and Smith, 1987; Smith and Shortle, 1988). Conversely, the presence of cavities or hollows in a tree trunk increase the stem resistivity since hollows are non-conductors of electricity (Larsson *et al*., 2004). The resistivity values of the decayed cambium of the candle tree presented in Table 4.2 are considerably decreased by an average factor of five in comparison to the healthy tree. Similarly, the resistivities of the hollowed xylem of the candle tree are markedly increased by an average factor of three than those of the healthy tree as presented in Table 4.3. Likewise, the resistivities of the hollowed candle tree in Table 4.4 are noticeably larger than those of the healthy candle tree by an average factor of four. This result is similar to that reported by Larsson *et al*. (2004) noting that the resistivity of Norway spruce trees with decay decreased by a factor of two than healthy trees. A similar trend was also observed in the resistivities of a decayed almond tree with hollow presented in Table 4.12. The resistivities of the decayed cambium of the almond tree decreased by an average factor of 10 compared to those of the healthy tree. Additionally, the resistivities of the hollowed xylem of the almond tree noticeably increased by an average factor of three than those of the healthy tree.

Furthermore, the copper wire lump inserted at different depths in the laboratory prototype to replicate wood decay in a tree stem was responsible for the relatively low resistivity values recorded at the various current electrode half separation, AB/2, where the resistivity anomaly was detected as shown in Tables 4.19 – 4.22. The copper wire lump inserted at 5, 10, 15 and 20 cm depths in the laboratory prototype, was detected at AB/2 = 4 – 8, 10 – 14, 16 – 20 and 22 – 26 cm, respectively as shown in Tables 4.19 – 4.22. The resistivity plot of the laboratory prototype with anomaly overlapped with that of the laboratory prototype without anomaly at the points where there was no copper wire lump as shown in Figs. 4.20, 4.22, 4.24, and 4.26. However, a disparity in trend was observed at the detection points of the copper wire lump. Additionally, the hollow modelled in the laboratory prototype at various depths resulted in the relatively high resistivity values recorded at the detection points of the anomaly as presented in Tables 4.23 – 4.25 and graphically in Figs. 4.28 – 4.33. The hollow positioned at 4, 12 and 20 cm depths in the laboratory prototype was detected at AB/2 = 4 – 10, 12 – 18 and 20 – 26 cm respectively, as shown in Tables 4.23 – 4.25.

Moreover, in addition to displaying the locations of the resistivity anomalies produced by the copper wire lump and hollows, the laboratory results offered useful information on the extent of the resistivity anomalies which is equivalent to the extent of decay and hollows in living trees. In agreement with the field measurements, wood decay modelled into the laboratory prototype (i.e., tree replica) was detected with low resistivity values ranging between 11 and 17 Ωm in the modelled cambium of the tree replica, and from 296 to 1,010 Ωm in the modelled xylem of the tree replica - representing a decrease of an average factor of four compared to the healthy tree replica. Similarly, hollows in the laboratory prototype were also detected with high resistivity values with a range of 155 to 271 Ωm in the modelled cambium of the tree replica, and 3,546 to 12,995 Ωm in the modelled xylem of the tree replica – representing an increase of average factor of three compared to the healthy tree replica. Hence, the resistivity profiles of the laboratory prototype with modelled wood decay and hollows serve as benchmarks for detecting decay and hollows in trees through curve matching. For instance, to detect decay or hollow in a candle tree, the resistivity profile of the tree will be compared to that of the healthy tree shown in Fig. 4.1 provided they are of similar diameter. If the two resistivity profiles match or overlap, it implies that the tree under examination is healthy; otherwise, the tree has decayed or may have hollow. The

location and extent of the decay or hollow in the tree are determined by comparing the resistivity profile of the tree to those of laboratory prototype with modelled wood decay and hollows presented in Figs. 4.20 – 4.27 and Figs. 4.28 – 4.33 respectively, for a possible match provided they are of similar diameter. Then, the 2-D image (Figs. 4.42 – 4.58) corresponding to the resistivity profile of the tree is identified and clearly displays the location and extent of the decay or hollow or both hollow and decay in the case of multiple anomalies. The 2-D images of modelled tree cross-sections transformed the resistivity profiles of the laboratory prototype into images, clearly showing the cross-sections of the equivalent trees with the location and extent of the wood decay and hollows highlighted.

Additionally, the possible occurrence of multiple decay and hollows in a tree is illustrated in Figs. 4.34 – 4.37 showing a sharp rise in resistivity values at the location of hollow and conversely, a rapid decrease in resistivity values at the position of wood decay. The resistivity profile of the laboratory prototype with multiple anomalies, serve as a benchmark for detecting a decayed tree with hollow of similar diameter by resistivity curve matching.

The four-point resistivity technique implemented in this study should not be limited to candle and almond trees alone. It can be applied to detect decay and hollows in other species of hardwood trees. However, to apply this technique to any hardwood tree, the diameter of the tree must first be known to determine appropriate electrode spacing for the vertical variation of resistivity with depth. The current electrode separation AB (Fig. 1.3) should not exceed the diameter of the tree because AB is proportional to the depth of current penetration (Herman, 2001). Secondly, an estimation of the cambium and xylem width from the resistivity profile of the tree is also required to replicate the cambium and xylem of the tree using the laboratory prototype and sawdust (Bieker and Rust, 2010).

CHAPTER FIVE
SUMMARY AND CONCLUSIONS

5.1 Summary

The various techniques for detecting wood decay and other defects, such as hollows or cavities, in living trees have been discussed extensively under two broad categories: invasive and non-invasive methods. The invasive methods comprise resistivity techniques, acoustic techniques (those using ultrasonic and stress-wave devices), traditional methods (involving the use of tools such as a portable hand or electric drill, and increment borer), acoustic tomography and impedance tomography. Conversely, the non-invasive techniques comprise ground penetrating radar methods, magnetic resonance imaging methods, microwave scanning techniques, X-ray tomography, and traditional techniques involving the use of mallets.

Furthermore, the implementation of the electrical resistivity method with modified Schlumberger electrode configuration for the detection of decay and hollows or cavities in candle (*Senna alata* L. Roxb.) and almond (*Terminalia catappa* L. Roxb.) trees has been discussed comprehensively in this thesis. One prime advantage of this technique over the four-point resistivity (RISE) method was its capability to determine the location and extent of decay and hollows in living candle and almond trees. It also provides a more quantitative measure of wood tissue decay status than other methods and can detect decay in the very early (or pre-visual) stages of the decay process (Shortle, 1990).

The field results show a similar trend in the resistivity values of the healthy candle and almond trees – a series of low resistivity values followed by a series of high resistivity values. The low resistivity values represent the cambium (soft, external layer) of the tree while the high resistivity values correspond to the xylem (hard, inner layer) of the tree. This trend was successfully replicated in the laboratory prototype by using compacted wet sawdust to model the cambium and compacted dry sawdust for the xylem. The outcome was that the resistivity profiles of the healthy candle and almond trees correlated strongly with those of the laboratory prototypes replicating the healthy trees ($r^2{}_{mean}$ = 0.956 for candle trees, and $r^2{}_{mean} = 0.998$ for almond trees). Hence,

the resistivity plots of the laboratory prototype serve as both replica and benchmark for healthy candle and almond trees of similar diameters. This claim was also supported by the outcome of one-way ANOVA conducted on the mean resistivities of the healthy trees and the laboratory prototypes.

Moreover, the resistivity values of the wood decay modelled into the laboratory prototype decreased remarkably with an average factor of four compared to those of the healthy tree replica. Similarly, the modelled hollows in the laboratory prototype displayed a marked increase in resistivity values with an average factor of three compared to the healthy tree replica. These laboratory results agree with the field results. Thus, the resistivity values of the laboratory prototypes with modelled wood decay and hollows serve as a benchmark for detecting decay and hollows of similar dimensions in candle and almond trees.

5.2 Conclusions

The four-point electrical resistivity method implemented in this research is a relatively low-cost technique developed to adapt earth resistivity meter, initially designed for ground survey, to measure tree resistivity. This study has proven that earth resistivity meter can be used for other purposes besides ground resistivity survey. Additionally, wood decay and hollow at any location in a tree stem can be detected using this resistivity technique by probing different sides and the entire stem of the tree under inspection. Also, detection points of the resistivity anomalies created by wood decay and hollows in a standing tree, expressed in terms of AB/2, provide information on the extent of decay and hollows. Another advantage of the resistivity method implemented in this research is that it does not involve the drilling of holes into the tree stem. The locally fabricated tiny electrodes, with a diameter of 0.382 cm, could easily be inserted into the tree stem without drilling a hole unlike the case of shigometer electrodes where a narrow hole is drilled towards the centre of the stem (Larsson *et al*., 2004). Therefore, the resistivity technique implemented is a non-destructive method since it does not endanger the tree to the invasion of fungi and other decay-forming organisms (Pellerin and Ross, 2002).

5.3 Field Applications of the Resistivity Method with Modified Schlumberger Electrode Configuration

The following steps are recommended for detecting wood decay and hollows in trees using the electrical resistivity method implemented in this research:

Step 1: Measure diameter (D) of the tree to determine the choice of electrode spacing for resistivity measurement. The current electrode separation (AB) is chosen such that it is not greater than the diameter of the tree, i.e., $AB \leq D$ since AB is proportional to the depth of current penetration.

Step 2: Take resistivity measurements of the tree.

Step 3: Obtain the tree resistivity plot.

Step 4: Compare the resistivity plot of the tree to that of the healthy tree provided they are of similar diameter. The tree is healthy if the two resistivity plots match. Otherwise, the tree has decayed or may have hollow.

Step 5: Compare the resistivity plot of the tree to that of laboratory prototype with modelled wood decay and hollows for a possible match, provided they are of similar diameter.

Step 6: Determine the extent and location of the decay or hollow from the resistivity plot.

Step 7: Convert the resistivity plot to a 2-D image to display the cross-section of the tree with the location and extent of the decay and hollow.

5.4 Major Contributions to Knowledge

I. Electrical resistivity method was adapted for the resistivity measurement of trees in this research using earth resistivity meter, locally fabricated electrodes and a modified form of Schlumberger electrode configuration, even though resistivity method was originally designed and commonly used for ground survey.

II. Electrical resistivity profile models were developed for healthy, decayed and hollowed trees.

5.5 Further Work

I. Development of computer software to automate the plotting of resistivity curves or profiles and generation of the 2-D images for detection of wood decay and hollows or cavities in living trees.

II. Extending the scope of the research to include other tropical trees e.g. Mango trees, Cashew trees, etc.

REFERENCES

Araujo, C.D., MacKay, A.L., Hailey, J.R.T., Whittall, K.P. and Le, H. 1992. Proton magnetic resonance techniques for characterization of water in wood: application to white spruce. *Wood Science Technology* 26.2: 101–113.

Arteca, R. 1996. *Plant Growth Substances: Principles and Applications*. New York: Chapman & Hall.

Axmon, J. 2000. On detection of decay in growing Norway spruce via natural frequencies. Licentiate Thesis. Department of Applied Electronics. Lund Institute of Technology, Lund, Sweden. 105

Bannan, M.W. 1962. The vascular cambium and tree ring development. *Tree growth*. New York: Ronald press. 3 – 21.

Bauer, C., Kilbertus, G. and Bucur, V. 1991. Ultrasound characterization technology of degree alteration of beech and pine wood subjected to the attack of different mushrooms. *Holzforschung* 45.1: 41–46.

Beall, F. and Wilcox, W. 1987. Relationship of acoustic emission during radial compression to mass loss from decay. *Forest Products Journal* 37: 38 – 42.

Bengtsson, B. 1997. Device and transmittance in the detection of rot attacks in biological applications, preferably trees. Swedish Patent No. 9703540–6.

Bethge, K., Mattheck, C. and Hunger, E. 1996. Equipment for detection and evaluation of incipient decay in trees. *Arboricultural Journal* 20: 13 – 37.

Bieker, D. and Rust, S. 2010. Non-destructive estimation of sapwood and heartwood width in Scots pine (*Pinus sylvestris* L.). *Silva Fennica* 44.2: 267–273.

Blanchette, R.A. 1991. Delignification by wood-decay fungi. *Annual Review of Phytopathology* 29: 381-98.

Brazee, N.J., Marra, R.E., Gocke, L. and Wassenaer, P.V. 2010. Non-destructive assessment of internal decay in three hardwood species of northeastern North America using sonic and electrical impedance tomography. *Forestry* 84: 33 – 39.

Bucur, V. 1995. *Acoustics of Wood*. Boca Raton, FL: CRC Press Inc. 286.

Bucur, V. 2003. *Nondestructive Characterization and Imaging of Wood*. Berlin: Springer-Verlag. 354.

Bucur, V. 2005. Ultrasonic techniques for nondestructive testing of standing trees. *Ultrasonics* 43: 237–239.

Bucur, V. 2006a. *Acoustics of Wood*. 2nd ed. Berlin: Springer-Verlag. 393.

Bucur, V., 2006b. *Urban Forest Acoustics*. Berlin: Springer-Verlag. 181.

Bulleit, W.M. and Falk, R.H., 1985. Modeling stress wave passage times in wood utility poles. *Wood Science Technol*ogy 19: 183–191.

Butin, H. 1995. *Tree diseases and disorders: causes, biology, and control in forest and amenity trees*. Oxford: Oxford University Press. 262.

Butnor, J.R., Pruyn, M. L., Shaw, D.C., Harmon, M.E., Mucciardi, A.N. and Ryan, M.G. 2009. Detecting defects in conifers with ground penetrating radar: applications and challenges. *Forestry Pathology* 39: 309–322.

Campbell, N.A. and Reece, J.B. 2005. *Photosynthesis: Biology*. San Francisco: Benjamin Cummings.

Catena, A. 2003. Thermography reveals hidden tree decay. *Arboricultural Journal* 27:27–42.

Catena, A. and Catena, G. 2008. Overview of thermal imaging for tree assessment. *Arboricultural Journal* 30: 259–270.

Chang, S.J., Olson, J.R. and Wang, P.C. 1989. NMR imaging of internal features in wood. *Forest Products Journal* 39: 43–49.

Choffel, D. 1999. Automation of wood mechanical grading. *Coupling of vision and microwave devices SPIE* 3836: 114–121.

Davies, P.J. 1995. *Plant Hormones: Physiology, Biochemistry and Molecular Biology*. Dordrecht: Kluwer.

Deflorio, G., Fink, S. and Schwarze, F.W.M. 2008. Detection of incipient decay in tree stems with sonic tomography after wounding and fungal inoculation. *Wood Science Technology* 42: 117–132.

Dolwin, J.A., Lonsdale, D. and Barnett, J. 1998. Detection of decay in trees. *The commonwealth Forestry Review* 77.4: 277–280.

Eriksson, K.E.L., Blanchette, R. A. and Ander, P. 1990. Microbial and enzymatic degradation of wood and wood components. New York: Springer-Verlag.

Fahn, A. and Werker, E. 1972. Anatomical mechanisms of seed dispersal. *Seed biology*. New York: Academic Press.

Flibotte, S., Menon, R.S., MacKay, A.L. and Hailey, J.R.T. 1990. Proton magnetic resonance of western red cedar. *Wood Fiber Science* 22: 362–376.

Fritts, H.C. 2001. Tree Rings and Climate. Blackburn Press.

Gao, S., Wang, X., Wiemann, M.C., Brashaw, B.K., Ross, R.J. and Wang L. 2017. A critical analysis of methods for rapid and nondestructive determination of wood density in standing trees. *Annals of Forest Science* 74: 27.

Gao, S., Yue, X. and Wang, L. 2019. Effect of the degree of decay on the electrical resistance of wood degraded by brown-rot fungi. *Canadian Journal of Forest Research* 49: 145–153.

Gilbert, E. and Smiley, E.T. 2004. Picus sonic tomography for the quantification of decaying white oak (Quercus alba) and hickory (Carya spp.). *Journal of Arboriculture* 30: 277 – 281.

Goh, C.L., Rahim, R.A., Rahiman, M.H.F., Talib, M.T.M. and Tee, Z.C. 2018. Sensing wood decay in standing trees: A review. *Sensors and Actuators A* 269: 276–282.

Goncz, B., Divos, F. and Bejo, L. 2017. Detecting the presence of red heart in beech *Fagus sylvatica*) using electrical voltage and resistance measurements. *European Journal Wood and Wood Prod*ucts 76.2: 679–686.

Guyot, A., Ostergaard, K.T., Lenkopane, M., Fan, J. and Lockington, D.A. 2013. Using electrical resistivity tomography to differentiate sapwood from heartwood: application to conifers. *Tree Physiology* 33:187–194.

Habermehl, A. 1982a. A new non-destructive method for detecting internal wood conditions and decay in living trees. Part 1: principles. method and apparatus. *Arboricultural Journal* 6: 1-8.

Habermehl, A. 1982b. A new non-destructive method for detecting internal wood conditions and decay in living trees. Part 2: Results and further developments. *Arboricultural Journal* 6: 121-130.

Hall, L.D., Rajanayagam, V., Steward, W.A. and Steiner, P.R. 1986a. Detection of hidden morphology by magnetic resonance imaging. *Canadian Journal of Forest Research* 16: 684–687.

Hall, L.D., Rajanayagam, V., Steward, W.A. and Steiner, P.R. 1986b. Magnet resonance imaging of wood. *Canadian Journal of Forest Research* 16: 423–426.

Harris, R.W., Clark, J.R. and Matheny, N.P. 2004. *Arboriculture: Integrated Management of Landscape Trees, Shrubs, and Vines*. 4th ed. New Jersey: Prentice Hall.

Heikura, T., Terho, M., Perttunen, J. and Sievanen, R. 2008. A computer-based tool to link Decay information to 3D architecture of urban trees. *Urban Forestry & Urban Greening* 7: 233–239.

Herman, R. 2001. An introduction to electrical resistivity in geophysics. *American Journal Physics* 69.9: 943–952.

Johnstone, D.W., Ades, G.M., Moore, G.M. and Smith, I.W. 2007. Predicting wood decay in eucalypts using an expert system and the IML-Resistograph drill, *Arboricult. Urban Forest* 33.2: 76.

Johnstone, D., Moore, G., Tausz, M. and Nicolas, M. 2010. The measurement of wood decay in landscape trees, *Arboriculture & Urban Forestry* 36.3: 121–127.

Karlinasari, L., Indahsuary, N., Kusumo, H.T., Santoso, E., Turjaman, M. and Nandika, D. 2015. Sonic and ultrasonic waves in agarwood trees (Aquilariamicrocarpa) inoculated with fusarium solani. *Journal of Tropical Forest Sci*ence. 351–356.

Kaestner, A.P. and Baath, L.B. 2005. Microwave polarimetry tomography of wood. *IEEE Senors Journal* 5.2: 209–215.

Kennard, D.K., Putz, F.E. and Niederhofer, M. 1996. The predictability of tree decay based on visual assessments. *Journal of Arboriculture* 22.6: 249–253.

Kirker, G.T., Zelinka, S., Gleber, S.C., Vine, D., Finney, L., Chen, S., Hong, Y.P., Uyarte, O., Vogt, S., Jellison, J., Goodell, B., and Jakes, J.E. 2017. Synchrotron based X-ray fluorescence microscopy enables multiscale spatial visualization of ions involved in fungal lignocellulose deconstruction. *Science Report* 7: 41798.

Kollman, F.F.P. and Cote, W.A., Jr. 1968. *Principle of wood science and Technology, Volume I, Solid Wood.* New York: Springer-Verlag. 57–65.

Kucera, L.J. 1986. Magnetic resonance tomography and electrical resistance measurement as diagnostic methods of the disease-affected trees. *Swiss Journal of Forestry* 137.8: 673–690.

Larson, P.R 1994. The concept of cambium. *New perspectives in wood anatomy*. The Hague: Martinus NIjhoff/Dr. W. Junk publishers. 85-121.

Larsson, B., Bengtsson, B. and Gustafsson, M. 2004. Nondestructive detection of decay in tree, *Tree physiology* 24: 853–858.

Lawday, G. and Hodges, P. A. 2000. The analytical use of stress waves for the detection of decay in standing trees. *Forestry* 73.5: 447–456.

Lin, C.J., Chung, C.H., Wu, M.L. and Cho, C.L. 2013. Detection of Phellinus noxius decay in Sterculia foetida tree. *Journal of Tropical Forest Science* 25: 487–496.

Lin, C.J., Kao, Y.C., Lin, T.T., Tsai, M.J., Wang, S.Y., Lin, L.D., Wang, Y.N. and Chan, M.H. 2008. Application of an ultrasonic tomographic technique for detecting defects in standing trees. *International Biodeterioration & Biodegradation* 43: 237–239.

Lin, C.J. and Yang, T.H. 2015. Detection of acoustic velocity and electrical resistance tomographies for evaluation of peripheral-inner wood demarcation in urban royal palms. *Urban Forestry & Urban Greening* 14: 583–589.

Lalonde, S., Wipf, D. and Frommer, W. B. 2004. Transport mechanisms for organic forms of carbon and nitrogen between source and sink. *Annual Review of Plant Biology* 55: 341–372.

Lonsdale, D. 1999. *Principles of Tree Risk Assessment and Management*. London: The Stationery Office.

Lyon, H.H. 2005. *Diseases of trees and shrubs*. 2nd ed. WA: Sinclair.

Manyazawale, B. and Ostrofsky, W.D. 1992. An assessment of internal decay of red spruce (picea rubens sarg.) using the shigometer. Maine Agricultural Experiment Station Miscellaneous Report 369.

Martone, P., Estevez, J., Lu, F., Ruel, K., Denny, M., Somerville, C. and Ralph, J. 2009. Discovery of Lignin in Seed Reveals Convergent Evolution of Cell-Wall Architecture, *Current Biology* 19.2: 169–75.

Martin, P., Collet, R., Barthelemy, P. and Roussy, G. 1987. Evaluation of wood Characteristics — internal scanning of the material by microwaves. *Wood Science Technology* 21: 361–371.

Martin, T. 2009. Complex resistivity (CR) of wood and standing trees. *Proceedings of the Non-Destructive Testing in Civil Engineering Conference, Nandes. France*.

Martin, T. and Gunther, T. 2013. Complex Resistivity Tomography (CRT) for fungus detection on standing trees, *European Journal of Forest Research* 132.5-6: 765–776.

Mattheck, C. and Bethge, K. 1993. Detection of decay in trees with the metriguard stress wave timer, *Journal of Arboriculture* 19: 374–378.

Mattheck, C., Breloer, H., Bethge, K.A., Albrecht, W.A. and Zipse, A.W. 1995. Use of the Fractometer to determine the strength of wood with incipient decay, *Journal of Arboriculture* 21.3: 105–112.

Maurer, C., Schubert, S.I., Bächle, F., Clauss, S., Gsell, D., Dual, J. and Niemz, P. 2006. A simple anisotropy correction procedure for acoustic wood tomography. *Holzforschung*, 60, 567–573.

Mauseth, J.D. 1991. Botany: An Introduction to Plant Biology, *Saunders*, Philadelphia, 348-415.

Miller, W.F. and Doolittle, J.A. 1990. The application of ground-penetrating radar to detection of internal defect in standing trees. *Proceedings of the 7th International Nondestructive Testing of Wood Symposium, September 27–29, 1990. Pullman, Washington: Washington State University*, 263–274.

Mishiro, A. 1996. Effect of density on ultrasonic velocity in wood. *Mokuzai Gakkaishi* 42: 887–894.

Mortimer, M.J. and Kane, B. 2004. Risk tree liability in the United States: Uncertain risks for owners and professionals *Urban Forestry and Urban Greening* 2: 159 –165.

Müller, U., Bammer, R., Halmschlager, E. and Wimmer, R. 2001. Detection of fungal wood decay using magnetic resonance imaging. *Holz Roh-Werkstoff* 59: 190–194.

Nicolotti, G., and Miglietta, P. 1998. Using high-technology instruments to assess defects in trees. *Journal of Arboriculture* 24: 297–302.

Nicolotti, G., Socco, L.V., Martinis, R., Godio, A. and Sambuelli, L. 2003. Application and Comparison of three tomographic techniques for the detection of decay in trees. *Journal of Arboriculture* 29: 66–78.

Nowak, T.P., Jasienko, J. and Hamrol-Bielecka, K. 2016. In-situ assessment of structural timber using the resistance drilling method – Evaluation of usefulness. *Construction Building Materiaals* 102: 403–415.

Okolie, E.C., Atakpo, E. and Okpikoro, F.E. 2010. Application of linear Schlumberger configuration in delineation of formation strata and groundwater distribution in Ifon, Ondo State, Nigeria, *International Journal of the Physical Sciences* 5.6: 642–650.

Olson, J.R., Chang S.J. and Wang, P.C. 1990. Nuclear magnetic resonance imaging: a noninvasive analysis of moisture distributions in white oak lumber. *Canadian Journal of Forest Research* 20: 586 – 591.

Osborne, N.L., Hoibo, O.A. and Maguire, D.A. 2016. Estimating the density of coast Douglas-fir wood samples at different moisture contents using medical X-ray computed tomography. *Computers and Electronics in Agriculture* 127: 50–55.

Ostrofsky, W.D. and Shortle, W.C. 1989. Application of the shigometer for assessing tree and forest health and wood product quality, *Review of Tropical Plant Pathology* 6: 39–57.

Ouis, D., 2003. Non-destructive techniques for detecting decay in standing trees. *Arboriculture Journal* 27: 159–177.

Pellerin, R.F. and Ross, R.J. 2002. Nondestructive Evaluation of Wood. *Forest Products Society, Madison, WI.*

Rabe, C., Ferner, D., Fink, S. and Schwarze, F.W.M.R. 2004. Detection of decay in trees with stress waves and interpretation of acoustic picus images, *Arboricultural Journal* 28: 3–19.

Raven, P.H., Evert, R.F. and Eichhorn, S.E. 1992. *Biology of Plants*. New York: Worth. 545–572.

Reynolds, J.M., 2011. *An Introduction to Applied and Environmental Geophysics*. 2nd ed. Wiley-Blackwell.

Rinn, F., 2011. Basic aspects of mechanical stability of tree cross-sections. *Arborist News*. Feb. 52–54.

Sakai, H., Minamisawa, A. and Takagi, K. 1990. Effect of moisture content on ultrasonic velocity and attenuation in woods. *Ultrasonics* 28.6: 382–385.

Schubert, S., Gsell, D., Dual, J., Motavalli, M. and Niemz, P. 2009. Acoustic wood tomography on trees and the challenge of wood heterogeneity. *Holzforschung* 63: 107–112.

Schwarze, F.W.M.R. 2008. *Diagnosis and Prognosis of the Development of Wood Decay in Urban Trees.* Rowville: Enspec. 336.

Schwarze, F.W.M.R., Engels, J., and Mattheck, C. 2000. *Fungal Strategies of Wood Decay in Trees*. Berlin: Springer-Verlag. 185.

Seweta, S., Kumar, R. and Singh, V.P. 2013. *Wood decaying fungi*. Germany: Lap Lambert Academic.

Shigo, A.L., 1991. *Modern arboriculture*. Durham: Shigo & Tree Associates.

Shigo, A.L. and Shortle, W.C. 1986. Shigometry: A reference guide. USDA Forest Service Agriculture Handbook 646: 48.

Shortle, W.C. 1990. Ionization of wood during previsual stages of wood decay. *Biodeterioration Research* 3: 333–348.

Shortle, W.C. and Smith, K.T. 1987. Electrical properties and rate of decay in spruce and firwood, *Phytopathology* 77: 811–814.

Skaar, C., 1988. *Wood – Water Relations*. New York: Springer-Verlag. 279.

Smith, K.T. and Shortle, W.C. 1988. Electrical resistance and wood decay by white rot fungi. *Mycologia* 80: 124–126.

Socco, L.V., Sambuelli, L., Martinis, R., Comino, E. and Nicolotti, G. 2004. Feasibility of ultrasonic tomography for nondestructive testing of decay on living trees. *Research in Nondestructive Evaluation* 15: 31–54.

Taiz, L. and Zeiger E. 2010. *Plant Physiology*. 5th ed. USA: Sinauer Associate Inc. USA.

Tattar, T.A. and Saufley, G.C. 1973. Comparison of electrical resistance and impedance measurements in wood in progressive stages of discoloration and decay. *Canadian Journal of Forest Research* 3.4: 593–595.

Tattar, T.A. and Shigo, A.L. 1972. Relationship between the degree of resistance to a pulsed electric current and wood in progressive stages of discoloration and decay in trees. *Phytopathology* 62: 792.

Telford, W.M., Geldart, L.P. and Sheriff, R.E. 1990. *Applied Geophysics*. Cambridge: Cambridge University Press.

Tomazello, M., Brazolin, S., Chagas, M.P., Oliveira, J.T., Ballarin, A.W. and Benjamin, C.A. 2008. Application of X-ray technique in non-destructive evaluation of eucalypt wood. *Maderas, Ciencia tecnologia* 10.2: 139–149.

Toole, E.R. and Grammage, J.L. 1959. Damage from increment borings in Bottomland hardwoods. *Journal of Forestry* 57: 909–911.

Ulaby, F.T. and Jedlicka, R.P. 1984. Microwave dielectric properties of plant materials. *IEEE Transactions on Geoscience and Remote Sensing* 22: 406–414.

Wade, P.J. 1975. The Fujikura-Arborsonic Decay Detector Concept, Development & Operation. Fujikura Europe Limited.

Waid, J. and Woodman, M. 1957. A non-destructive method for detecting diseases in wood, *Nature* 80: 45–75.

Wang, X., Allison, R.B., Wang, L. and Ross, R.J. 2007. Acoustic tomography for decay detection in Red Oak Trees. *Research Paper FPL-RP-642. US Department of Agriculture, Madison, WI.*

Wang, X. and Allison, R.B. 2008. Decay detection in red oak trees using a combination of visual inspection, acoustic testing, and resistance micro drilling. *Arboriculture & Urban Forestry* 34.1: 1–4.

Wang, P.C. and Chang, S.J. 1986. Nuclear magnetic resonance imaging of wood. *Wood and Fiber Science* 18: 308–314.

Wang, X., Wiedenbeck, J. and Liang, S. 2009. Acoustic tomography for decay detection in black cherry trees. *Wood Fiber Science* 41: 127–137.

Weihs, U., Dubbel, V. Krummheuer, F. and Just, A. 1999. Electrical resistivity tomography—a promising method for diagnosing red heart in standing beech. *Forst und Holz* 6: 166–170.

Wilcox, W.W. 1988. Detection of early stages of wood decay with ultrasonic pulse velocity. *Forest Products Journal* 5: 68–73.

Xu, Z., Leininger, T.D., Williams, J.G. and Tainter, F.H. 2000. Examination of the Arborsonic Decay Detector for detecting bacterial wetwood in red oaks. *Southern Journal of Applied Forestry* 24.1: 6–10.

Yamaguchi, T., Sasaki, K. and Sakamoto, Y. 2001. Evaluation of a stress-wave timer for the minimally destructive detection of decay in living trees in northern-Japan forests. *Journal of Forest Resources* 6. 117–120.

Zakaria, Z., Mansor, M.S.B., Rahim, R.A., Balkhis, I., Rahiman, M.H.F., Rahim, H.A. and Yaacob, S., 2013. Magnetic induction tomography: a review on the potential application in agricultural industry of Malaysia, *Journal of Agricultural Science* 5.9: 78.

Appendix 1

A Car Crushed by a Fallen Tree

Source: Metro UK, http://metrouk2.files.wordpress.com/2013/10/ad_119148649.jpg, retrieved on 14 April 2014

Appendix 2

A Fallen Tree Wreaked Havoc on Buildings and a Car

Source: Daily Telegraph, www.cdn.nolet.com/node/6096007/articles?page=28, retrieved on 14 April 2014

Appendix 3

Miller 400D Digital Resistance Meter

Appendix 4

Conventional Electrode and Improvised Tiny Electrode

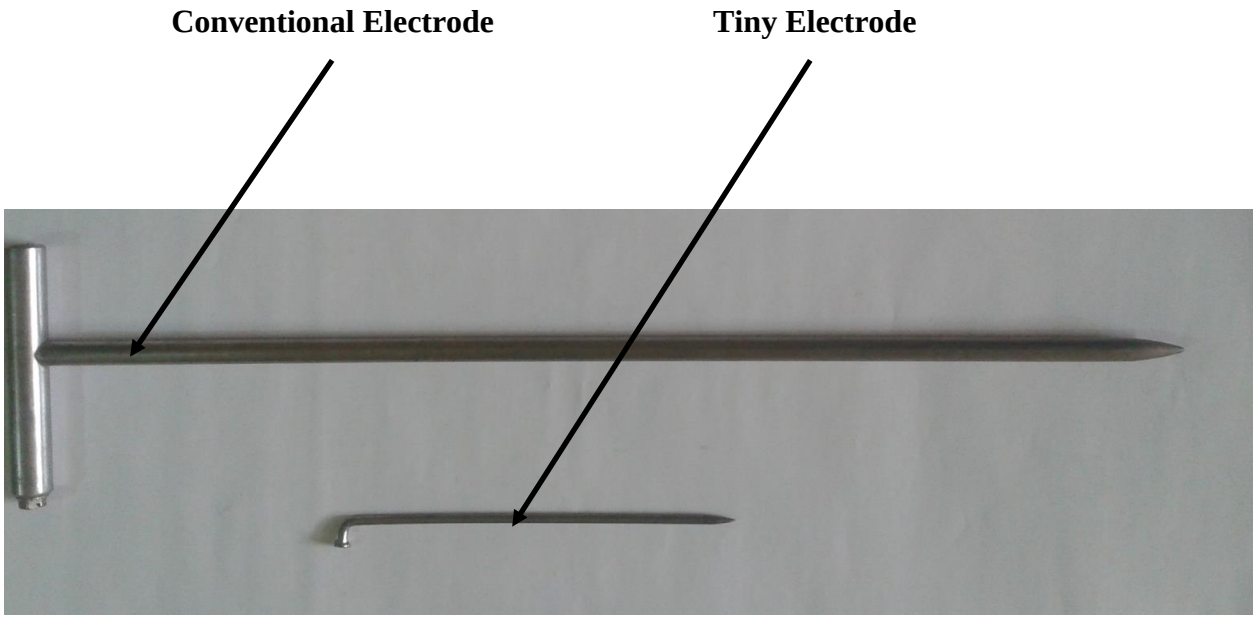

Appendix 5

Electrode configurations designed for tree diameters of 20, 30, 40, 50 and 60 cm, Respectively

Tree Diameter									
20 cm		**30 cm**		**40 cm**		**50 cm**		**60 cm**	
AB/2 (cm)	**MN/2 (cm)**	**AB/2 (cm)**	**MN/2 (cm)**	**AB/2 (cm)**	**MN/2 (cm)**	**AB/2 (cm)**	**MN/2 (cm)**	**AB/2 (cm)**	**MN/2 (cm)**
4	1	4	1	4	1	4	1	4	1
6	1	6	1	6	1	6	1	6	1
8	1	8	1	8	1	8	1	8	1
10	1	10	1	10	1	10	1	10	1
		12	2	12	1	12	1	12	1
		14	2	14	2	14	1	14	2
		16	2	16	2	16	2	16	2
				18	2	18	2	18	2
				20	2	20	2	20	2
						22	2	22	2
						24	2	24	3
						26	2	26	3
								28	3
								30	3

AB/2: Current electrode half separation
MN/2: Potential electrode half separation

Appendix 6

Electrode Configurations Designed for Tree Diameters of 70, 80, 90, 100 and 110 cm, Respectively

Tree Diameter									
70 cm		**80 cm**		**90 cm**		**100 cm**		**110 cm**	
AB/2 (cm)	**MN/2 (cm)**	**AB/2 (cm)**	**MN/2 (cm)**	**AB/2 (cm)**	**MN/2 (cm)**	**AB/2 (cm)**	**MN/2 (cm)**	**AB/2 (cm)**	**MN/2 (cm)**
4	1	4	1	4	1	4	1	4	1
6	1	6	1	6	1	6	1	6	1
8	1	8	1	8	1	8	1	8	1
10	1	10	1	10	1	10	1	10	1
12	1	12	1	12	1	12	1	12	1
14	1	14	2	14	1	14	2	14	1
16	2	16	2	16	2	16	2	16	2
18	2	18	2	18	2	18	2	18	2
20	2	20	2	20	2	20	2	20	2
22	2	22	2	22	2	22	2	22	2
24	2	24	3	24	2	24	3	24	2
26	2	26	3	26	2	26	3	26	2
28	3	28	3	28	3	28	3	28	3
30	3	30	3	30	3	30	3	30	3
32	3	32	3	32	3	32	3	32	3
34	3	34	4	34	3	34	4	34	3
36	3	36	4	36	3	36	4	36	3
		38	4	38	3	38	4	38	3
		40	4	40	4	40	4	40	4
				42	4	42	4	42	4
				44	4	44	5	44	4
				46	4	46	5	46	4
						48	5	48	4
						50	5	50	5
								52	5
								54	5
								56	5

AB/2: Current electrode half separation
MN/2: Potential electrode half separation

Appendix 7

An Example of Schlumberger Electrode Configuration (Okolie *et al*., 2010)

Current Electrode Half Separation AB/2 (m)	Potential Electrode Half Separation MN/2 (m)
1	0.5
2	0.5
3	0.5
4	0.5
6	0.5
6	1.0
9	1.0
12	1.0
15	1.0
15	2.0
25	2.0
32	2.0
40	2.0
40	5.0
65	5.0
100	5.0
100	10.0
150	10.0
200	10.0
200	20.0
250	20.0
300	20.0
350	20.0

Appendix 8

Measurement of the Electrical Resistance of a Tree

RESEARCH PUBLICATIONS

The following three research articles have been published in learned journals indexed in SCOPUS to report the outcome of this research:

1. **Soge, A. O.**, Popoola, O. I., and Adetoyinbo, A. A., 2020. Detection of wood decay and cavities in living trees: A review. *Canadian Journal of Forest Research*, in press.
   Publisher: Canadian Science Publishing (NRC Research Press), Canada

2. **Soge, A. O.**, Popoola, O. I., and Adetoyinbo, A. A., 2019. A four-point electrical resistivity method for detecting wood decay and hollows in living trees. *European Journal of Wood and Wood Products* 77:465-474.
   Publisher: Springer-Verlag, Germany

3. **Soge, A.**, Popoola, O., and Adetoyinbo, A., 2018. Detection of decay and hollows in living almond trees (Terminalia catappa L. Roxb.) using electrical resistivity method. *Journal of the Indian Academy of Wood Science* 15.2:181-189.
   Publisher: Springer, India